ANNEX A: Gasification of sewage sludge using a throated downdraft gasifier and uncertainty analysis.

M.Dogru, A. Midilli, C.R. Howart

ELSEVIER

Fuel Processing Technology 75 (2002) 55–82

FUEL PROCESSING TECHNOLOGY

www.elsevier.com/locate/fuproc

Gasification of sewage sludge using a throated downdraft gasifier and uncertainty analysis

Murat Dogru [c], Adnan Midilli [a,b,c,*], Colin R. Howarth [c]

[a] *Mechanical Engineering Department, University of Nigde, Nigde, Turkey*
[b] *Visiting Research Fellow, University of Newcastle, Newcastle upon Tyne, UK*
[c] *Department of Chemical and Process Engineering, University of Newcastle, NE1 7RU, UK*

Accepted 6 September 2001

Abstract

The most important objectives to gasify sewage sludge are to produce a clean gas of acceptable composition for synthesis or combustion, and to convert this solid resource into combustible-clean gas at high efficiency. The experiments of the gasification were conducted using a 5 kWe-throated downdraft gasifier. It was concluded that sewage sludge can be gasified to produce low-quality combustible gas, and would be an acceptable alternative source to fossil fuels for the production of the clean energy. It is suggested that the downdraft gasifier should be operated at 3.69–3.71 kg/h $\pm$ 1.43% of the feed rate, at 2.28–2.34 N m^3/kg $\pm$ 1.84% of the air fuel ratio, around 497.74–514 N m^3/m^2 h $\pm$ 1.50% of specific gasification rate and around 93.64–94.15% $\pm$ 1.92% of turndown ratio in order to achieve good quality gas and to avoid clinker formation at the throat of the gasifier because of high ash content of sludge. The thermal efficiency was calculated as between 39% and 40% at the optimum operation levels given above.

Keywords: Gasification; Sewage sludge; Downdraft gasifier; Air fuel ratio; Specific gasification rate; Turndown ratio; H/C

1. Introduction

Sewage sludge is a waste product from sewage treatment plant, and also contains significant amounts of heavy metals, organic toxins and pathogenic microorganism [1],

* Corresponding author. Mechanical Engineering Department, University of Nigde, 51000 Nigde, Turkey. Tel.: +90-462-3772960; fax: +90-462-3255526.
E-mail addresses: midilli@gmx.co.uk, midilli@nigde.edu.tr (A. Midilli).

0378-3820/02/$ - see front matter
PII: S0378-3820(01)00234-X

Nomenclature:

A_t	Cross-sectional area across throat, m^2
C_{dss}	Dry sewage sludge capacity, kg/h
C_{mdss}	Maximum dry sewage sludge capacity, kg/h
d_d	Diameter of the drying zone, m
d_{fb}	Diameter of the filter box, m
d_o	Diameter of the oxidation zone, m
d_s	Diameter of the packed bed scrubber, m
d_t	Diameter of the throat zone, m
F_{dss}	Flow rate of dry sewage sludge, kg/h
F_{dvg}	Total volumetric flow of dry gas, N m^3/h
F_{vda}	Volumetric flow of dry air input, N m^3/h
h_b	Height of the reactor bed, m
h_d	Height of the drying zone, m
h_{fb}	Height of the filter box, m
h_{fb}	Height of the oxidation zone, m
h_p	Height of the pyrolysis, m
h_s	Height of the packed bed scrubber, m
R_{af}	Air fuel ratio, N m^3/kg
R_{sg}	Specific gasification rate, N m^3/m^2 h
R_{td}	Turndown ratio, kg/kg
w_{A_t}	Average uncertainty in the calculation of cross-sectional area across throat, %
$w_{C_{dss}}$	Average uncertainty in the calculation of dry sewage sludge capacity, %
$w_{C_{mdss}}$	Average uncertainty in the calculation of maximum dry sewage sludge capacity, %
$w_{F_{ao}}$	Total uncertainty in the measurement of ash output, %
$w_{F_{ca}}$	Total uncertainty in the measurement of condensate output in the produced wet gas after cleanup, %
$w_{F_{cb}}$	Total uncertainty in the measurement of condensate output in the produced wet gas before cleanup, %
$w_{F_{cdo}}$	Total uncertainty in the measurement of condensate output, %
$w_{F_{co}}$	Total uncertainty in the measurement of char output, %
$w_{F_{dss}}$	Average uncertaintyin the calculation of total mass flow of dry ash free sewage sludge, %
$w_{F_{dvg}}$	Average uncertainty in the calculation of total volumetric flow of dry gas, %
$w_{F_{tda}}$	Total uncertainty in the measurement of tar–dust output in the produced wet gas after cleanup, %
$w_{F_{tdb}}$	Total uncertainty in the measurement of tar–dust output in the produced wet gas before cleanup, %
$w_{F_{to}}$	Total uncertainty in the measurement of tar output, %
$w_{F_{vda}}$	Average uncertainty in the calculation of volumetric flow of dry air input, %
$w_{F_{ws}}$	Total uncertainty in the measurement of the flow rate of wet sewage sludge, %
$w_{F_{wg}}$	Total uncertainty in the measurement of the produced wet gas, %
$w_{F_{wo}}$	Total uncertainty in the measurement of water output, %

$w_{P_{bfo}}$	Total uncertainty in the measurementof the pressure drop at the filter box outlet, %
$w_{P_{go}}$	Total uncertaintyin the measurement of the pressure drop at the gasifier outlet, %
$w_{P_{so}}$	Total uncertainty in the measurement of the pressure drop at the packed bed scrubber outlet, %
$w_{R_{af}}$	Total uncertainty in the calculation of air fuel ratio, %
$w_{R_{sg}}$	Total uncertainty in the calculation of specific gasification rate, %
$w_{R_{td}}$	Total uncertainty in the calculation of turndown ratio, %
$w_{T_{bfo}}$	Total uncertainty in the measurement of the outlet temperature of filter box, %
$w_{T_{dz}}$	Total uncertainty in the measurement of the drying zone temperature, %
$w_{T_{o}}$	Total uncertainty in the measurement of the ambient temperature,%
$w_{T_{pz}}$	Total uncertainty in the measurement of the pyrolysis zone temperature, %
$w_{T_{so}}$	Total uncertainty in the measurement of the outlet temperature of packed bed scrubber, %
$w_{T_{tz}}$	Total uncertainty in the measurement of the throat zone temperature, %

which are considered to be harmful to the environment and all living organisms. Although sewage sludge has been widely used as a fertiliser in many regions all over the world, it can also contribute in solving a number of local energy problems and to the renewable energy sources. The production rate of sewage sludge is significant; for instance, nearly 1 million m^3/year of sewage sludge in the UK [2], 4.2 millions m^3/year in Switzerland, 50 millions m^3/year in the old Federal Republic of Germany [2], 170,000 m^3/year in Singapore [2] are produced. Within UK, the fees of the landfill gate tax have been rising well about the rate of inflation. This increasing weight of environmental, legislative and economic pressure is forcing EU and, particularly, the water companies in the UK to rise the challenge and provide innovative solutions for beneficial processing of sewage sludge. It is evident that there is a growing change in the perception of sludge from an unwanted waste to a beneficial resource, and important to develop a suitable technology or use an existing technology in order to reduce the environmental problem and costs of sludge treatment. Thus, gasification technology can be applied to convert the sewage sludge into a useable energy and to reduce the waste volume. Additionally, it prevents from the toxic organic compounds and fixes the heavy metals in the resultant solid ash as well as produces gas mixture, which can be efficiently utilised in the boilers for heat recovery and/or power generators for electricity generation. However, the lack of the reported comprehensive work on sewage sludge gasification also leads to a preliminary investigation.

During the gasification process presented in this article, sewage sludge was converted into the clean and useable gases at high efficiency for synthesis and combustion, and gasification potential of dried sewage sludge and the effects of this fuel on the gasifier operation was investigated and discussed. In addition to these, this paper reports the physical characteristics, proximate and ultimate analyses of sewage sludge, the composi-

tion of the produced gas, the H/C ratio, the percentages of the combustible and noncombustible gases, the mass balance closure, the composition of the waste products, the efficiencies of the hot and cold gas, the rate of specific gasification and turndown ratio. Accordingly, the small-scale downdraft gasifiers can make an important contribution to the economy of such rural areas where sewage sludge is abundantly produced and some operational data is provided for suitable gasifiers. Therefore, the investments in gasification processes should be also encouraged for, in particular, England and Turkey, the future of European Nations by governments and other authoritative bodies who, for strategic reasons, wish to have a clean alternative to fossil fuels.

2. Theory and method

2.1. Theory—sewage sludge gasification

The gasification of sewage sludge is a series of complex concurrent and consecutive chemical and thermal process, which is not well understood [3]. The process is energetically self-sustaining (auto-thermal) as no thermal input is required at steady-state conditions. During the gasification process, sewage sludge undergoes a complex physical and chemical change starting with the drying or removal of water contained as moisture. The dried sewage sludge is then pyrolysed or thermally decomposed. Finally, the pyrolysis products, condensable and noncondensable vapours and char undergo gasification, where they are concurrently oxidised and then reduced to permanent gases at the reduction zone. The principle stages in the gasification are drying, pyrolysis, oxidation and reduction; however, these processes differ from the unusual types of the gasifiers [4].

In the drying zone, sewage sludge descends into the gasifier and moisture is evapourated using the heat generated in the zones below. The rate of drying depends on the surface area of the fuel, the recirculation velocity, the relative humidity of these gases and temperature differences between the feed and hot gases as well as internal diffusivity of moisture within the fuel [4]. Sewage sludge with less than 15% moisture loses all moisture in this zone. During the experiments, drying process of sewage sludge in the reactor has carried out at temperatures between about 70 and 200 °C.

In the pyrolysis zone, the irreversible thermal degradation of dried sewage sludge descending from the drying zone takes place using the thermal energy, released by the partial oxidation of the pyrolysis products. The release of volatile from sewage sludge begins at about 250 °C, and 60–70% of sewage sludge is converted to a complex liquid fraction comprising water, tars, oils and a gaseous phase including CO, CO_2, H_2 and hydrocarbons remaining char and ash [4]. Pyrolysis of sewage sludge in the reactor has occurred at the temperatures between 350 and 500 °C.

In the throat zone (as often referred as oxidation zone), the volatile products from pyrolysis process are partially oxidised in highly exothermic reactions resulting in a rapid rise in temperature up to 1100 °C in that region. The heat generated is used to drive the drying and pyrolysis of sewage sludge and the gasification reactions. The

oxidation reactions of the volatile are very rapid and the oxygen is consumed before diffusing to the surface of the char. No combustion of the solid char can, therefore, take place. Oxidation of the condensable organic fraction to form lower molecular weight products is important in reducing the amount of tar produced by the downdraft gasifier. However, during the sewage sludge gasification, oxidation zone temperatures have been measured between 1000 and 1100 °C. The products, including CO_2, CO, H_2, H_2O, high chain hydrocarbon gases, residual tars and char, then pass on into the gasification zone below.

In the reduction zone (as often referred as gasification zone), the char is converted into gas by reaction with the hot gases from the upper zones. The gases are reduced to form a greater proportion of H_2 and CO. Temperatures of the gases entering this zone are about 1000–1100 °C and leaving around 700 °C.

2.2. Theory—downdraft gasifier

In a downdraft gasifier, both the fuel (sewage sludge) and the producer gas flow downwards through the reactor enabling the pyrolysis gases to pass through a throated hot bed of char (1100 °C), and this results in the cracking of most of the tars into light chain hydrocarbon gases and water. Also, the air or oxygen is usually admitted to the fuel bed through intake nozzles from throat causing pyrolysis to charcoal and volatile that partially burn as they are produced. The gaseous products of this 'flaming pyrolytic combustion' then consume the charcoal, produced during the pyrolysis, and are converted into combustible gases [4]. These gases are much more appropriate for the purpose of the operation of clean gas burners and Internal Combustion Engines (ICE). High char conversion, low ash carry over, lower tar level, quick response to load different solid wastes and simple construction are some of the most important advantages of the downdraft gasifier over other fixed bed gasifiers [4]. These properties make this type most suitable in a combined heat/power generation requirement, such as in a sewage sludge treatment plant, where drying and power are required [4].

2.3. Method—experimental setup and procedure

2.3.1. Experimental setup

The 5 kWe pilot-scale downdraft gasification system designed and developed by Dogru [4] shown in Fig. 1 consists of a downdraft gasifier, packed bed scrubber, filter box, circulation fan and a pilot burner. *Downdraft gasifier* has four reaction zones, which are drying, pyrolysis, oxidation and reduction zones from top to bottom of the gasifier, respectively.

In *drying zone*, sewage sludge descends into the gasifier and moisture is removed using the heat generated in the zones below by evapouration. In *pyrolysis zone*, the irreversible thermal degradation of dried sewage sludge descended from the drying zone takes place using the thermal energy released by the partial oxidation of the pyrolysis products. In *oxidation zone*, the volatile products of pyrolysis are partially oxidised in the exothermic reactions resulting in a rapid rise of temperature up to 1200 °C in the throat region. The heat generated is used to drive the gasification reactions. In the

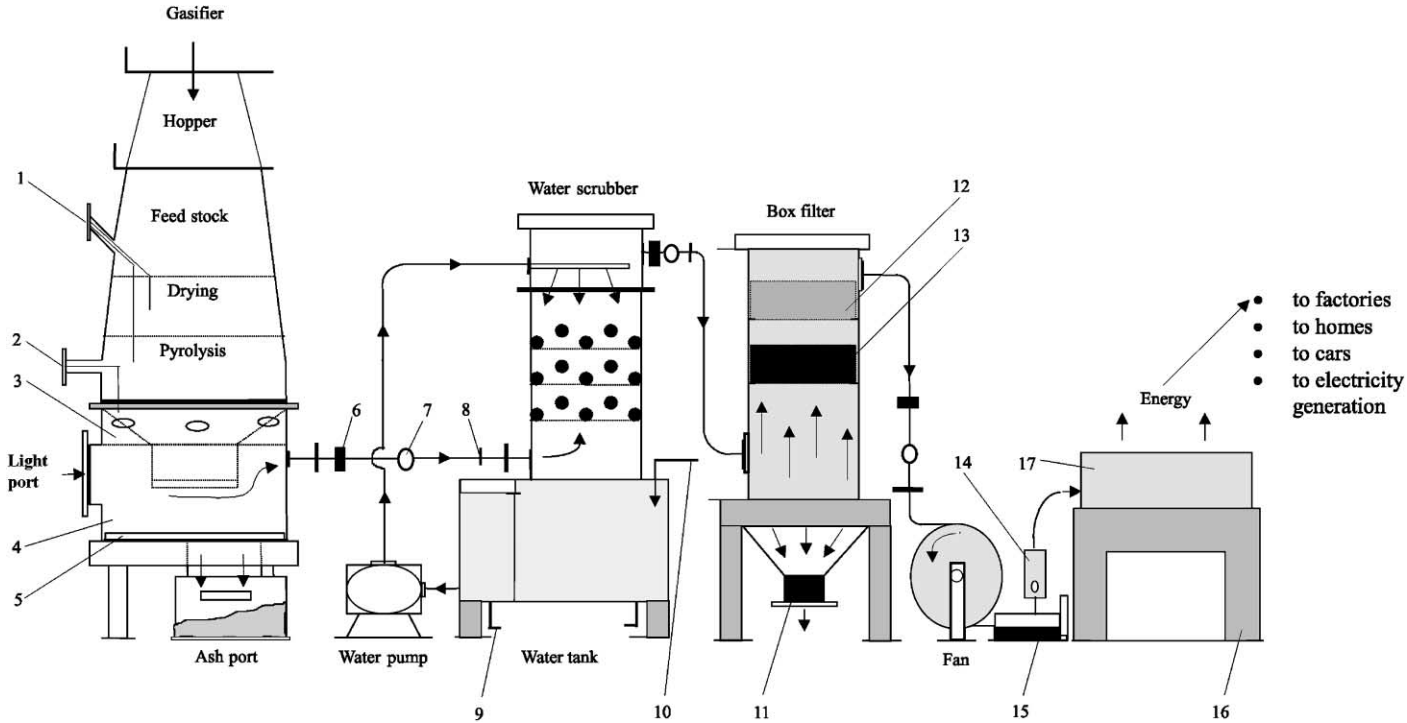

Fig. 1. Schematic figures of the experimental setup. (1) Temperature measurement of drying and pyrolysis zone. (2) Temperature measurement of oxidation zone. (3) Oxidation zone. (4) Reduction zone. (5) Grate. (6) Produced gas outlet temperature measurement. (7) Sampling gas. (8) Pressure measurement of the produced gas. (9) Wastewater outlet. (10) Fresh water inlet. (11) Tar collection chamber. (12) Wood chip. (13) Charcoal. (14) Rotameter. (15) Tar and dust trap. (16) Steal table. (17) Energy generator.

reduction zone as often referred as *gasification zone*, the char is converted to the producer gas by reaction with the hot gases from the upper zones. The gases are reduced to form a greater proportion of H_2, CO, CH_4, C_2H_2 and C_2H_6. While leaving the gasifier at temperatures between 200 and 300 °C, the produced gases carry over some dust, pyrolytic products (tar) and water vapour.

The *packed bed scrubber* consists of water tank to recirculate the spray water and a cooling tower packed with sprays. The gases, left the gasifier, are cooled to 30 °C and 80–90% of tar, dust, fly ash and condensate is removed by packed bed scrubber. After scrubbing, the produced wet gas is further cleaned and moisture removed by vertical filter box. The *filter box* has two layers including wood chips and charcoal, respectively. The contaminated filter can be recycled as fuel for the gasifier. To prevent excessive pressure drop over the box filter, the wood chips and charcoal are thoroughly sieved to remove any fines before installed. Remaining tar and condensate from the produced wet gases are collected at the base of the box filter.

2.3.2. Experimental procedure

Detailed flow diagram of the process of downdraft gasification was shown in Fig. 2 and the following procedure was applied during the experiments.

Preweighted batches of sewage sludge are carefully loaded into the downdraft gasifier until the sewage sludge filled up to a predetermined level. Clean and dry wood chips and charcoal for use as filters are placed in the respective trays in the filter box. Gas flow meter is regulated to the required flow rate. Air fan is switched on. Circulation pump (water scrubber pump) at the side of the water tank is turned on. Pilot lighter to ignite the fuel is lighted. After these processes, the flow rate of the produced wet gas was measured by gas flow meter, located after suction of the circulation fan. During the experiments, the samples were taken two times from the outlet of the gasifier and the outlet of the water scrubber in order to analyse the produced wet gas, and to determine the amounts of tar and condensate in the produced wet gas. A gas chromatography (Shimadzu GC-8A) was used to analyse the gas samples using helium carrier gas.

Gas Chromatography (GC) has dual columns (chromosorp 101 and molecular sieve) and a thermal conductivity detector. Carbon monoxide (CO), methane (CH_4), carbon dioxide (CO_2), oxygen (O_2), nitrogen (N_2), ethane (C_2H_6) and ethylene (C_2H_2) were determined utilising helium as the carrier gas. Hydrogen (H_2) can be determined by difference or using argon as the carrier gas.

The U-tube apparatus was utilised to collect tar and condensate, and to clean the gas samples for GC analysis. The U-tube apparatus, basically, consists of a stainless steel sampling probe (5-mm diameter) linked to a plastic pipe according to the necessary relative position of the sampling ports and the rest of the gear. Following, three "U" tubes (Pyrex) were placed in series into ice bath (bucket) for trapping tar and moisture. The first trap contained the glass tubes with smaller diameter to provide a large surface area to the produced wet gas, while the second trap also included silica gel between two pieces of glass wool, and the third trap contained glass wool. All U-tubes were placed in an ice bath. Then, a sampling bottle with two teflon taps was used to collect the samples. A differential pressured mercury column manometer (Gallencamp) and a rotameter (MFG Fischer 10 l/min) were placed between the gas bottle and the vacuum pump. A

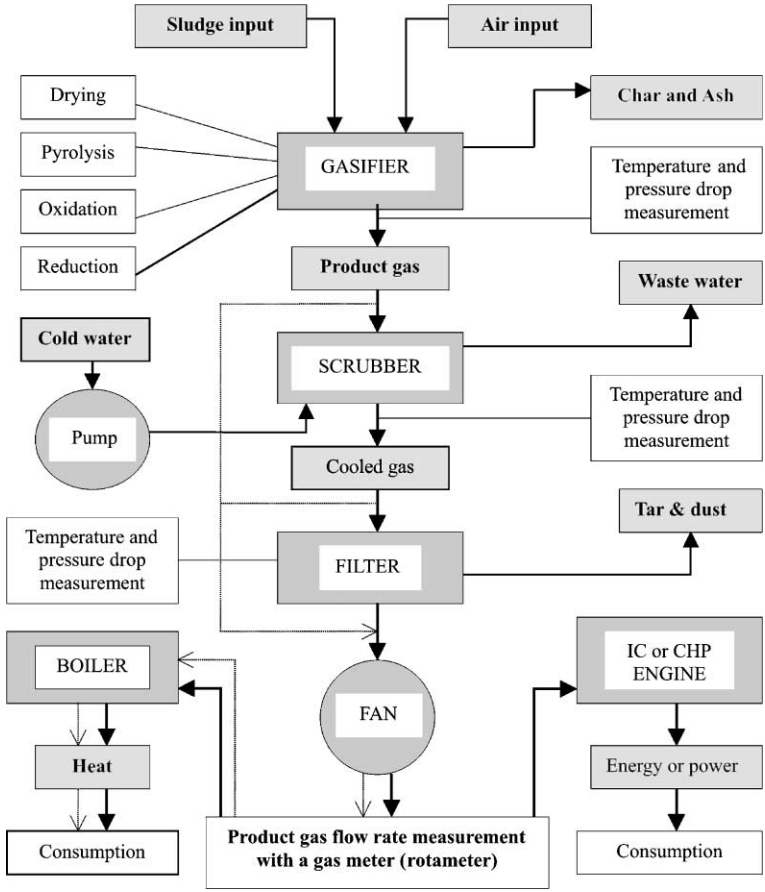

Fig. 2. Detailed flow diagram of the gasification of sewage sludge.

vacuum pump (AEI type BS 2406 0.25 hp) was utilised to draw the gases through the sampling bottle. As an auxiliary equipment, a mechanical balance with two-digit scale was used for weighting the U-tubes before and after the collection of each sample and a chronometer was also used for measuring time of 3 min at the outlet of the gasifier and 5 min at the outlet of filter box.

3. Results and discussion

Gasification of sewage sludge was successfully carried out in five runs. During the experimental works, there was a minor clinker formation on the grate and around the throat of the gasifier. This clinker was easily removed at the end of each run, but this could be reduced introducing any means of agitation.

3.1. Characteristics of sewage sludge

Table 1 lists the average major physical properties, the proximate and ultimate analyses of sewage sludge with standard deviations. The physical properties define the particulate size, absolute density and bulk density. The moisture content, volatile matter, the content of ash and fixed carbon were, however, determined by the proximate analysis, while the chemical composition (includes the carbon, hydrogen, oxygen, nitrogen, sulfur and ash content of the dry sewage sludge on a weight percentage basis) and higher heating value were designated by the ultimate analysis. The ultimate analysis of a fuel never indicates the suitability for gasification, but is the main tool for predicting the composition of the gas and temperature limits of the gasifier. Gross Calorific Value of sewage sludge was measured with Gallenkamp-Auto-bomb calorimeter and also calculated using the IGT method [5].

The moisture content of the fuel greatly effects on both the operation of the gasifier and the quality of the produced wet gas. The moisture content constrains for the fuels are dependent on the gasifier used. The upper limit of moisture for a downdraft reactor is generally considered to be not more than 30% wet basis [4].

In this study, the moisture content of sewage sludge was found almost 11.75%. Hence, it is clear that sewage sludge is a suitable fuel and well within the range for use in a downdraft gasifier. However, with respect to the quality and quantities available, sewage sludge does not seem to be a very promising bio-fuel because of high ash content.

Earp [6] recommended the maximum particle size to be used in a downdraft gasifier as one-eighth of the reactor diameter. However, the particle size of sewage sludge, used in this experiment, was $3.5 \times 1 \times 0.5$ on average, and it is not observed that any problem in the gasifier during the processes of the downdraft gasification because the size of sewage sludge is very close to this recommendation.

Table 1
Physical characteristics, proximate and ultimate analysis of sewage sludge

Physical properties of sewage sludge (average of 4)

Size (cm)	Absolute density (kg/m^3)	Bulk density (kg/m^3)
$3.5 \times 1 \times 0.5$	314.33	207.5

Proximate analysis % wet basis (average of 4)

Volatile matter (%)	Moisture (%)	Fixed carbon (%)	Ash (%)	GCV (MJ/kg)
53.48 ± 1.69	11.75 ± 0.31	11.27 ± 1.17	23.51 ± 0.33	17.14 ± 0.36

Ultimate analysis % dry basis (average of 4)

Carbon (%)	Hydrogen (%)	Oxygen (%)	Nitrogen (%)	Sulfur (%)	Ash (%)
39.48 ± 0.30	6.19 ± 0.12	25.46 ± 0.50	3.93 ± 0.17	1.45 ± 0.34	23.51 ± 0.33

The absolute and bulk densities are very important for process design in terms of handling and storage [5] and high bulk density requires less reactor space for a given refuelling time. However, low bulk fuels sometimes give rise to insufficient flow under gravity resulting in low gas heating value and possibly burning char in the reduction zone [7]. It was observed that, although the bulk density of sewage sludge was 207.5 kg/m^3, there was no char burning in the reduction zone.

The ash content of biomass is typically much less than that of coal ($< 3\%$), however, some forms have a high ash content, such as sewage sludge [5]. Proximate analysis showed that the amount of ash in sewage sludge was quite high (23.51%, wet basis). Although the ash was removed quite frequently and continuously from the gasifier, some clinker formation occurred in the oxidation zone because of the high temperature (> 1100 °C). The clinker occasionally formed on the grate during the gasification process by bridging and blocking the fuel flow in the reduction zone, and this caused to decrease the quality of the produced gas.

3.2. Gas composition and the ratio of H / C

The composition of the produced wet gases and the ratio of H/C are presented in Table 2. The produced wet gases contain both the combustible gases and noncombustible gases.

The *combustible gases*, produced from sewage sludge by downdraft gasification, contain the gases, such as H_2, CO, CH_4, C_2H_2 and C_2H_6, while the noncombustible gases also include N_2 and CO_2. The percentage of the combustible gases altered between approximately 20% and 23% of the total produced wet gas. However, the most of the combustible gases were produced as 21.86–23.05% at the values between 3.69

Table 2
The composition of the produced wet gas and the ratio of H/C

Runs	Unit	R1	R2	R3	R4	R5
Wet feed rate	kg/h	2.86	3.69	3.71	3.81	3.94
Wet gas flow	$N\ m^3/h$	6.22	8.14	8.14	9.18	10.07
H_2	%	8.80	11.15	10.41	10.79	10.31
CH_4	%	1.25	1.85	1.25	2.07	1.86
CO	%	9.28	8.03	10.63	7.02	6.31
C_2H_2	%	0.74	0.62	0.62	0.94	0.83
C_2H_6	%	0.19	0.21	0.14	0.16	0.27
Combustible gases	%	20.26	21.86	23.05	20.98	19.58
GCV of produced gas	$MJ/N\ m^3$	3.52	3.84	3.82	4.01	3.79
O_2	%	0.16	0.09	0.27	0.93	0.84
N_2	%	64.41	63.04	62.32	63.05	63.92
CO_2	%	13.24	12.79	11.11	12.66	13.12
H_2O	%	1.96	2.23	3.24	2.37	2.54
Noncombustible gases	%	79.77	78.15	76.94	79.01	80.42
H_i/C_i	kg H_2/kg C	0.207	0.212	0.212	0.213	0.209
H_o/C_o	kg H_2/kg C	0.139	0.198	0.181	0.177	0.195

and 3.71 kg/h of the feed rate. However, the least of the noncombustible gases were as 76.94–78.15% (N_2 and CO_2) of the volume percentage of the produced wet gas although generally varying between 76% and 81% of the produced wet gas depending on the operating conditions.

The *rates of* H_i/C_i were almost constant around 0.210 kg H_2/kg C with the increase of the amounts of the produced wet gases. However, it was seen that the rates of H_o/C_o changed from 0.139 to 0.198 kg H_2/kg C and the rates of H_o/C_o are particularly low because of the little clinker formation on the grate in the reduction zone of the gasifier. The highest value of H_o/C_o was obtained at which the highest percentage of hydrogen was at 8.14 N m^3/h of the produced wet gas. This means that the combustible gases containing more amounts of the hydrocarbon compounds are more produced at the higher rates of H_o/C_o. It can be, however, said that this affects the rates of H_o/C_o partially now that sewage sludge is not exactly gasified and converted into the combustible gases.

3.3. Contaminants in produced wet gas

Table 3 shows the contaminants in the produced wet gas. The amounts of tar–dust and condensate were determined before and after cleanup. During the experiments, it was observed that large amounts of tar–dust were deposited at the inner parts of the fan blade and outlet of the circulation fan. During cooling of the gasifier, tars from the produced wet gas condensed inside the gasifier and at the outlet of the circulation fan and filter box. Due to the presence of tars in the produced wet gas, some problems were encountered in the measurement of flow rate of the produced wet gas through the gas flow meter. The tar in the produced wet gas, condensing at the inlet manifold of the gas flow meter, proved to be particularly difficult to remove, and this factor limited the accuracy of the data to be collected in the flow meter. Because of these reasons, the produced wet gas should be analysed to bring out the harmful particulars in the composition of the gas, damaging to the gasifier system and the power engine.

The samples of the produced wet gas were first taken from the outlet of the gasifier before the produced wet gas introduced to the water scrubber. In this stage, it was determined that the produced wet gas contained higher amounts of tar–dust and condensate at the increased rates of the volumetric flow of the produced wet gas before cleaning processes. If the produced wet gas containing more than 0.5 g/N m^3 of tar and dust before introducing the engine, it can damage some parts of the engine, and decrease

Table 3
The contaminants in the produced wet gas before and after cleanup

Runs	Unit	R1	R2	R3	R4	R5
Tar and dust before cleanup	g/N m^3	8.38	5.47	5.50	5.60	6.37
Tar and dust after cleanup	g/N m^3	1.96	1.39	1.47	1.55	1.64
Condensate before cleanup	g/N m^3	97.39	163.25	144.10	172.80	142.50
Condensate after cleanup	g/N m^3	28.98	26.82	21.08	29.22	23.47

its performance [2]. Therefore, it was passed through the water scrubber and followed by the filter box. After the gas samples were taken from the outlet of the filter box, it was found that they still contained the lower quantities of tar and condensate. Consequently, it was noticed that the amounts of tar and condensate in the produced wet gas were particularly reduced after cleaning process, and gas cleanup degree was achieved as high as 95% in terms of tar and condensate removal.

3.4. Composition of waste products

Waste products from the gasification of sewage sludge were presented in Figs. 3 and 4 as a function of the feed rate and the air fuel ratio for five runs. Additionally, Table 4 tabulates the main operating parameters along the gasifier side. The rates of char and tar can be assumed as the best indicators of the performance of the gasifier.

As shown in Figs. 3 and 4, the output of the char and the flow rate of water in the produced wet gas increased and, however, the output of tar and ash went through a minimum depending on the increase of the feed rate of sewage sludge. The waste products from the gasification of sewage sludge are char, ash, tar, condensate and water. The output rates of the waste products should be commented for the determination of the optimum operational region of downdraft gasifier. The output of char as 0.59–0.63 kg/h $\pm$ 1.50%, the output of ash as 0.52–0.57 kg/h $\pm$ 1.37%, the output of tar around 0.05 kg/h $\pm$ 1.34%, the output of condensate as 1.28–1.47 kg/h $\pm$ 1.37%, and the output of water as 0.18 kg/h $\pm$ 1.37% were obtained at the values of 3.69 kg/h–3.71 kg/h $\pm$ 1.43% of the feed rate of sewage sludge. Lower outputs of tar and ash showed that the temperature in the gasifier ascended by entering of more fuel and less air, and that the high quality gas was produced at high temperature in the reactor. Thus, it can be

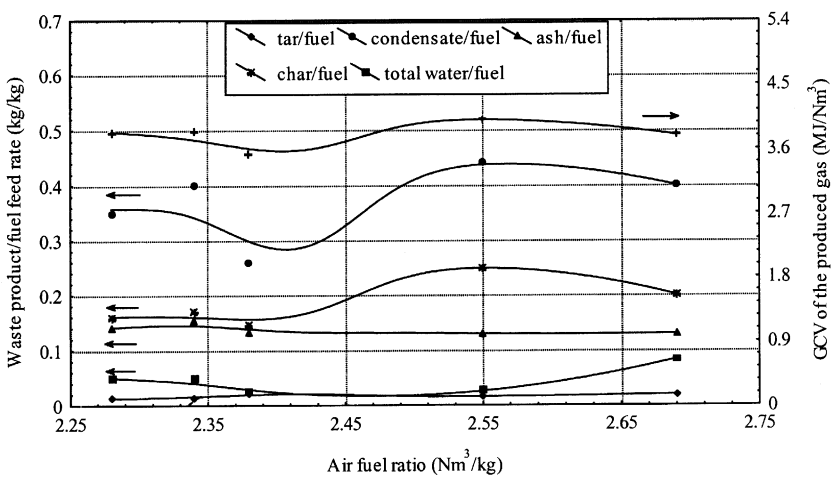

Fig. 3. Variations of waste product/fuel on the left ordinate and GCV of the produced gas on the right ordinate vs. air fuel ratio on the axis.

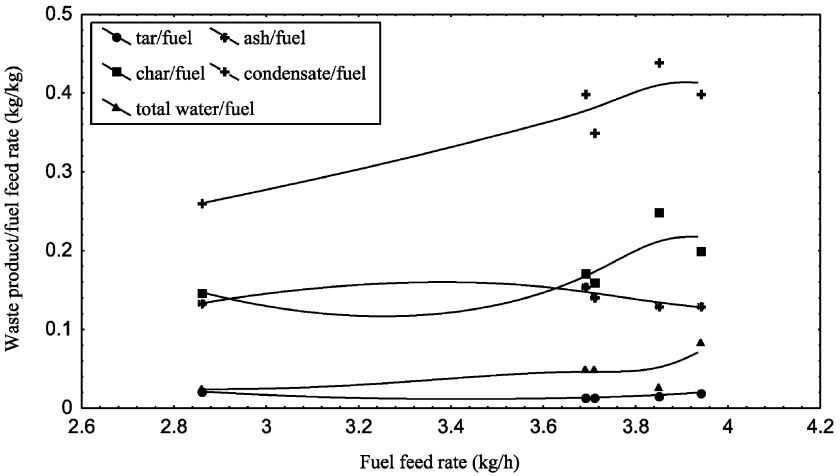

Fig. 4. Variations of side products/fuel feed rate vs. the fuel feed rate.

expressed that the efficiency of the gasifier system was also the best analysed by the ratio of waste product/fuel flow.

3.5. Air fuel ratio

Fig. 5 shows the variation of the capacity of given feed rate, the produced wet gas and the combustible gas on the left ordinate and gross calorific value of the produced gas on the right ordinate vs. air fuel ratio, and gives a good idea for optimum operational region of the gasifier. As shown in Fig. 5, the air fuel ratio was mainly between 2.28 and 2.69 N m^3/kg $\pm$ 1.84% for all runs, and also the flow rates of the produced wet gas increased with an increase of air fuel ratios as expected. The lowest air fuel ratios were estimated as 2.28–2.34 N m^3/kg $\pm$ 1.84% at the values of 3.69–3.71 kg/h $\pm$ 1.43% of the wet feed rate. The maximum gross calorific value of the produced gas was found as

Table 4
The waste products and the operation parameters of the gasifier

Runs	Unit	R1	R2	R3	R4	R5
Ambient temperature	°C	9	12	12	9	11
Throat temperature	°C	1026	1049	1077	1009	1042
Char output	kg/h	0.42	0.63	0.59	0.96	0.79
Ash output	kg/h	0.38	0.57	0.52	0.49	0.50
Tar output	kg/h	0.06	0.05	0.05	0.05	0.08
Condensate output	kg/h	0.74	1.47	1.28	1.70	1.59
Total water output	kg/h	0.07	0.18	0.18	0.10	0.33
Air/fuel ratio	N m^3/kg	2.38	2.34	2.28	2.55	2.69
Specific gasification rate	N m^3/m^2 h	396.06	514.60	497.74	576.59	626.66
Turndown percentage	%	72.58	93.64	94.15	97.70	99.98

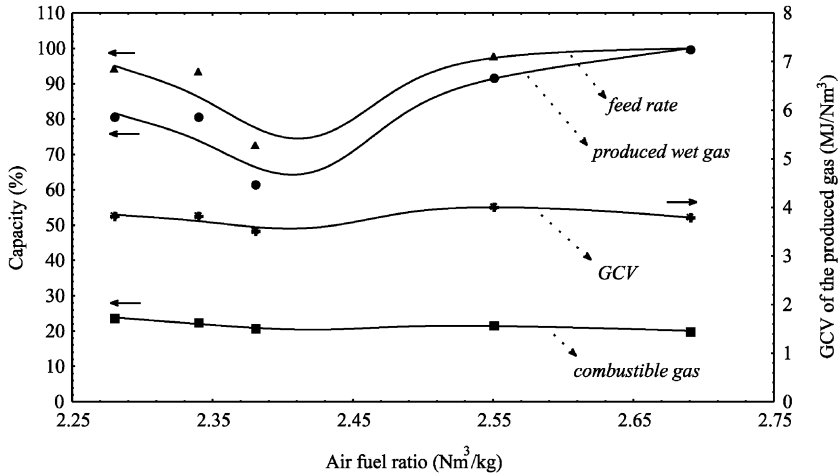

Fig. 5. The variation of the capacity of the produced wet gas and combustible gas on the left ordinate and GCV of the produced gas on the right ordinate as a function of the air fuel ratio.

4.01 MJ/N m^3 at 2.55 N m^3/kg $\pm$ 1.84% of air fuel ratio. On the contrary, the maximum production of combustible gas was carried out at approximately 2.28–2.34 N m^3/kg $\pm$ 1.84% of air fuel ratios and at 80.8% of the capacity of the produced wet gas. The high-quality combustible gases, which was 3.82–3.84 MJ/N m^3 of GCV of the produced gas and 22.35–23.83% of the capacity of the produced wet gas, were produced when this gasifier was operated by the capacity of the feed rate of almost 93.65–94.16% and at the air fuel ratios of 2.28–2.34 N m^3/kg $\pm$1.84%. The amount of air, entering the downdraft gasifier, was less than the others and, thus, the clinker and as a result bridging was believed to be formed in the throat region of the reactor and carried over to the grate at 2.28–2.34 N m^3/kg $\pm$ 1.84% of air fuel ratios because of high temperature of oxidation zone temperature ($>$ 1000 C). However, it was observed that the clinker and bridging formed at the other values of air fuel ratios except for 2.28–2.34 N m^3/kg $\pm$ 1.84% because the temperatures of oxidation zone was high enough to induce slag and the clinker formation. The increase in air fuel ratio could almost result in combustion instead of gasification in the reactor and also combustion from the oxidation zone travels to the pyrolysis zone undesirably caused burnout in the upper zones of the reactor. Therefore, it is suggested that the optimum values of air fuel ratio and the capacity of the wet feed should be employed as the constant operating parameters of the gasifier during the steady-state operation.

Fig. 6 shows the variations of the average zone temperatures vs. the air fuel ratio. As shown in Fig. 6, the temperature of 1077 °C $\pm$ 0.75% of oxidation zone, of 471 °C $\pm$ 0.82% of pyrolysis zone and of 203 °C $\pm$ 1.14% of drying zone were measured at the lowest air fuel ratios. However, the maximum temperatures of the gasifier zones were also determined between approximately 2.28 and 2.34 N m^3/kg $\pm$ 1.84% of the air fuel ratio. Then, this denotes that the downdraft gasifier continuously operates by producing low tar and ash output and high calorific value product gas, and can indicate

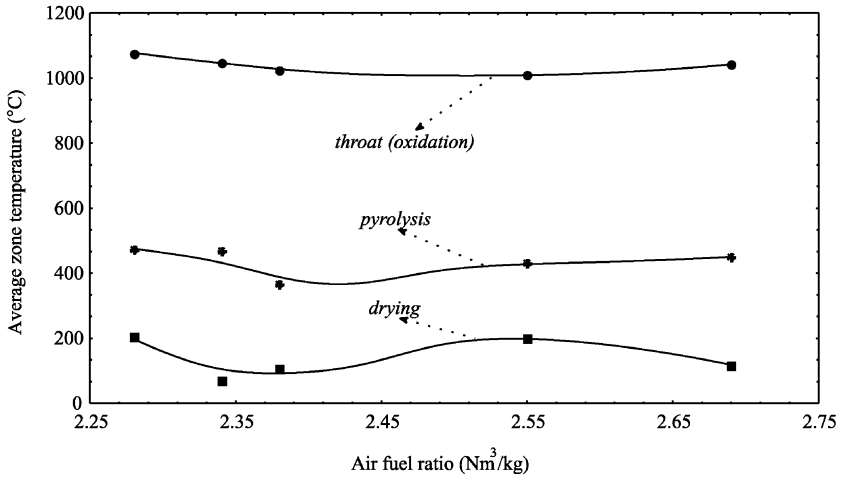

Fig. 6. Variations of average zone temperatures vs. air/fuel.

that optimum operational region of the gasifier was between these values of air fuel ratio. However, it is particularly pointed out that the higher air fuel ratio increased the disturbances in the reaction zones as oxidation zone traveled upwards in the reactor, which, therefore, result oxidation in the pyrolysis zone and also high levels of tar during the gasification process.

Moreover, the pressure drops were determined at the gasifier outlet, across the scrubber and across the filter box. The pressure losses were 0.10–0.80 mm Hg $\pm$ 1.41% at the outlet of the gasifier and 0.20–1.80 mm Hg $\pm$ 1.25% at across the water scrubber and 2.15–4.60 mm Hg $\pm$ 1.16% at across the filter box. It can be said that these are satisfactory to allow an Internal Combustion Engine to run.

3.6. Specific gasification rate

The specific gasification rate is an indicator of the size of the gas producer for a given throughput, and is strongly depending on the type of gas producer and on the fuel characteristics [3,4]. Fig. 7 shows the variation of the produced wet gas and the percentage of combustible gas on the right ordinate and the ratios of H_o/C_o on the left ordinate vs. the specific gasification rates.

As shown in Fig. 7, *specific gasification rates* of downdraft gasifier altered between 396.06 and 626.66 N m^3/m^2 h. The great amounts of combustible gases and the lowest air fuel ratios were obtained at around 514.60 N m^3/m^2 h $\pm$ 1.50%. The amounts of the produced wet gas and the combustible gas went up with the increase of specific gasification rates. However, the ratios of H_o/C_o showed an increase almost linearly to 514.60 N m^3/m^2 h $\pm$ 1.50% of specific gasification rate while decreasing after this value. The ratio of H_o/C_o can also be assumed as a specification of gasification process of sewage sludge as well as the specific gasification rate. The highest ratio of H_o/C_o was found as 0.198 kg H_2/kg C at 514.60 N m^3/m^2 h $\pm$ 1.50% of specific gasification

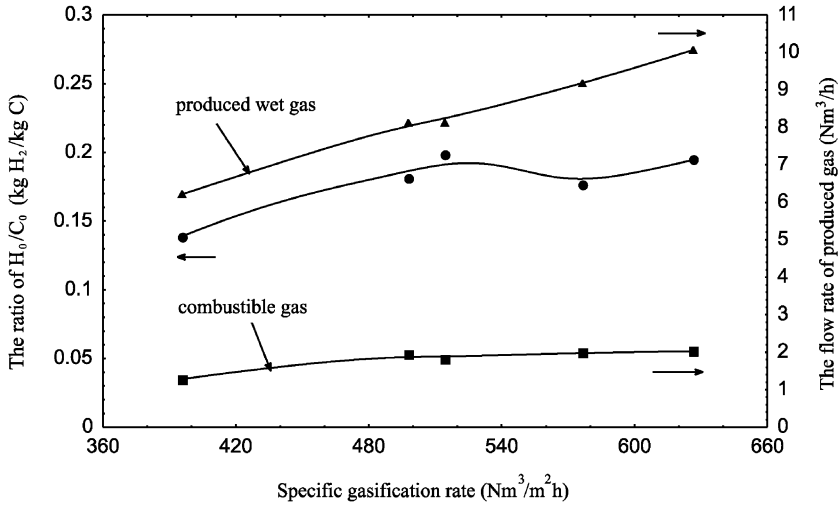

Fig. 7. The variation of the produced wet gas, the percentage of combustible gas on the right ordinate and the ratios of H_o/C_o on the left ordinate as a function of the specific gasification rate.

rate. This means that the great amount of hydrocarbons are almost produced at 0.198 kg H_2/kg C of the ratio of H_o/C_o. Therefore, it can be said that the most productive region for the gasification of sewage sludge would be selected around 514.60 N m^3/m^2 h $\pm$ 1.50% of specific gasification rate. On the other hand, the downdraft gasifier during the gasification of sewage sludge could produce the appropriate and useful experimental results at 497.74–514.60 N m^3/m^2 h $\pm$ 1.50% of the specific gasification rate.

3.7. Turndown ratio

Turndown is defined as the ability of the gasifier to respond to the changes in demand for the produced wet gas with different capacity of sewage sludge, and at the same time, operated with a stable reaction zone [4]. Turndown ratio is often quoted in the gasifier trade leaflets, but most of these are ambiguous. Fig. 8 shows the variations of the flow rate of the capacity of dry fuel (dry sewage sludge) on the right ordinate and the produced wet gas and combustible gas on the left ordinate as a function of turndown ratio.

As shown in Fig. 8, the capacity of dry fuel altered between 1.93 and 2.66 kg/h $\pm$ 1.20%, and the turndown ratio was estimated between 72% and 99.98% $\pm$ 1.92%. It was observed that turndown ratio went up almost linearly with the increase of the capacity of dry fuel as well as the amounts of the produced wet gas and combustible gas. Although the maximum capacity of dry fuel was determined as 2.66 kg/h $\pm$ 1.20%, this value was not enough to say something about optimum capacity of downdraft gasifier. Taking the ratios of H_o/C_o and the amounts of combustible gases into consideration, it can, however, be much more productive to run the gasifier between 93.64% and 94.15% $\pm$ 1.92% of turndown ratio.

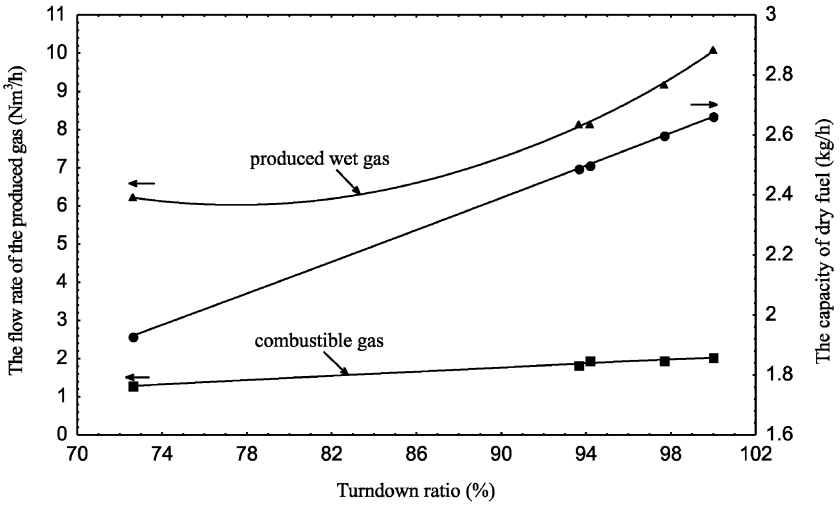

Fig. 8. The variations of the flow rate of the produced wet gas and combustible gas on the left ordinate and the capacity of dry fuel (dry sewage sludge) on the right ordinate as a function of turndown percentage ratio.

3.8. Efficiencies of produced wet gas

Fig. 9 presents the variation of the efficiency of raw gas, hot gas and cold gas on the left ordinate and the ratio of H_o/C_o on the right ordinate as a function of specific gasification rate.

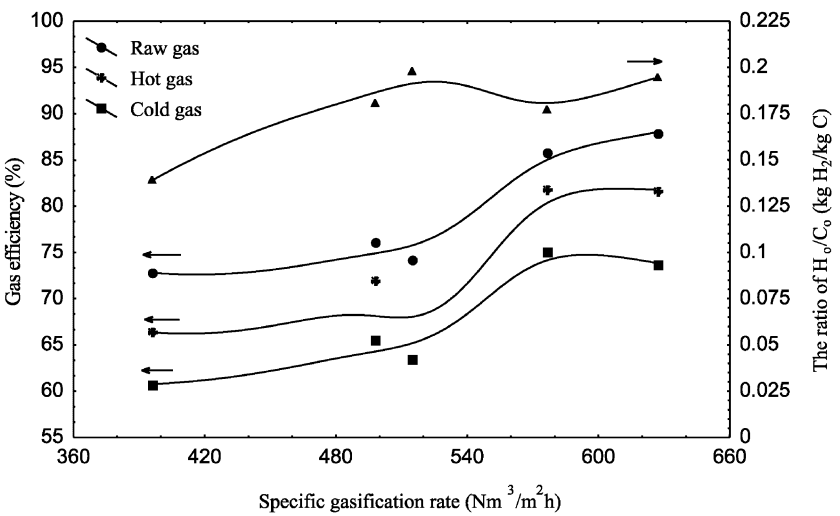

Fig. 9. The variations of gas efficiency and the ratio of H_o/C_o as a function of the specific gasification rate.

As shown in Fig. 9, the ratios of the cold gas efficiency changed between 60% and 75%, while the ratios of hot gas efficiency altered between 63% and 81%, and the ratios of raw gas efficiency varied between 72% and 87%. In order to determine the cold gas efficiency of the produced gas, the ratios of H_o/C_o can be also considered as an indicator. Moreover, the cold gas efficiency of the produced gas should be taken much more into consideration in the usage of the gas in the operation of Internal Combustion Engines during the process of power generation. Therefore, it can be said that the cold gas efficiency, which was obtained after scrubbing, cooling and filtration, was estimated between 63.54% and 65.52% around 514.60 N m^3/m^2 h $\pm$ 1.50% of the specific gasification rate at which the highest ratio of H_o/C_o was estimated.

3.9. Thermal efficiency

Thermal efficiency shows the performance of downdraft gasifier in the production of energy from sewage sludge, and is defined as the ratio of net energy recovery from sewage sludge with downdraft gasification to total energy input into the gasifier for the gasification of sewage sludge [4]. In this part of the article, the variations of thermal efficiency were analysed as a function of air fuel ratio, specific gasification rate and energy balance closure. They are presented in Figs. 10–12, respectively.

As shown in Fig. 10, thermal efficiency changed between 36.40% and 47.70% as a function of air fuel ratio, and decreased to 36.40% at 2.38 N m^3/kg $\pm$ 1.84% of air fuel ratio and then increased to 47.70% at 2.69 N m^3/kg $\pm$ 1.84% of air fuel ratio. On taking the highest ratio of H_o/C_o (0.198 kg H_2/kg C) into consideration, it was noticed that the thermal efficiency went up with the increase of air fuel ratio on condition that net energy recovery increased, and the gasification process took place instead of combustion

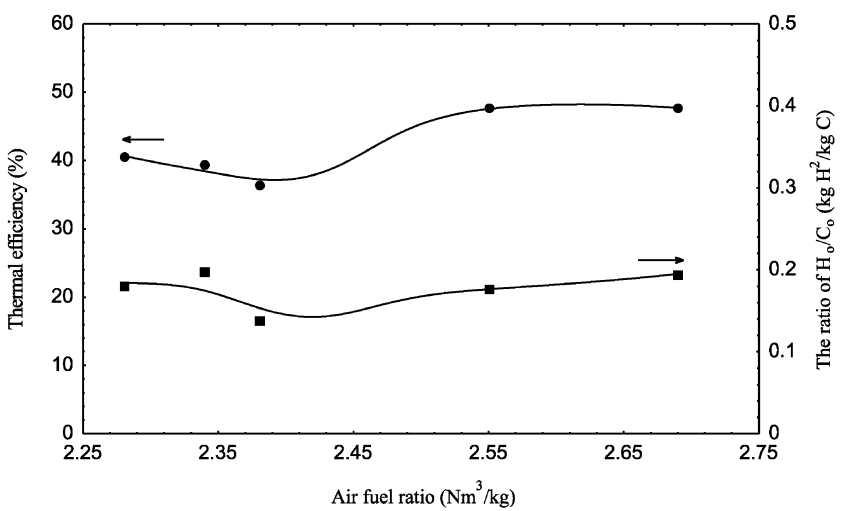

Fig. 10. The variations of thermal efficiency on the left ordinate and the ratio of H_o/C_o on the right ordinate as a function of air fuel ratio on the axis.

in the gasification zone. It can, thus, be assumed that the optimum thermal efficiency could be around 39.4%.

As shown in Fig. 11, the thermal efficiency ascended with the increase of specific gasification rate and also of the amounts of combustible gas. However, the optimum thermal efficiency can be almost assumed between 497.74 and 514.60 N m^3/m^2 $h \pm 1.50\%$ of specific gasification rate because of the low amounts of contaminants in the produced wet gas and waste products, and the production of the clean and much more combustible gas.

As shown in Fig. 12, the thermal efficiency increased linearly to 90% with the rise of energy balance closure. After that value, thermal efficiency was almost constant as 47.7% at 95% of energy balance closure. This means that net energy recovery from the gasification of sewage sludge gasification was as high as 90% of thermal efficiency, and then constant at 47.7% of thermal efficiency. Thus, it can be said that, total energy input effects the thermal efficiency as well as the net energy recovery.

3.10. Gasification results

The general results of sewage sludge gasification were also summarised in Table 5, which includes the rates of total mass input and output, the rates of total energy input and output, an the ratios of mass and energy balance closure. Total mass inputs involve dry sewage sludge, air and total water input, while total mass outputs comprise total outputs of char, ash, tar, condensate, water and dry gas. The *mass balance closure* should be also identified depending on total mass inputs and outputs. The usual method quantifying the discrepancies in the mass balance is the closure, which is defined as the percentage ratio of the total mass output to the total mass input. The majority of the

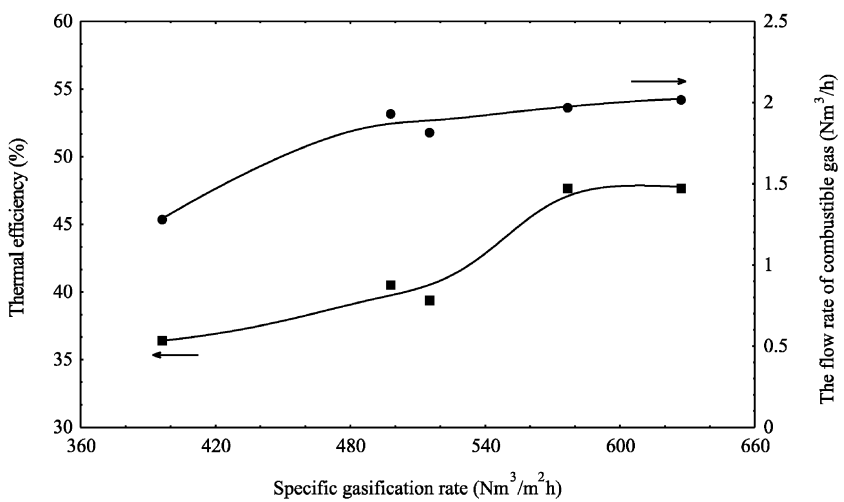

Fig. 11. The variations of thermal efficiency on the left ordinate and the ratio of H_o/C_o on the right ordinate as a function of specific gasification rate on the axis.

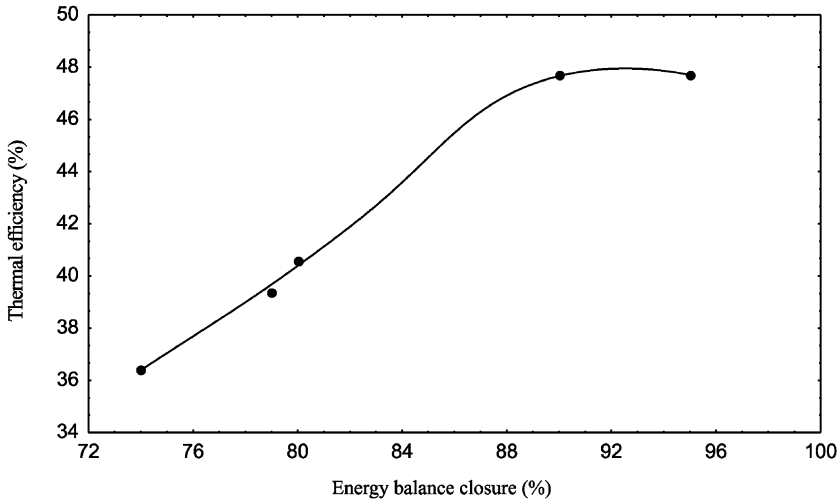

Fig. 12. The variations of thermal efficiency as a function of energy balance closure.

mass balance closures lie in the range 90–100%. It means that total mass input is almost equal to total mass output and the gasification of sewage sludge has been carried out by less error. This is also probably associated with the poor performance of the water scrubber and due to the tar deposition around the circulation fan and pipes. However, if moisture in fuel increases, the mass closures dramatically increase and, hence, the difficulties are also encountered in maintaining the gas quality resulting in poor yields.

Energy balance closure is also calculated as the ratio of total energy output to total energy input. Total energy inputs include the energy in sewage sludge and moisture, the energy in air and moisture in air, while the energy outputs contain the energy in product gas, the energy in char and tar, and the energy in condensate and heat loses. Because the mass balance closure was estimated as 90–100%, and the energy balance closure were calculated as 75–90%, they can be assumed as appropriate ranges for the gasification of sewage sludge by using downdraft gasifier. Therefore, the main source of little difference in the energy balance was considered as the estimation of the heat losses.

Table 5
The balance closure of the sewage sludge gasification

Parameters	Units	R1	R2	R3	R4	R5
Total mass input	kg/h	9.41	12.01	11.86	13.35	14.16
Total mass output	kg/h	8.72	11.64	10.60	13.35	13.85
Mass balance closure	%	92.66	96.92	89.37	100.0	97.81
Total energy input	MJ/h	49.12	63.68	63.34	66.01	67.66
Total energy output	MJ/h	36.71	50.54	50.74	62.96	61.39
Energy balance closure	%	0.74	0.79	0.80	0.95	0.90

4. Uncertainty analysis

All instruments and measurements have certain general characteristics. An understanding of these common qualities is the first step towards accurate measurement. Errors and uncertainties are inherent in both the instrument and the process of making the measurement, and too much reliance should not be placed on any single reading from one affected by the environment. Final accuracy depends on a sound program and on correct methods for taking reading on the proper instruments. When readings are repeated, they tend to produce a band of results rather than a point or a line. Errors and uncertainties in the experiments can arise from instrument selection, instrument condition, instrument calibration, environment, observation and reading, and test planning [8].

In the experiments of sewage sludge gasification, the temperatures, flow rates, pressure drops were measured with appropriate instruments and, however, air fuel ratio, specific gasification rate and turndown ratio were calculated using the data measured before.

4.1. Total uncertainties in temperatures

In order to calculate total uncertainties of each temperature, the average uncertainties arisen from each temperature should be determined. During the gasification process of sewage sludge, the average uncertainties arisen from the measurement of temperatures are systematically classified as follows:

(a1) The average uncertainty arisen from the fabrication of thermocouples $= \pm 0.25\%$

(a2) The average uncertainty arisen from the connecting devices and settling of thermocouples $= \pm 0.25–0.5\%$

(a3) The average uncertainty arisen from the interaction of thermocouples with the system $= \pm 0.01\%$

(a4) The average uncertainty arisen from the measurement of drying zone temperature $= \pm 0.5–1\%$

(a5) The average uncertainty arisen from the measurement of pyrolysis zone temperature $= \pm 0.3–0.6\%$

(a6) The average uncertainty arisen from the measurement of throat zone temperature $= \pm 0.25–0.5\%$

(a7) The average uncertainty arisen from the measurement of gas outlet temperature $= \pm 0.5–0.75\%$

(a8) The average uncertainty arisen from the measurement of scrubber outlet temperature $= \pm 0.25–0.5\%$

(a9) The average uncertainty arisen from the measurement of box filter outlet temperature $= \pm 0.25–0.5\%$

(a10) The average uncertainty arisen from the measurement of air temperature $= \pm 0.5\%$

The uncertainties of (a1), (a2) and (a3) affect the calculation of total uncertainties arisen from temperatures. However, total uncertainties for each temperature can be calculated by using Eq. (1):

$$w_A = \left[(\mathrm{a1})^2 + (\mathrm{a2})^2 + (\mathrm{a3})^2 + (A)^2\right]^{1/2}. \quad (1)$$

In Eq. (1) [8,9], A defines the uncertainties from (a4) to (a9), respectively. Total uncertainties of temperatures were presented in Table 6 by using the temperatures classified above systematically.

4.2. Total uncertainties in pressure drops

In order to calculate total uncertainties of pressure drops, the average uncertainties should be determined. During the gasification process of sewage sludge, the average uncertainties arisen from the measurement of pressure drops are systematically classified as follows:

(b1) The average uncertainty arisen from fabrication and connecting devices of pressure transducers = ± 0.5–1%

(b2) The average uncertainty arisen from the measurement of pressure drop of gasifier outlet = ± 0.5–1%

(b3) The average uncertainty arisen from the measurement of pressure drop of scrubber outlet = ± 0.25–0.75%

(b4) The average uncertainty arisen from the measurement of pressure drop of filter box outlet = ± 0.3–0.6%

Table 6
Total uncertainties

Total uncertainties in each temperature

Total uncertainty	$w_{T_{dz}}$	$w_{T_{pz}}$	$w_{T_{tz}}$	$w_{T_{go}}$	$w_{T_{so}}$	$w_{T_{bfo}}$	w_{T_o}
Unit	%	%	%	%	%	%	%
Comments	± 1.14	± 0.82	± 0.75	± 0.93	± 0.75	± 0.75	± 0.50

Total uncertainties in the pressure drops

Total uncertainty	$w_{P_{go}}$	$w_{P_{so}}$	$w_{P_{bfo}}$
Unit	%	%	%
Comment	± 1.41	± 1.25	± 1.16

Total uncertainties in the waste products

Total Uncertainty	$w_{F_{ws}}$	$w_{F_{wg}}$	$w_{F_{co}}$	$w_{F_{ao}}$	$w_{F_{to}}$	$w_{F_{co}}$	$w_{F_{wo}}$
Unit	%	%	%	%	%	%	%
Comment	± 1.436	± 1.040	± 1.500	± 1.374	± 1.346	± 1.346	± 1.224

Total uncertainties in the contaminants of the produced wet gas

Total Uncertainty	$w_{F_{tdb}}$	$w_{F_{tda}}$	$w_{F_{cb}}$	$w_{F_{ca}}$
Unit	%	%	%	%
Comment	± 1.346	± 1.346	± 1.224	± 1.268

Table 7
Total uncertainties in the indicators of downdraft gasifier

Total uncertainty of indicators	$\frac{w_{R_{af}}}{R_{af}}$	$\frac{w_{R_{sg}}}{R_{sg}}$	$\frac{w_{R_{td}}}{R_{td}}$
Unit	%	%	%
Comment	±1.843	±1.500	±1.920

The uncertainties of (b2), (b3) and (b4) were affected by the uncertainty of (b1) during the pressure drops measurement. However, total uncertainties for each pressure drops can be calculated by using Eq. (2):

$$w_B = \left[(\mathrm{b1})^2 + (B)^2\right]^{1/2}. \quad (2)$$

In Eq. (2) [8,9], B defines the uncertainties from (b2) to (b4), respectively. Total uncertainties of temperatures were presented in Table 6 by using the temperatures classified above systematically.

4.3. Total uncertainties in flow rates of wet gas and waste products

The average uncertainties arisen from the measurement of flow rates were systematically presented below:

(c1) The average uncertainty arisen from time recorder = ±0.5–1%
(c2) The average uncertainty arisen from the vibration of balance instrument = ±0.01%
(c3) The average uncertainty arisen from weighing of sewage sludge = ±0.5–1%
(c4) The average uncertainty arisen from the determination of wet feed rate of sewage sludge = ±0.1–0.25%

Total uncertainty in the determination of wet feed rate ($w_{F_{ws}}$) was affected by the uncertainties of (c1), (c2) and (c3), and calculated by Eq. (3), and presented in Table 7. In Eq. (3), C_1 defines the uncertainties from (c1) to (c3), respectively:

$$w_{C_1} = \left[(\mathrm{c1})^2 + (\mathrm{c2})^2 + (\mathrm{c3})^2 + (C_1)^2\right]^{1/2}. \quad (3)$$

(c5) The average uncertainty arisen from the gas flow meter = ±0.25%
(c6) The average uncertainty arisen from connecting devices of gas flow meter = ±0.1%
(c7) The average uncertainty arisen from losses of gas flow meter = ±0.1%
(c8) The average uncertainty arisen from reading wet gas flow = ±0.5–1%

Total uncertainty in determination of wet gas flow ($w_{F_{wg}}$) was affected by the uncertainties of (c5), (c6) and (c7), and calculated by Eq. (4) [8,9], and presented in Table 7.

$$w_{F_{wg}} = \left[(\mathrm{c5})^2 + (\mathrm{c6})^2 + (\mathrm{c7})^2 + (\mathrm{c8})^2\right]^{1/2}. \quad (4)$$

(c9) The average uncertainty arisen from the capacity of sensitive electronic balance = ±0.25–0.5%
(c10) The average uncertainty arisen from the vibration of sensitive balance during the measurement = ±0.5–1%
(c11) The average uncertainty arisen from the determination of char output = ±0.5–1%
(c12) The average uncertainty arisen from the determination of ash output = ±0.5–0.8%
(c13) The average uncertainty arisen from the determination of tar output = ±0.5–0.75%
(c14) The average uncertainty arisen from the determination of the output of condensate = ±0.4–0.8%
(c15) The average uncertainty arisen from the determination of the output of water = ±0.5–0.8%
(c16) The average uncertainty arisen from the determination of the output tar and dust in the produced wet gas before cleanup = ±0.5–0.75%
(c17) The average uncertainty arisen from the determination of condensate before cleanup (F_{cd}) = ±0.5–0.75%
(c18) The average uncertainty arisen from the determination of tar and dust output after cleanup (F_{cd}) = ±0.25–0.5%
(c19) The average uncertainty arisen from the determination of condensate after cleanup (F_{cd}) = ±0.30–0.60%

Total uncertainties in determination of the output of char, ash, tar, condensate and water, and of tar–dust and condensate in the produced wet gas before and after cleanup were affected by the uncertainties of (c9) and (c10), and were presented in Table 7. In Eq. (5) [8,9], C_3 defines the uncertainties from (c11) to (c19), respectively:

$$w_{C_2} = \left[(\mathrm{c9})^2 + (\mathrm{c10})^2 + (C_2)^2\right]^{1/2}. \quad (5)$$

4.4. The uncertainty in air fuel ratio

In order to estimate total uncertainty in the calculation of air fuel ratio, the average uncertainties arisen from air fuel ratio can be written as below:

(d1) The average uncertainty arisen from the calculation of volumetric flow of dry air input ($w_{F_{vda}}$) = ±0.75–1.4%
(d2) The average uncertainty arisen from the calculation of total mass flow of dry ash free sewage sludge ($w_{F_{dss}}$) = ±0.5–1.2%

Air fuel ratio is calculated by the following equation:

$$R_{af} = \frac{F_{vda}}{F_{dss}}. \quad (6a)$$

In Eq. (6a), the air fuel ratio is a function of two variables, each subject to an uncertainty:

$$R_{af} = f(F_{vda}, F_{dss}). \tag{6b}$$

Eqs.(6c and 6d) were derived from Eq. (6a):

$$\frac{\partial R_{af}}{\partial F_{vda}} = \frac{1}{F_{dss}}, \tag{6c}$$

$$\frac{\partial R_{af}}{\partial F_{dss}} = -\frac{F_{vda}}{F_{dss}^2}, \tag{6d}$$

$$w_{R_{af}} = \left[\left(\frac{\partial R_{af}}{\partial F_{vda}} w_{F_{vda}} \right)^2 + \left(-\frac{\partial R_{af}}{\partial F_{dss}} w_{F_{dss}} \right)^2 \right]^{1/2}. \tag{6e}$$

By substituting Eqs. (6c and 6d) into Eq. (6e):

$$w_{R_{af}} = \left[\left(\left(\frac{1}{F_{dss}} \right)^2 w_{F_{vda}}^2 \right) + \left(\left(-\frac{F_{vda}}{F_{dss}^2} \right)^2 w_{F_{dss}}^2 \right) \right]^{1/2}. \tag{6f}$$

By substituting Eq. (6a) into Eq. (6f), the total uncertainty equation for air fuel ratio was derived as Eq. (6g). Total uncertainty in the air fuel ratio may now be calculated by assembling these derivatives in accordance with the following equation. The value of total uncertainty in air fuel ratio was presented in Table 7:

$$\frac{w_{R_{af}}}{R_{af}} = \left[\left(\frac{w_{F_{vda}}}{F_{vda}} \right)^2 + \left(-\frac{w_{F_{dss}}}{F_{dss}} \right)^2 \right]^{1/2}. \tag{6g}$$

4.5. The uncertainty in specific gasification rate

In order to estimate total uncertainty in the calculation of specific gasification rate, the average uncertainties arisen from specific gasification rate can be written as below:

(e1) The average uncertainty arisen from the calculation of total volumetric gas flow ($w_{F_{dvg}}$) = ±1–1.5%. This uncertainty is affected by the total uncertainty of wet gas.

(e2) The average uncertainty arisen from the calculation of cross-sectional area across throat (w_{A_t}) = ±0.0001%. This uncertainty is affected by the average uncertainty from the measurement of throat diameter = ±0.35%.

Specific gasification rate is calculated by the following equation:

$$R_{sg} = \frac{F_{dvg}}{A_t}. \tag{7a}$$

In Eq. (7a), the specific gasification rate is a function of two variables, each subject to an uncertainty:

$$R_{sg} = f(F_{dvg}, A_t). \tag{7b}$$

By applying the same derivation and calculation process in air fuel ratio, total uncertainty in the specific gasification rate may now be calculated by assembling appropriate derivatives in accordance with the following equation. The value of total uncertainty in air fuel ratio was presented in Table 7:

$$\frac{w_{R_{sg}}}{R_{sg}} = \left[\left(\frac{w_{F_{dvg}}}{F_{dvg}} \right)^2 + \left(- \frac{w_{A_t}}{A_t} \right)^2 \right]^{1/2}. \tag{7c}$$

4.6. The uncertainty in turndown ratio

In order to estimate total uncertainty in the calculation of turndown ratio, the average uncertainties arisen from turndown ratio can be written as below:

(f1) The average uncertainty arisen from the calculation of the capacity of dry sewage sludge $(w_{C_{dss}}) = \pm 0.5–1.2\%$.
(f2) The average uncertainty arisen from the calculation of the maximum capacity of sewage sludge $(w_{C_{mdss}}) = \pm 0.5–1.2\%$.

Turndown ratio is calculated by the following equation:

$$R_{td} = \frac{C_{dss}}{C_{mdss}}. \tag{8a}$$

In Eq. (8a), the turndown ratio is a function of two variables, each subject to an uncertainty.

$$R_{td} = f(C_{dss}, C_{mdss}). \tag{8b}$$

By applying the same derivation and calculation process in air fuel ratio, total uncertainty in turndown ratio may now be calculated by assembling appropriate derivatives in accordance with the following equation. The value of total uncertainty in air fuel ratio was presented in Table 7:

$$\frac{w_{R_{td}}}{R_{td}} = \left[\left(\frac{w_{C_{dss}}}{C_{dss}} \right)^2 + \left(- \frac{w_{C_{mdss}}}{C_{mdss}} \right)^2 \right]^{1/2}. \tag{8c}$$

5. Conclusion

Gasification trials were successfully carried out in a 5 kWe-throated downdraft gasifier because some fuel properties of sewage sludge were appropriate for the process of gasification.

The following conclusions are given.

• During the experiments, there was a minor clinker formation problem on the grate of the gasifier at the higher feed rates, and this arisen from the nonuniform temperature

distribution in the oxidation zone. However, it is suggested that minor agitation of the grate or better grate design will overcome this problem.

- The combustible gases were produced in spite of the clinker formation on the grate. The combustible gases, produced from sewage sludge, contained as volume by volume percentages: 8.89–11.17% of H_2, 1.26–2.09% of CH_4, 6.28–10.77% of CO, 0.62–0.95% of C_2H_2 and 0.15–0.27% of C_2H_6.
- The quality product gas $(4\ MJ/m^3)$ from sewage sludge would still allow an Internal Combustion Engine to operate because of less pressure drops.
- The highest value of H_o/C_o was found as 0.198 kg H_2/kg C at the value of which the percentage of hydrogen was at 8.14 N $m^3/h \pm 1.04\%$ of the produced wet gas, and at 514.60 N m^3/m^2 h $\pm$ 1.50% of specific gasification rate. The clinker formation in the oxidation zone of the gasifier ceased the output ratio of H_o/C_o. At the highest value of H_o/C_o, the great amounts of the combustible gases containing more amounts of the hydrocarbon compounds were almost produced.
- Due to presence of contaminants, in particular, tar and moisture carry over in the producer gas, the gas flow meter was difficult to read. The amounts of tar and condensate in the produced wet gas were particularly reduced after cleaning process, and gas cleanup degree was achieved as high as 95% in terms of tar and condensate removal using the water scrubber and filter box, respectively.
- The most productive region of the gasification of sewage sludge could be selected around 514.60 N m^3/m^2 h $\pm$ 1.50% of specific gasification rate.
- The optimum efficiency of cold gas was estimated between 63.54% and 65.52% around 514.60 N m^3/m^2 h $\pm$ 1.50% of specific gasification rate at which the highest ratio of H_o/C_o was estimated as 0.198 kg H_2/kg C.
- The thermal efficiency ascended with the increase of specific gasification rate and of the amounts of the combustible gases. On taking the highest ratio of H_o/C_o into consideration, thermal efficiency went up with the increase of air fuel ratio on condition that net energy recovery increased and the gasification process took place instead of combustion because of more air entering the gasifier. The optimum thermal efficiency would be almost assumed as 39.4% between 497.74 and 514.60 N m^3/m^2 h $\pm$ 1.50% of specific gasification rate because of low amount of waste products.
- Total energy input effected the thermal energy as well as the net energy recovery.
- The flow rates of dry gas and char with feed flow rate increased, while tar flow was increasingly constant. However, ash output decreased after wet sewage sludge feed rate of 3.50 kg/h. Beyond this increases in char and tar coupled with decreases in ash indicated a fall off in performance. The ash should be removed quite frequently to provide continuously operation of the gasifier. Additionally, the optimum operational region for this size of the gasifier was also determined and assumed according to feed rate, the maximum flow of combustible gas, air fuel ratio, specific gasification rate, turndown ratio, the ratio of H_o/C_o, the optimum outputs of char, ash, tar and condensate, the optimum rate of GCV of the combustible gases and optimum throat temperature:

1. Optimum wet feed rates are 3.69–3.71 kg/h $\pm$ 1.43%.
2. Maximum flows of combustible gas are 1.77–1.87 N m^3/h.

3. Optimum air fuel ratios are 2.28–2.34 N $m^3/kg \pm 1.84\%$.
4. Optimum specific gasification rates are 497.74–514.60 N m^3/m^2 h $\pm 1.50\%$.
5. Optimum turndown ratios are 93.64–94.15% $\pm 1.92\%$.
6. The ratios of H_o/C_o is around 0.198 kg H_2/kg C.
7. Optimum char output is around 0.59 kg/h $\pm 1.50\%$.
8. Optimum ash output is around 0.52 kg/h $\pm 1.37\%$.
9. Optimum tar output rate is around 0.05 kg/h $\pm 1.34\%$.
10. Optimum condensate output is 1.28–1.47 kg/h $\pm 1.50\%$.
11. Maximum GCV is 3.82 MJ/N m^3.
12. Optimum throat temperature is measured around 1077 °C $\pm 0.75\%$.

Consequently, the gasifier should be operated at these operational regions to prevent the clinker formation and as a result bridging in the throat zone, and to produce maximum energy output from sewage sludge using the small-scale gasifier–CHP system. The small-scale gasifiers can make an important contribution to the economy of such rural areas where sewage sludge is abundantly produced and some design/operating data was provided for suitable gasifiers. Therefore, the investments in gasification processes should be also encouraged for, especially England and Turkey, European Nations' Future by governments and other authoritative bodies who, for strategic reasons, wish to have a clean alternative to fossil fuels.

Acknowledgements

Authors wish to thank Mr. Mike J. Ling, Managing Director of Waste to Energy for the financial support through out the research project.

References

[1] J.E. Hall, Recent developments in sludge disposal and use, Chemistry and Industry 6 (1993) 188–191.
[2] A. Midilli, M. Dogru, C.R. Howarth, M.J. Ling, T. Ayhan, Combustible gas production from sewage sludge with a downdraft gasifier, Energy Conversion and Management 42 (2001) 157–172.
[3] T.B. Reed, A. Das, Hand Book on Biomass Downdraft Gasifier Engine Systems 1988, USA, ISBN: 1-890607-00-2.
[4] M. Dogru, Fixed Bed Gasification of Biomass, PhD thesis, University of Newcastle, UK, 2000.
[5] A.V. Bridgewater, J.M. Double, D.M. Earp, Technical and Market Assessment of Biomass Gasification in the United Kingdom, Report submitted to Energy Technology Support Unit, UKAEA, Harwell, UK, 1986.
[6] D.M. Earp, The Gasification of Biomass in a Downdraft Reactor, PhD Thesis, Chemical Engineering Department, Aston University, UK, 1988.
[7] D.B.G. Boocock, S.M. Konar, A. Makay, P.T.C. Cheung, J. Liu, Fuels and chemicals from sewage sludge: 2. The production of alkanes and alkenes by the pyrolysis of triglycerides over activated alumina, Fuel 71 (11) (1992) 1291–1297.
[8] J.P. Holman, Experimental Methods for Engineers, 4th edn., McGraw-Hill, New York, USA, 1984.
[9] H. Schenck, Theories of Engineering Experimentation, 2nd edn., McGraw-Hill, New York, USA, 1968.

ANNEX B: Computer simulation of a downdraft wood gasifier for tea drying.

T.H. Jayah, L. Aye, R.J. Fuller, D.F. Stewart

Available online at www.sciencedirect.com
SCIENCE DIRECT®
PERGAMON
Biomass and Bioenergy 25 (2003) 459–469
BIOMASS & BIOENERGY
www.elsevier.com/locate/biombioe

Computer simulation of a downdraft wood gasifier for tea drying

T.H. Jayah, Lu Aye*, R.J. Fuller, D.F. Stewart

International Technologies Centre (IDTC), Department of Civil & Environmental Engineering, The University of Melbourne, Parkville, Victoria 3010, Australia

Received 20 June 2002; received in revised form 3 February 2003; accepted 4 February 2003

Abstract

A gasifier has been fabricated in Sri Lanka for the tea industry, but there is a lack of knowledge of the effect of certain key operating parameters and design features on its performance. Experimental testing of the design under various conditions has produced data that has then been used to calibrate a computer program, developed to investigate the impact of those parameters and features on conversion efficiency. The program consists of two sub-models of the pyrolysis and gasification zones, respectively. The pyrolysis sub-model has been used to determine the maximum temperature and the composition of the gas entering the gasification zone. The gasification zone sub-model has been calibrated using data gathered from the experiments. It was found that a wood chip size of 3–5 cm with a moisture content below 15% (d.b.) should be used in this gasifier. Feed material with a fixed carbon content of higher than 30% and heat losses of more than 15% should be avoided. For the above parameters, the gasification zone should be 33 cm long to achieve an acceptable conversion efficiency.

Keywords: Downdraft gasifier; Tea drying; Simulation; Conversion efficiency

1. Introduction

A previous feasibility study conducted by Jayah et al. [1] indicates that wood gasifiers appear to be a viable option to produce the hot air for drying tea in Sri Lanka. A subsequent study [2] compared the performance of a locally produced downdraft gasifier with an imported unit and found that the units had a similar conversion efficiency.[1] The study also showed that the life cycle cost of energy from the gasifier would be 8% lower than the cost of energy from the current wood fired air heating system. At the same time, savings in wood consumption of 12% could be expected. Furthermore, the study concluded that adequate expertise and support for the use of gasifier technology

* Corresponding author. Tel.: +61-3-8344-6879; fax: +61-3-8344-6868.
E-mail addresses: lua@unimelb.edu.au, 1.aye@devtech.unimelb.edu.au (L. Aye).

[1] In this paper, the conversion efficiency is based only on the heating value or chemical content of the cooled output gas and does not include the sensible heat the hot gas contains when produced. Hence the conversion efficiency figures reported in this paper are approximately 30% lower than those reported in [2].

0961-9534/03/$ - see front matter
doi:10.1016/S0961-9534(03)00037-0

by the tea industry was also available in Sri Lanka because of its success in their crematoria industry.

However, there is still a lack of knowledge of the optimum range of operating parameters and the influence of some design features of the locally produced downdraft gasifier on conversion efficiency. This paper therefore describes the selection and development of a model used to study the downdraft gasifier designed by the National Engineering Research and Development (NERD) Centre in Sri Lanka. Data from a series of experiments was used to calibrate this model, which has then been used to investigate the effect of chip size, moisture content, inlet air temperature, heat loss and throat angle on conversion efficiency. Based on these simulations, the optimum range of these operating and design parameters, and the optimum gasification zone length for the NERD downdraft gasifier are selected.

2. Model selection

Jayah et al. [3] conducted a survey to identify the possible models that could be used to investigate the performance of the NERD downdraft gasifier. It was found that the model developed by Chen [4] could be used, but with some modifications. The objectives of Chen's model were to estimate the length of the gasification zone, reactor diameter and to investigate the dependence of reactor performance on operating parameters such as the feedstock moisture content, chip size, reactor insulation, input air temperature and gasifier load. Chen's model consists of three parts. The first part determines the amount of oxygen needed for a fixed input of fuel at a specific operating condition. The fuel-to-air ratio estimated from this first part is then used as an input to the second part of the model, where the drying, pyrolysis and combustion zones are all lumped together and considered as a single zone. The outputs from this "lumped" zone are the product concentrations and the temperatures of the gaseous and solid phases leaving the zone. These calculated concentrations and temperatures are then used as inputs to the third part of the model. Here the temperature profile along the axis of the gasification zone, gas composition, conversion efficiency and the length of the gasification zone at any given time interval are predicted.

The main weakness of Chen's model is the over-prediction of the gas exit temperature from the "lumped" zone due to an unrealistically low estimate of heat loss and the omission of CO and H_2 in the pyrolysis gas. Therefore modifications were required to overcome these deficiencies and also to suit a reactor with a variable rather than a constant gasification zone diameter.

3. Model development

In order to overcome the over-prediction of the pyrolysis zone exit temperature, the flaming pyrolysis model developed by Milligan [5] has been used in place of the algorithms used by Chen. The aim of Milligan's flaming pyrolysis zone model is to calculate the composition of the product gas entering the gasification zone in terms of CO, H_2, CO_2, H_2O, CH_4 and N_2. It has been found that the predictions of Milligan's flaming pyrolysis model are more realistic than those made using Chen's "lumped" zone concept [5]. The constant reactor diameter, assumed in the final section of Chen's model, was modified with a variable diameter to suit the throat configuration of the NERD gasifier. As a result, the model used in this study consists of two sub-models, namely of the flaming pyrolysis and gasification zones.

The flaming pyrolysis zone sub-model is used to determine the maximum temperature and the product concentration of gas leaving that zone. The concepts of equilibrium in chemical reactions with mass and energy balance principles are used in the model development. The calculated concentrations and temperatures predicted by the flaming pyrolysis zone sub-model are then used as inputs to the gasification zone sub-model. The gasification zone sub-model assumes that a single char particle moves vertically downwards along the vertical axis of the gasifier. This sub-model includes a description of the physical and chemical processes, flow equations, transport phenomena and conservation principles. A Fortran computer program has been written [6] to calculate the characteristic profiles of temperature, gas concentration and conversion efficiency along the reactor axis. While the focus of this project was to investigate the effect of various parameters on efficiency, the model

could be used to determine the variation of $CO:H_2$ ratio with fuel moisture content, but only at a fixed pressure.

4. The experimental system

The experimental test rig used to collect data to calibrate the gasification zone sub-model consisted of the gasifier, blower, airflow meter, data logger, computer, orifice plate, manometer, cooling system, gas sample collector and thermocouples. Figs. 1 and 2 show the experimental system both schematically and pictorially, while Fig. 3 gives the main dimensions of the gasifier.

The 80 kW_{th} test gasifier has an inner reactor diameter of 0.92 m and is 1.15 m long. The inner and outer walls of the drum are made from 22 gauge mild steel and 1.4 mm thick galvanized iron respectively and there is a small air gap between the walls. Air is supplied to the combustion zone through 12 air nozzles, 6-mm in diameter, located 100-mm above the throat. The 100-mm diameter throat is lined with high alumina castable and is surrounded by firebricks to withstand the high temperatures in the combustion zone. No insulating materials have been used in this gasifier design. The 220-mm long gasification zone diverges at angle of 61° from the horizontal. Below this zone there is a grate to catch any unreacted char and an ash chamber lies below the grate. A 50-mm diameter galvanized steel pipe delivers the gas from the system to the load.

5. Experimental procedure

The main fuel wood used in the tea industry in Sri Lanka is rubber wood. It accounts for 70% of the total fuel wood consumption by the industry [7] and thus rubber wood has been selected as the feed material for this study. Accordingly, rubber wood logs with initial moisture content of 54–100% (d.b.) were initially sun-dried for three weeks. The partially dried wood was then cut into variously sized chips (3.3–5.5 cm) and then sun-dried again for another week until the desired moisture level of 11–18% (d.b.) was reached. The moisture content of rubber wood was determined by the percent weight loss of a 10 g sample at 105°C constant temperature for 1 h. Three samples were tested for each run and the average value was taken.

The process of gasification is governed by the characteristics of the feed materials used and so an understanding of the properties of feed materials is necessary in order to evaluate their utility as feed stocks for the gasification process [4]. The higher

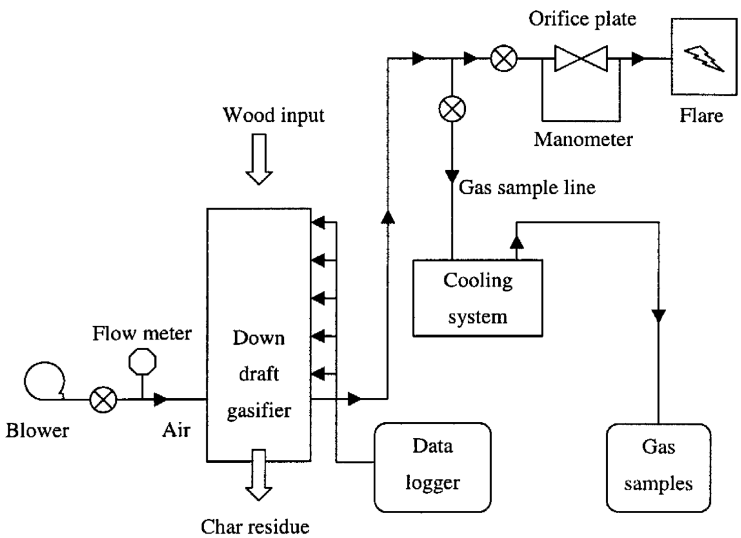

Fig. 1. Schematic diagram of the experimental system.

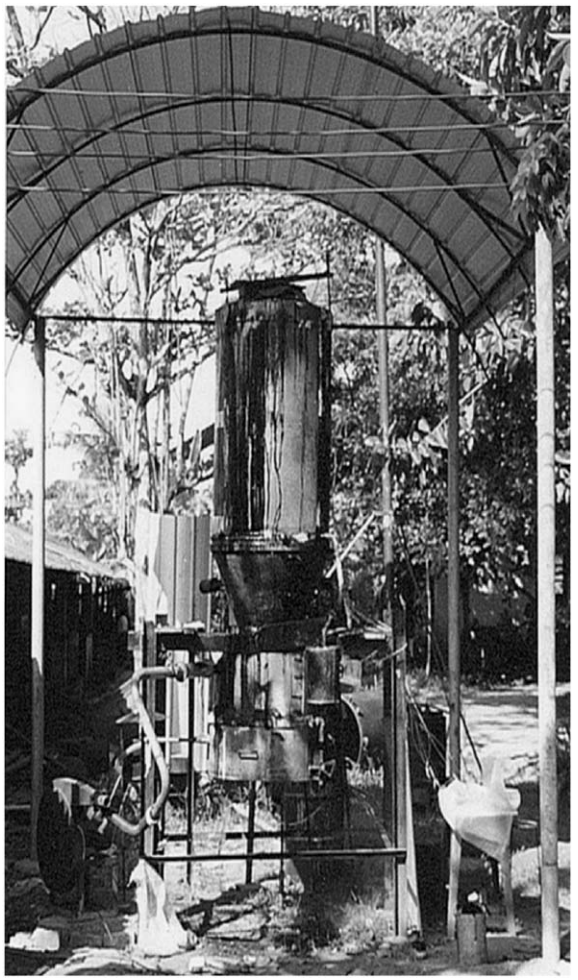

Fig. 2. The test gasifier.

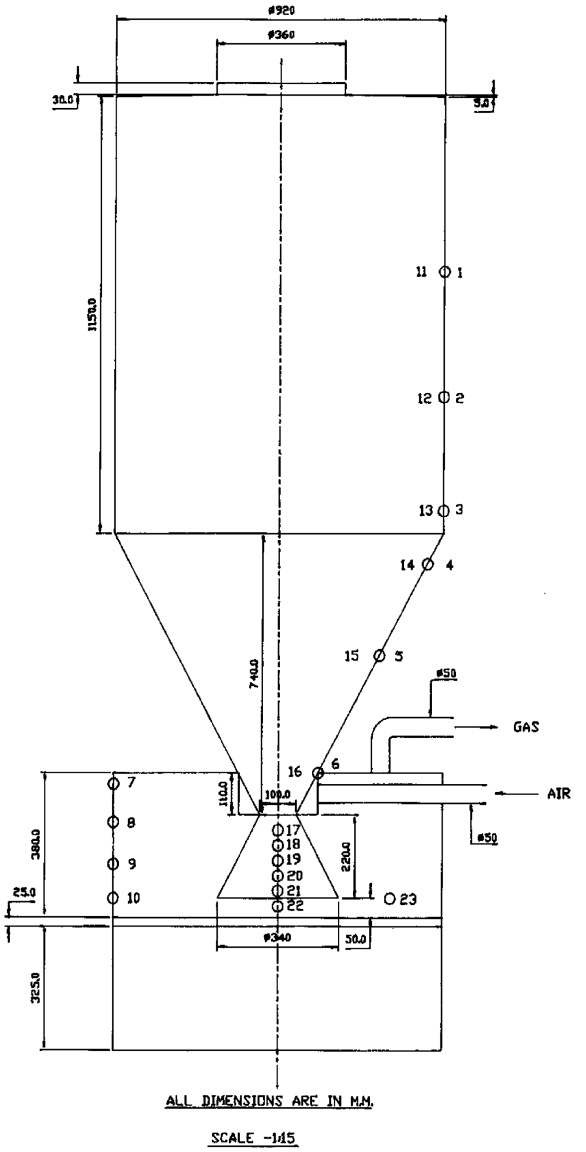

Fig. 3. Schematic diagram of the test gasifier.

heating value, proximate and ultimate analyses of the rubber wood were therefore all determined. This work was carried out by a commercial company.

Prior to each operation of the gasifier, the weight of wood chips to be used was recorded. The blower was then switched on and the airflow was adjusted to the desired level. The chips were ignited through a port in the throat of the gasifier. Once gas production began, measurements of the key variables were made. Airflow was measured on the exit side of the blower by the flow meter and pressure measurements were made either side of the orifice plate using the manometer (Fig. 1). Axial temperatures in the gasification zone and the outer surface of the gasifier were measured using K- and T-type thermocouples. Ambient conditions were measured using a dry bulb-wet bulb thermometer and the outlet gas temperature was measured using a digital thermometer.

To ensure that there was no "bridging" i.e. fuel lodging in the throat and possibly leading to a shortage of char in the gasification zone, the gasifier was "shaken" once during the experimental and trial runs.

The gas burned steadily with a blue-red colour flame, and was considered to indicate reliable operation. A sample of product gas was collected during each operation of the gasifier. A commercial company using gas liquid chromatography analyzed the samples. A molecular sieve column was used to analyze H_2, O_2, N_2, CO and CH_4while a Carboxine 1000 column with temperature program 50–225°C at 20°C min^{-1} was used to determine CO_2.

The experiments were conducted for three chip sizes and for four air–fuel ratios.

6. Experimental results

The proximate and ultimate analyses of rubber wood used in the experiments are given in Tables 1 and 2. The proximate analysis agrees well with the data reported by Hoi et al. [8]. The measured higher heating value of the rubber wood used was 19.6 MJ kg^{-1}, which is 6% higher than the figure reported by the same authors. The bulk density of rubber wood, calculated by dividing the weight of air dried chip samples by the volume occupied, was found to be 314–330 kg m^{-3}. The range of moisture content of the samples varied between 12.5% and 18.5% (d.b.). Gas composition data is available for nine of the experimental runs of the gasifier and varies with moisture content, chip size and air–fuel ratio.Table 3 shows the results of the analysis of the gas sampled during these runs. A mass balance on the gasifier was also carried out (Table 4). In this analysis, tar and water vapour in the product gas and ash production were not measured directly and are included in "unaccounted material", which represent 7–9% of the output material. Fig. 4 shows typical temperatures in the gasifier, measured by a selection of the thermocouples (Fig. 3) during one trial. The temperature profile clearly shows that in a gasifier the area of interest, in terms of conversion efficiency and heat loss, is in the last 40 cm of the unit.

Table 1
Proximate analysis of rubber wood

Parameter	Proximate analysis (% d.b.)
Volatile matter	80.1
Fixed carbon	19.2
Ash content	0.7

Table 2
Ultimate analysis of rubber wood

Parameter	Ultimate analysis (%)
C	50.6
H	6.5
N	0.2
Ash content	0.7
$O = \{100 - (C + H + N + Ash)\}$	42.0

7. Model calibration and use

The purpose of the modeling is to be able to study the effects of various operating and design parameters on the conversion efficiency of the NERD gasifier. In order to carry out this parametric study, it was first necessary to calibrate the model using the gas compositions measured in the experiments. In calibrating the sub-model, the amount of methane predicted was adjusted in such a way that it was equal to the amount of methane measured experimentally in the product gas. A typical comparison between the model predictions and measurements using the 2.5 cm chips (Run No 7) is shown in Table 5. It can be seen that the gas compositions predicted by the gasification zone sub-model are within ±5.8% of the measured values. A typical comparison between the measured and predicted temperatures in the gasification zone is shown in Fig. 5. While there was a tendency to under-predict and over-predict the temperatures generated in the central and end portions of the gasification zone, respectively, the expected trend is nevertheless evident with sufficient accuracy. The predictions of the gasification zone sub-model were therefore considered to be satisfactory to study the performance of the NERD gasifier and a set of computer simulations have been carried out to investigate the effects of various operating parameters on conversion efficiency. The parameters and range of values used in these simulations is shown in Table 6.

Table 3
Summary of gas analyses from nine experimental runs of test gasifier

Run no.	Chip size (cm)	M/C (%) (d.b.)	Air/fuel ratio	CO (%)	H_2 (%)	CO_2 (%)	CH_4 (%)	N_2 (%)	Gas flow rate ($m^3\,h^{-1}$)
1	3.3	18.5	2.03	19.6	17.2	9.9	1.4	51.9	52.4
2	3.3	16.0	2.20	20.2	18.3	9.7	1.1	50.7	57.7
3	3.3	14.7	2.37	19.4	17.2	9.7	1.1	52.6	59.7
4	4.4	16.0	1.96	18.4	17.0	10.6	1.3	52.7	53.6
5	4.4	15.2	2.12	19.7	13.2	10.8	1.3	55.0	62.1
6	4.4	14.0	2.29	18.9	12.5	8.5	1.2	59.1	62.5
7	5.5	14.7	1.86	19.1	15.5	11.4	1.1	52.9	51.9
8	5.5	13.8	2.04	22.1	12.7	10.5	1.3	53.4	62.5
9	5.5	12.5	2.36	19.1	13.0	10.7	1.2	56.0	63.5

Table 4
Material balance of the gasifier

Material input (kg/h)					Material output ($kg\,h^{-1}$)				
Air	Feed	Wood moisture	Air moisture	Ash	Gas	Water	Char	Ash	Unaccounted material
55.6	18.6	3.4	1.0	0.1	71.0	1.4	0.7	0.1	5.5
55.6	20.9	2.6	1.0	0.1	69.9	1.2	2.1	0.1	6.9

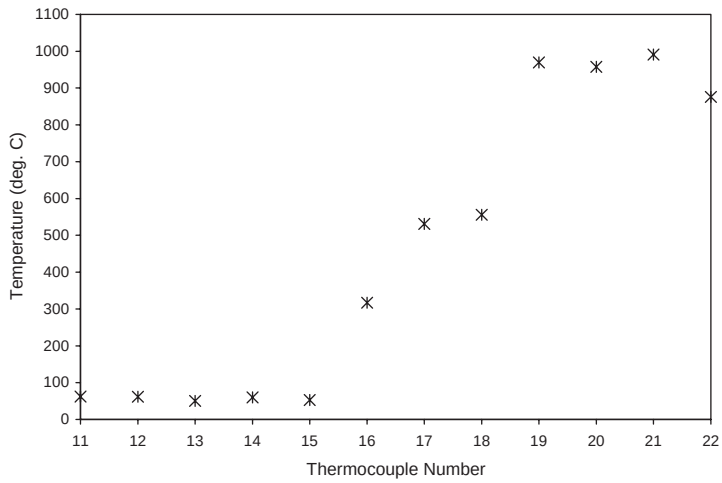

Fig. 4. Typical temperature profile through gasifier during operation.

Table 5
Comparison of predicted and measured gas composition for 2.5-cm chips

Dry gas composition (% by vol.)	Predicted	Measured
CO	18.3	19.1
H_2	16.4	15.5
CO_2	11.1	11.4
N_2	53.2	52.9
CH_4	1.1[a]	1.1

[a] Assumed.

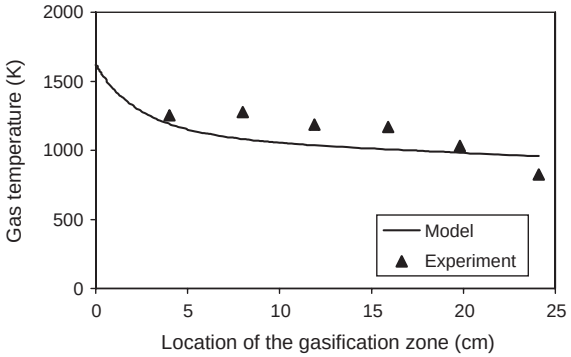

Fig. 5. Comparison of measured and predicted temperatures along axis of gasification zone for air–fuel ratio of 2.20.

Table 6
Range of parameters used for simulation study

Parameter	Range
Wood moisture content (% d.b.)	0–30
Heat loss (% input energy)	5–15
Chip size (cm)	1–5
Air temperature (K)	300–600
Throat angle (°)	30–90

8. Simulation results and discussion

Three of the parameters studied (air inlet temperature, chip size and moisture content) are operating parameters over which the user has control and the remaining two parameters (heat loss and throat angle) are functions of the gasifier design. The variation in conversion efficiency along the gasification zone for each of these parameters was investigated and the simulation results are presented and discussed below. For various values of four of these parameters, the optimum length of gasification zone and the efficiency at that length is then summarised and compared with the efficiency levels achievable with the current NERD design.

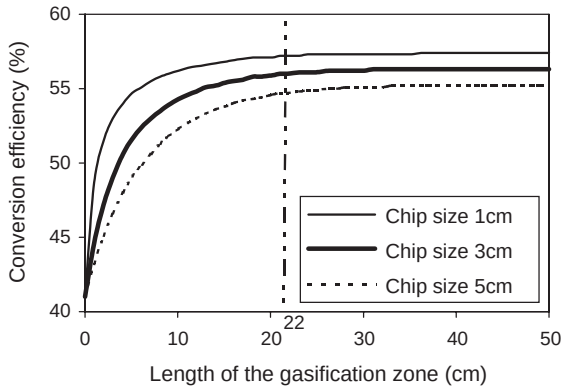

Fig. 6. Variation of conversion efficiency for different chip sizes.

8.1. Chip size

The size of fuel wood chip is an important parameter which affects the char conversion rate and hence the conversion efficiency. The size of the chips used mainly depends on the diameter of the gasifier. Milligan [5] used 0.6 cm chips in a laboratory-scale gasifier with a reactor diameter of 7.5 cm. In contrast, Walawender et al. [9] used chips as large as 4.7 cm for a commercial scale gasifier with a reactor diameter of 60 cm.

The variation of conversion efficiency along the gasification zone for different chip sizes is shown in Fig. 6. It can be seen that as the chip size increases the length of the gasification zone must also increase before the conversion reaches its maximum. Thus larger particles need longer reactor lengths to achieve the maximum conversion. Char conversion consists of two processes namely, fast conversion and slow conversion. Fast conversion of char takes place at the entrance of the gasification zone due to the fast reaction rate [4]. Smaller particles are more likely to get converted to gases completely before the slow conversion begins because of their size and fewer

diffusional limitations during the reaction process [4]. Thus gasifiers with shorter reactor lengths need small chips. With the same environmental conditions, larger chips also undergo the same fast conversion but because of their size, complete conversion may not be possible. Larger chips undergo the remaining slow conversion and thus need a longer reactor length prior to leaving the gasification zone. As a result of faster char conversion, smaller chips increase the conversion efficiency compared to larger chips. Sizes of chips used in the NERD gasifier varied from 1 to 5 cm. But in general, 5 cm chips are preferred due to their lower preparation cost, which is significant for commercial gasifiers. The gasification zone length of the NERD is 22 cm. It can be seen from Fig. 6 that for a gasification zone length of 22 cm, the conversion efficiency is almost 55% for chip size of 5 cm. If this size is reduced to 3 cm, the conversion efficiency increases by 1%. The optimum gasification zone length is defined as the length at which the efficiency is 99.5% of the ultimate conversion efficiency. For a 5 cm chip size, the optimum length of the gasification zone is approximately 33 cm.

8.2. Moisture content

The moisture content of the feed material is one of the main characteristics, which affects the composition of the product gas [10]. The effects of moisture on the recoverable heat are very significant due to the heat requirement for vapourizing the moisture and superheating the vapour [11]. Generally for gasifier operations, fuel wood with a low moisture content is preferred because of its higher gross energy content. Reed and Das [12] have reported that moisture contents higher than 67% (d.b.) make the product gas too lean for ignition. Although lower moisture contents are preferred to produce a high-quality gas, they further stated that it is desirable to maintain a level at least below 33% (d.b.) to produce a combustible gas.

Fig. 7 shows the variation of conversion efficiency along the gasification axis for various moisture contents. Although it is not practically possible to achieve a 0% moisture content, this figure has been included to show the maximum possible efficiency. It can be seen that the conversion efficiency decreases with increasing moisture contents. This is due to the fact that a higher amount of energy is consumed in evaporating

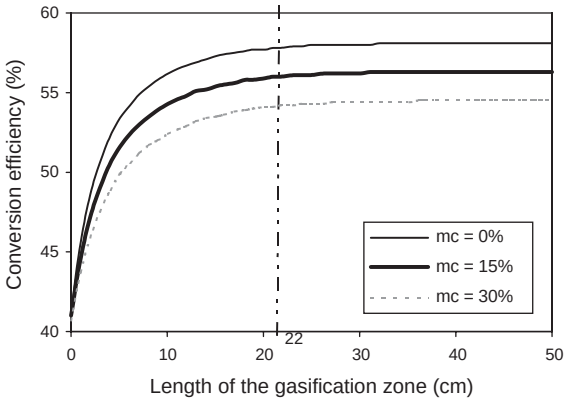

Fig. 7. Variation of conversion efficiency for different moisture contents.

the moisture in the wood, which subsequently reduces the temperature of the gas. The lower temperature reduces the reaction rate and thereby the conversion efficiency. The moisture content of the wood chips used in NERD gasifier varied from 12.5 to 18.5 (d.b.). It can be seen from Fig. 7 that for average moisture content of 15% (d.b.), the conversion efficiency of the NERD gasifier is 56% at 22 cm along the gasification zone whereas the optimum length occurs at approximately 32 cm.

8.3. Inlet air temperature

Generally ambient air at 300 K is used for gasification. However, Chen [4] stated that a higher inlet air temperature improves the conversion efficiency. Conversion efficiency increases as the inlet air temperature increases because hot air provides additional enthalpy necessary for reaction, thereby decreasing the air fuel ratio. The effect of preheating the input air temperatures to 450 and 600 K has therefore been investigated. Fig. 8 shows that higher inlet air temperatures are beneficial to gasifier performance, but the effect is only marginal. The conversion efficiency increases from 56.0% to 56.5% when the inlet temperature increases from 300 to 450 K. For an air input of 50 kg h^{-1}, which a typical figure for the NERD gasifier, approximately 2 kW of energy would be required to raise the temperature of air from 300 to 450 K. This is approximately 3% of the 70 kW_{th} gasifier capacity. However, in tea drying, the temperature of the exhaust

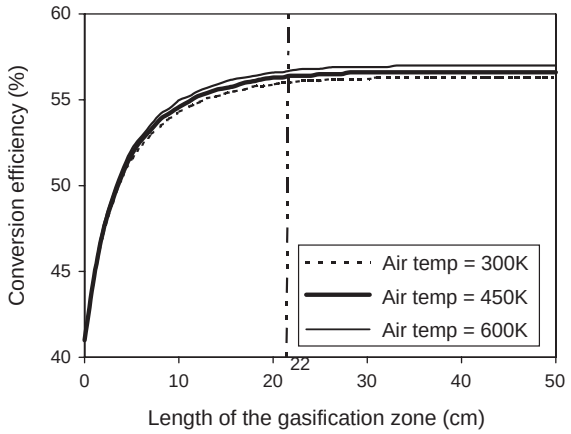

Fig. 8. Variation of conversion efficiency for different air temperatures.

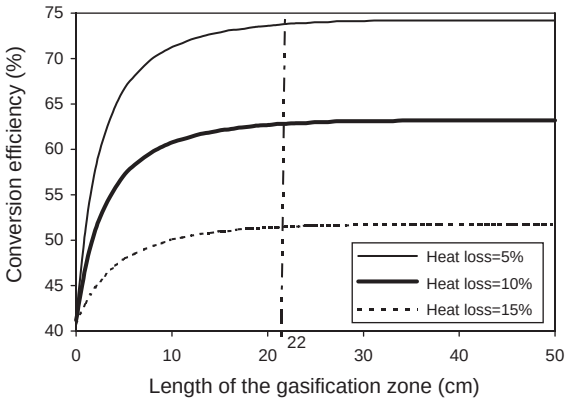

Fig. 9. Variation of conversion efficiency for different heat losses.

gas is around 150°C [13] and this could be used in combination with a heat exchanger to raise the temperature of inlet air. However, due to the additional expense involved, it is unlikely that achieving only a small increase in conversion efficiency in this way is economically viable.

8.4. Heat loss

According to Chern [14], a heat loss of 10% is acceptable for a commercial gasifier. The results of an energy balance conducted on the NERD gasifier found the heat loss was approximately 12.8% [6], the lack of insulation on the gasifier body being a major contributor to this loss. Unaccounted losses in the balance represented about 5% of the energy output. This included losses due to tar production, which could not be accurately measured. The variation of conversion efficiency for varying degrees of heat losses is shown in Fig. 9. It can be seen that of all the parameters investigated, the heat loss has the greatest effect on the conversion efficiency, which decreases by approximately 11% for every 5% increase in heat loss. This is because the high heat loss lowers the reactor temperature, which in return reduces the gasification reaction rates and the conversion efficiency. This is more significant for smaller reactors because in terms of fluxes (based on reactor cross-section area) the heat loss is high for gasifiers with smaller reactor diameters as the surface-to-volume ratio will be higher. Fig. 9 indicates that a 12.8% heat loss (i.e. the NERD gasifier) will result in a conversion efficiency of approximately 56% at a gasification zone length of 22 cm, although the optimum gasification zone length is approximately 26 cm. Although the decrease in conversion efficiency is considerable for any increase in heat loss, the cost associated in reducing the heat loss e.g. increasing gasifier insulation must be considered to ensure economic benefit.

8.5. Throat angle

Throat angle is a special unique feature of downdraft gasifiers and the effect of this on conversion efficiency is important. In selecting the range of the throat angles, the values of 30°, 60° and 90° were selected to include the existing angle of 61°. Fig. 10 shows the variation of conversion efficiency along the gasification zone axis for different throat angles. The conversion efficiency decreases as the throat angle increases, because the divergent effect of the throat decreases the temperature and hence the reaction rate. However, the smaller angles also need a longer gasification zone length to reach their optimum efficiency. The effect of throat angles is not significant until the conversion process reaches the gasification zone length of 10 cm. For a throat angle of 61° i.e. the NERD gasifier, the conversion efficiency is 56% at the gasification zone length of 22 cm.

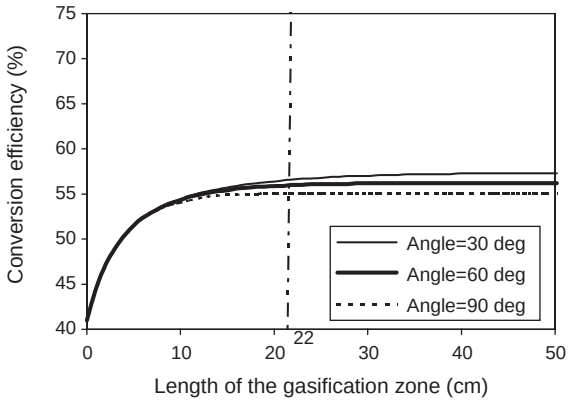

Fig. 10. Variation of conversion efficiency for different throat angles.

8.6. Optimum gasification zone length

Table 7 compares four of the above operating and design parameters with the efficiency achievable at 22 cm and at the optimum gasification zone length. In this comparison, the effect of increasing the inlet air temperature is not included because the efficiency gains achievable are considered to be too small. It can be seen that 1 cm chips tend to increase the maximum efficiency by only 1% compared to 3 cm chips, although the gasification zone length may be reduced by 25%. However, these benefits would only be achieved with a higher fuel wood preparation cost. Although it would be advantageous to use rubber wood with a moisture content below 10% (d.b.), in reality it would be difficult to dry the large quantities of chips needed for a commercial type gasifier to this level. If wood chips are given sufficient sun exposure, the moisture content can be reduced to 15%, which gives a conversion efficiency of 56%.

As noted earlier, a decrease in heat loss has the greatest effect in terms of improving efficiency. However, the optimum gasification zone length needs to be increased at the same time as reducing the heat loss. However, the resulting gains in efficiency are likely to far outweigh the increased cost of increased insulation and reactor length. An increase in the existing throat angle would have some beneficial effect in terms of efficiency, but as already noted the length of the gasification zone would have to be increased. Therefore the relative costs of this exercise would have to be carefully evaluated against the potential gains.

9. Conclusions

Of the five parameters investigated in this section, the moisture content of fuel wood and heat loss are the main variables affecting downdraft gasifiers. Moisture content and heat loss have greater effects on reactor temperature and hence on the conversion efficiency. Reducing the heat loss from the gasifier is very beneficial in terms of conversion efficiency and this can be achieved by insulating the reactor body. Chips (3–5 cm) can be sun dried to a moisture content of approximately 15% in commercial quantities, and although a lower moisture content and smaller chip size would be preferable, in practice this is unlikely to be economically viable. High inlet air temperatures are beneficial to gasifier performance but heating the inlet air is probably not economical when compared with the small gain in conversion efficiency. A smaller throat angle increases the conversion efficiency but at

Table 7
Comparison of efficiencies with gasification zone length

Parameter	Chip size (cm)			Moisture content (% d.b.)			Heat loss (%)			Throat angle (deg)		
	1	3	5	0	15	30	5	10	15	30	60	90
Efficiency at 22 cm	57.2	56.0	54.7	57.8	56.0	54.2	73.8	62.8	51.5	56.6	56.0	55.1
Optimum length (cm)	24	32	33	31	32	35	29	28	25	28	24	19
Efficiency at optimum length	57.3	56.3	55.2	58.1	56.3	54.5	74.2	63.2	51.7	57.4	56.2	55.1

the same time the gasification zone length must be increased to achieve the same conversion efficiency.

From the above study it can be concluded that the length of the gasification zone is a vital design parameter for downdraft gasifiers. A longer length enables the gasifier to operate at its maximum efficiency but it also increases the fabrication cost. A shorter length is not desirable as the gasifier may perform below its design capacity due to insufficient length for char conversion. The optimum gasification zone length has to be selected for maximum output for a given range of operating parameters. Assuming that 3–5 cm rubber wood chips with moisture content of approximately 15% (d.b.) will be used, then the gasification zone length needs to be increases from the current 22 cm to approximately 33 cm. This increase will also mean that increased insulation levels can be introduced to achieve the significant gains in efficiency that this modification will produce.

Acknowledgements

Authors wish to thank to Mr. Victor Mendis and staff members of NERD Centre, Sri Lanka for the information about the gasifiers. The financial support of the Asian Development Bank-Japanese Scholarship Programme is also acknowledged.

References

[1] Jayah TH, Fuller RJ, Lu Aye. Renewable energy options for the tea industry in Sri Lanka. Proceedings of the 36th Annual Conference of the Australia and New Zealand Solar Energy Society, Christchurch, New Zealand, 25–27 November 1998. p. 15–21.

[2] Jayah TH, Fuller RJ, Lu Aye, Stewart DF. The potential for wood gasifiers for tea drying in Sri Lanka. RERIC International Energy Journal 2002;2(2):85–91.

[3] Jayah TH, Lu Aye, Fuller RJ, Stewart DF. Wood gasifiers for tea drying in Sri Lanka. Proceedings of the 37th Annual Conference of the Australia and New Zealand Solar Energy Society, Geelong, Australia, 1–3 December 1999. p. 1–10.

[4] Chen JS. Kinetic engineering modelling of co-current moving bed gasification reactors for carbonaceous material. Ph.D. thesis, Cornell University, New York, 1987.

[5] Milligan JB. Downdraft gasification of biomass. Ph.D. thesis, Aston University, Birmingham, UK, 1994.

[6] Jayah TH. Evaluation of a downdraft wood gasifier for tea manufacturing in Sri Lanka. M.Eng. Sc. thesis, Department of Civil and Environmental Engineering, University of Melbourne, 2002.

[7] Haskoning. Energy conservation in the Tea Industry in Sri Lanka; conclusive results. The Netherlands-Sri Lanka Energy Programme, Sri Lanka, 1989.

[8] Hoi WK, Razak AM, Bridgewater AV. Performance data of rubber wood gasification. Energy from Biomass, Second International Energy Conference, Kuala Lumpur, Malaysia, August 17–19, 1992.

[9] Walawender WP, Chern SM, Fan LT. Wood chip gasification in a commercial downdraft gasifier. In: Overend RP, Milne TA, Mudge LK, editors. Fundamentals of thermochemical biomass conversion. London: Elsevier Applied Science Publishers, 1985.

[10] Hos JJ, Groeneveld MJ. Biomass gasification. In: Hall DO, Overend RP, editors. Biomass regenerable energy. Chichester: Wiley, 1987.

[11] Graboski M, Bain R. Properties of biomass relevant to gasification. In: Reed TB, editor. Biomass gasification, principles and technology. New Jersey: Noyes Data Corp., 1981. p. 41–69.

[12] Reed TB, Das A. Handbook of biomass downdraft gasifier engine system. Golden, CO: SERI, 1988.

[13] Keegel EL. Tea manufacture in Ceylon. Monographs on Tea Production in Ceylon, No. 4, Tea Research Institute, Ceylon, 1983.

[14] Chern SM. Equilibrium and kinetic modelling of co-current (downdraft) moving-bed biomass gasifier. Ph.D. thesis, Kansas State University, Kansas, 1989.

ANNEX C: Pyrolytic characteristics of sewage sludge.

P. Thipkhunthod, V. Meeyoo, P. Rangsunvigit, B. Kitiyanan, K.Siemanond, T. Rirksomboon

ELSEVIER

Chemosphere 64 (2006) 955–962

CHEMOSPHERE

www.elsevier.com/locate/chemosphere

Pyrolytic characteristics of sewage sludge

Puchong Thipkhunthod [a], Vissanu Meeyoo [b,*], Pramoch Rangsunvigit [a], Boonyarach Kitiyanan [a], Kitipat Siemanond [a], Thirasak Rirksomboon [a]

[a] *The Petroleum and Petrochemical College, Chulalongkorn University, 245 Soi Chula 12, Phyathai Road, Pathumwan, Bangkok 10330, Thailand*

[b] *Centre for Advanced Materials and Environmental Research, Mahanakorn University of Technology, 51 Cheum-Sampan Road, Nong Chok, Bangkok 10530, Thailand*

Received 19 September 2005; received in revised form 28 December 2005; accepted 6 January 2006
Available online 17 February 2006

Abstract

In this study, a number of different sewage sludge including sludge samples from industrial and hospital wastewater treatment plants were characterized for pyrolysis behavior by means of thermogravimetric analysis up to 800 °C. According to the thermogravimetric results, five different types of mass loss behaviors were observed depending on the nature of the sludge used. Typical main decomposition steps occurred between 250 and 550 °C although some still decomposed at higher temperatures. The first group (Types I, II and III) was identified by main decomposition at approximately 300 °C and possible second reaction at higher temperature. Differences in the behavior may be due to different components in the sludge both quantitatively and qualitatively. The second group (Types IV and V), which rarely found, has unusual properties. DTG peaks were found at 293, 388 and 481 °C for Type IV and 255 and 397 °C for Type V. Kinetics of sludge decomposition can be described by either pseudo single or multicomponent overall models (PSOM or PMOM). The activation energy of the first reaction, corresponding to the main pyrolysis typically at 300 °C, was rather constant (between 68 and 77 kJ mol^{-1}) while those of second and third reactions were varied in the range of 85–185 kJ mol^{-1}. The typical order of pyrolysis reaction was in the range of 1.1–2.1. The pyrolysis gases were composed of both saturated and unsaturated light hydrocarbons, carbon dioxide, ethanol and chloromethane. Most products, however, evolve at a quite similar temperature regardless of the sludge type.

Keywords: Sewage sludge; Pyrolysis; Kinetics

1. Introduction

Sewage sludge is generated and collected from several parts of wastewater treatment system in both community and industrial sections. All indications suggest that sludge production will continue to increase, and a suitable solution for the disposal of the expected large quantity of sludge would be needed (Werther and Ogada, 1999). The most common methods to handle the problem are incineration, agricultural use, and landfill disposal. However, the problem is not totally solved because one may cause subsequent problems and require secondary treatment. A promising way for sewage sludge disposal that has been widely studied is the thermal application such as pyrolysis. Pyrolysis has been considered as an alternative to the problems of both secondary pollution in thermal processing and of large energy consumption.

Development for sewage sludge conversion to energy and chemicals by pyrolysis process requires better understanding of its thermal properties and reaction kinetics. For highly heterogeneous materials with a wide variety of unknown components such as sewage sludge, it is believed that many decomposition reactions involve in the pyrolysis. Moreover, complex details of each reaction are generally unknown and difficult to analyze. There have been many

* Corresponding author. Tel./fax: +66 2 988 4039.
E-mail address: vissanu@mut.ac.th (V. Meeyoo).

0045-6535/$ - see front matter © 2006 Elsevier Ltd. All rights reserved.
doi:10.1016/j.chemosphere.2006.01.002

attempts to describe pyrolysis of sewage sludge with suitable kinetic models by different authors (Conesa et al., 1997, 1998; Chu et al., 2000; Chen et al., 2001; Conesa et al., 2001; Chao et al., 2002). The models usually inherit their own assumptions and supported data. Nonetheless, any evaluation of complex reaction scheme may not be accomplished due to limitation in a number of samples. In this work, with an extensive number of samples, kinetics of the sludge pyrolysis was investigated by means of thermogravimetric analysis.

2. Materials and methods

2.1. Sample preparation

Samples used in this study were collected from 20 sources comprising municipal, hospital, and industrial wastewater treatment plants located in Bangkok, Thailand and its vicinity. The sample collection was repeated monthly over a two-year period, resulting in exceeding a total number of 210 samples. The sample collecting method was in accordance with the standard method (ASTM D346-90, 1999). The samples were naturally dried for 1–2 d and ground by a ball mill. The fraction of 150–250 μm in particle size was selected for further study.

Physical and chemical properties of sludge samples were given in Table 1. On the whole, a broad range of sludge characteristics was observed. The lower and higher volatile matter limits of the samples are 17 and 60 wt%, corresponding to ash contents of 80 and 31 wt%, respectively, in dry basis. The samples contain only a small fraction of fixed carbon, with an average of 5 wt%. Typical heating values of the samples varied from 2.6 to 16.3 MJ kg^{-1}. Small differences between the sludge characteristics from the same source were also found. Most samples in this work, however, have lower volatile matter (higher ash) and heating values than those reported in the literature (Dogru et al., 2000; Menéndez et al., 2001; Shen et al., 2001; Inguanzo et al., 2002; Otero et al., 2002; Folgueras et al., 2003).

Table 1
Properties of sludge samples used in this study

Property	Average
Proximate analysis (wt%)[a]	
Moisture	5.2 ± 1.1
Volatile matter	42.6 ± 4.9
Ash	52.8 ± 5.7
Fixed carbon	4.6 ± 1.1
Ultimate analysis (wt%)[a]	
Carbon content	21.1 ± 3.2
Hydrogen content	3.4 ± 0.4
Nitrogen content	3.2 ± 0.6
Sulfur content	1.1 ± 0.3
Oxygen content	18.4 ± 2.2
Heating value (MJ kg^{-1})	9.9 ± 1.6

[a] Dry basis except moisture is in air-dried basis.

2.2. Pyrolysis experiment

The samples were pyrolized using a TG7 Perkin–Elmer thermogravimetric analyzer. A sample weight of approximately 10 mg was used for each experiment under non-isothermal conditions. The sample was heated up from ambient temperature to 105 °C and held until its weight was constant in which free moisture was removed out. Then, the sample was further heated to 800 °C with a heating rate of 20 °C min^{-1}. The experiments were carried out under the nitrogen flow of 20 ml min^{-1}. Some samples were randomly selected for repeating the experiment to ensure the reproducibility, which was found to be very consistent. The effect of heating rate was also studied between 5 and 20 °C min^{-1}. The thermogravimetric and differential thermogravimetric (TG–DTG) data were used to characterize the pyrolysis behavior of the sludge samples as well as to provide estimates of their kinetic parameters.

2.3. Gas evolution

Evolution of various gases produced from the sludge pyrolysis was analyzed by coupled temperature programmed pyrolysis/mass spectroscopy (TPP/MS). A mass spectrometer (Blazers Omnistar™) was directly connected to a temperature programmed pyrolyzer (TPDRO 1100, ThermoFinnigan). A sample weight of approximately 10 mg was placed in a quartz tube. The sample was heated in a nitrogen flow from room temperature to 800 °C with a heating rate of 10 °C min^{-1} and held for 10 min. Evolved gases of m/z of less than 60 were monitored during the heat up. The ion intensities were normalized to the sample mass as well as the intensity of the $^{28}N_2$ isotope of the carrier gas, in order to minimize errors caused by a shift in the mass spectrometer sensitivity.

3. Results and discussion

3.1. Thermal decomposition behavior of sewage sludge

Typical DTG curves for the sludge pyrolysis are shown in Fig. 1 and the DTG characteristics were given in Table 2. It should be noted that the pyrolysis reaction occurred within 600 °C. For most samples, a small fraction of mass loss occurred as indicated by a DTG peak in the temperature range of 120–180 °C. The mass loss in this region corresponds to the vaporization of sorbed water in the sludge, called dehydration or drying process (Chen and Jeyaseelan, 2001; Calvo et al., 2004). Its magnitude depends on the nature of individual sludge, typically varying from 5% to 10% of the total mass loss. A main decomposition step was normally observed at higher temperature. Five different types of DTG patterns were observed in this study. They were designated as Types I–V as shown in Fig. 1. All five behavior types were distinguished as the following descriptions.

Type I: The main decomposition or pyrolysis step starts slowly after dehydration and more sharply after 200 °C.

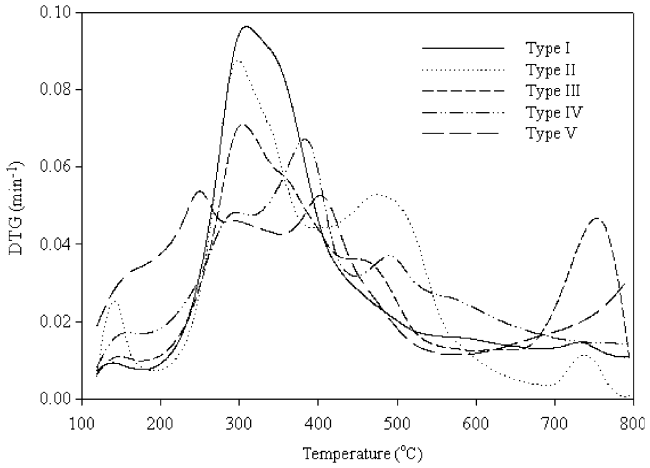

Fig. 1. DTG profiles of the sludge decomposition (heating rate = 20 °C min^{-1}).

Table 2
DTG peak temperature and height in accordance with the sludge decomposition (excluding dehydration)

	Peak temperature	Corresponding peak height
I	299 ± 1	0.21 ± 0.02
II	292 ± 2, 488 ± 11	0.20 ± 0.03, 0.11 ± 0.02
III	301 ± 2, 458 ± 7, 755 ± 8	0.17 ± 0.03, 0.07 ± 0.01, 0.10 ± 0.02
IV	293 ± 1, 388 ± 7, 481 ± 5	0.10 ± 0.01, 0.14 ± 0.01, 0.08 ± 0.01
V	255 ± 3, 397 ± 6	0.10 ± 0.01, 0.08 ± 0.01

The decomposition profile presents the main DTG peak at 299 °C and ceases at the temperature of ca. 550 °C. Overall decomposition (excluding dehydration) is accounted to be a single step with the magnitude of more than 80% of the total mass loss.

Type II: The sludge has an almost similar behavior as Type I up to 400 °C. The DTG curve presents the peak at 292 °C. At higher temperature, the mass loss presents a distinguished DTG peak at 488 °C. These two steps account for approximately 50% and 30% of the total mass loss, respectively. This, in turns, may refer to the two distinguished composition groups in the sludge.

Type III: A main decomposition takes place at 301 °C and next decomposition centered at 458 °C. These two steps were thought to be the same as Type II. However, for this type, another sharp peak occurs at the temperature higher than 700 °C. This region is accounted to be 15–20% of the total mass loss. The decomposition at such a high temperature is due to the degradation of calcium carbonate (Caballero et al., 1997).

Type IV: The decomposition takes place in three steps. Like other types, the first step at 293 °C takes place but as a shoulder. The main decomposition step occurs at 388 °C as the highest peak. At higher temperature, another shoulder was observed at 481 °C and overall decomposition ceases at 600 °C.

Type V: A mass loss in drying step is higher than those of other types, corresponding to high moisture in proximate analysis (Table 3). Other than the drying step, the decomposition can be clearly separated into two steps. The former occurs at 255 °C, which is lower than usual case. The later occurs at 397 °C with an almost similar magnitude to the first peak and stops at 550 °C.

In general, small variances in DTG characteristics such as peak height and temperature are possible due to the variation of samples (Table 2). It was also noticed that most sludge samples behave as Types I, II and III as the samples in these three types exceeds 90% of the total samples. Such thermograms also have been reported by many literatures (Caballero et al., 1997; Chen and Jeyaseelan, 2001; Tian et al., 2002; Calvo et al., 2004). In addition to the common case, Types IV and V as minor have only been observed in this work.

The characteristics of the sludge that represent each decomposition type were reported in Table 3. The behavior type was reported in the orders of increasing ash content and of lowering volatile matter, heating value, carbon and oxygen contents and C/O ratio. It was observed that Types I, II and III are not highly different in both proximate and ultimate analyses. For example, the volatile matter are 47, 43 and 42 wt%, C/H ratios are 6.39, 6.34 and 6.64 and C/O ratios are 1.37, 1.21 and 1.13 for Types I, II and III, respectively. This might be the reason why these three types have quite similar decomposition behaviors. Coincidence that these three types having a main decomposition step at approximately 300 °C, which almost constant, is however comparable to premature coal (Speight, 1994). The difference in these three types is the second

Table 3
Properties of sludge samples (indicated in average) corresponding to each sludge type[a]

Type	Proximate analysis[b]				HHV (MJ kg^{-1})	Ultimate analysis						
	M	*V*	*A*	FC		C	H	N	S	O	C/H	C/O
I	5.3 ± 0.9	47.0 ± 3.8	47.7 ± 4.4	5.3 ± 1.0	11.5 ± 1.1	24.5 ± 2.3	3.8 ± 0.3	3.9 ± 0.3	1.0 ± 0.1	19.1 ± 2.1	6.39 ± 0.1	1.37 ± 0.3
II	4.1 ± 1.1	43.2 ± 3.9	51.3 ± 4.6	5.5 ± 1.0	10.4 ± 1.2	22.0 ± 2.3	3.5 ± 0.3	3.4 ± 0.3	0.8 ± 0.2	18.9 ± 2.1	6.34 ± 0.1	1.21 ± 0.2
III	4.4 ± 1.0	42.4 ± 4.9	54.4 ± 5.5	3.2 ± 1.0	8.9 ± 1.4	20.5 ± 3.2	3.1 ± 0.5	2.7 ± 0.5	1.2 ± 0.3	18.1 ± 1.7	6.64 ± 0.1	1.13 ± 0.1
IV	4.9 ± 0.7	37.3 ± 0.6	59.6 ± 1.0	3.0 ± 0.6	8.5 ± 0.2	17.3 ± 0.2	3.4 ± 0.2	1.7 ± 0.1	1.9 ± 0.2	16.1 ± 1.1	5.12 ± 0.2	1.09 ± 0.1
V	8.5 ± 1.3	24.0 ± 1.1	73.5 ± 1.0	2.5 ± 0.4	3.6 ± 0.4	9.3 ± 0.5	2.3 ± 0.5	1.5 ± 0.1	1.6 ± 0.4	11.8 ± 0.9	4.18 ± 0.3	0.81 ± 0.1

[a] Dry basis except for moisture in air-dried basis.
[b] M, V, A, FC and HHV are moisture, volatile matter, ash, fixed carbon and high heating value.

decomposition pronounced at higher temperature approximately 450 °C). This peak is believed to owe to the decomposition of higher molecular weight or more complex molecules (Gascía-Pèrez et al., 2001; Sørum et al., 2001).

The properties of other two sludge types (IV and V) are considerably different from the others. C/H ratio of Type IV was found to be lower (reported at 5.12) than that of Types I, II and III. Notably, the characteristic of Type V sludge is highly different from the others. It has drastically low volatile matter, 24 wt%, as well as C/H and C/O ratios at 4.18 and 0.81. This may be due to the fact that this type of the sludge contains significant amount of inorganic substances or ash content, which is uncommonly found in most organic solids. As such manner, the property of material such as its heating value is unpredictable (Thipkhunthod et al., 2005).

Table 4 shows the decomposition temperatures of samples comparing to other materials collected from literatures (Chen et al., 2001; Gascía-Pèrez et al., 2001; Peng et al., 2001; Grønli et al., 2002; Gong et al., 2003; Heikkinen et al., 2004). It was found that the decomposition temperatures of the sludge are comparable to that of various materials. It should be noted that the mass loss for composted sludge and API separator sludge was also found at 250 °C. It was reported for composted sludge that the decomposition at such low temperature was corresponded to the combustion of carbohydrate (Pietro and Paola, 2004). In case of API separator sludge, it was proposed to be the volatilization process (Punnaruttanakun et al., 2003). The decomposition at 300–350 °C most likely belongs to the degradation of natural polymers such as cellulose, micro algae, starch, leather and wool. Whereas the decomposition at higher temperature, up to 500 °C, is believed to be due to the degradation of complex and/or aromatic structures in various materials such as API separator sludge, petroleum residue, scrap tire, asphalt and some plastics (Chen et al., 2001; Gascía-Pèrez et al., 2001; Sørum et al., 2001; Gong et al., 2003; Punnaruttanakun et al., 2003; Heikkinen et al., 2004).

Table 4
The DTG peak temperature and C/H ratio of various materials

Materials	Temperature (°C) at presence of DTG peak	C/H ratio
Micro algae[a]	330–360	–
Cellulosic material[b,c,d]		
Xylan	298	–
Cellulose	350	–
Lignin	350	–
Leather[d]	342	–
Wool[d]	339	–
Composted sludge[e]	250, 400	–
API separator sludge[f]	250, 440	–
Asphalt[g]	350, 474	7.85–8.44
Petroleum residue[b]	450	8.27
Scrap tire[d,h]	400, 450	11.24
Various plastics[i]		
PS	413	11.73
PP	456	6.28
LDPE	472	6.04
HDPE	479	6.62
PVC	294, 316, 455	7.81

[a] Peng et al. (2001).
[b] Gascía-Pèrez et al. (2001).
[c] Grønli et al. (2002).
[d] Heikkinen et al. (2004).
[e] Pietro and Paola (2004).
[f] Punnaruttanakun et al. (2003).
[g] Gong et al. (2003).
[h] Chen et al. (2001).
[i] Sørum et al. (2001).

It was also observed that all thermogram types are generally shifted to higher temperatures when the heating rate is increased from 5 to 20 °C min^{-1}. General decomposition behaviors (DTG patterns) do not significantly change for all sludge types. With the same trend, DTG peak heights were increased. This fact is also true for various materials, for instance, biomass or cellulosic materials, API sludge and plastics (Dubdub and Tiong, 2001; Punnaruttanakun et al., 2003).

3.2. Kinetic modeling

The global reaction kinetics of sewage sludge pyrolysis can be described by the following rate equation:

$$\frac{dx}{dt} = kf(x), \tag{1}$$

where x is the mass loss fraction. Constant k obeys Arrhenius correlation

$$k = A\exp\left(-\frac{E}{RT}\right), \tag{2}$$

where A is the frequency factor; E is the activation energy; R is the universal gas constant and T is the absolute temperature. With some mathematic manipulation, Eq. (1) is converted to

$$\frac{dx}{dT} = \frac{A}{\beta}\exp\left(-\frac{E}{RT}\right)f(x), \tag{3}$$

where β is the heating rate. The specific form of $f(x)$ represents the hypothetical model of the reaction mechanism or 'model function', which may be presented here in the form of an nth order of reaction

$$f(x) = (1-x)^n, \tag{4}$$

where n is the order of reaction. Eq. (3) is in a suitable form for the application with constant heating rate TG–DTG data. An integral form of Eq. (3) is normally written as

$$g(x) = \int_0^x \frac{dx}{f(x)} = \frac{A}{\beta}\int_{T_0}^{T}\exp\left(-\frac{E}{RT}\right)dT. \tag{5}$$

Following Coats and Redfern approximation method (Coats and Redfern, 1964), Eq. (5) becomes

$$\ln\left[\frac{g(x)}{T^2}\right] = \ln\frac{AR}{\beta E}\left[1-\frac{2RT}{E}\right] - \frac{E}{RT}, \tag{6}$$

$$\text{where } g(x) = \begin{cases} -\ln(1-x) & n = 1, \\ \dfrac{1-(1-x)^{1-n}}{1-n} & n \neq 1. \end{cases} \tag{7}$$

As shown in Fig. 1, mass loss mechanism changes during an increase in temperature, at which pyrolysis occurs and the corresponding reaction seems not to complete in a single step (except for Type I only). The decomposition reaction of the sludge then should be represented by either the pseudo single component overall model (PSOM) or the pseudo multi-component overall model (PMOM) (Liu et al., 2002). With the PSOM, the sludge was considered as a single pseudo component and decomposed in a single step over a temperature range. On the other hand, the PMOM assumes that the sludge decomposition is resulted from the multi-component decomposes in separated stages. One of the PMOMs is written in the form of pseudo bi-component separated state model (PBSM) (Liu et al., 2002; Punnaruttanakun et al., 2003)

$$\frac{dx}{dT} = \begin{cases} \dfrac{w_{10}-w_{1\infty}}{w_{10}-w_{2\infty}}\dfrac{dx_1}{dT} & w_{10} < w < w_{1\infty}, \\ \dfrac{w_{20}-w_{2\infty}}{w_{10}-w_{2\infty}}\dfrac{dx_2}{dT} & w_{20} < w < w_{2\infty} \end{cases} \quad \text{and} \tag{8}$$

$$\begin{cases} \dfrac{dx_1}{dT} = \dfrac{A_1}{\beta}\exp\left(-\dfrac{E_1}{RT}\right) f_1(x_1) & w_{10} < w < w_{1\infty}, \\ \dfrac{dx_2}{dT} = \dfrac{A_2}{\beta}\exp\left(-\dfrac{E_2}{RT}\right) f_2(x_2) & w_{20} < w < w_{2\infty}, \end{cases} \tag{9}$$

where subscripts 1, 2 correspond to the pseudo components 1 and 2 and subscripts 0, ∞ correspond to the initial and final mass percentages, respectively.

The analogy to these two equations is considered when single and more than two pseudo components involve. To obtain the kinetic parameters, the TG–DTG information was used. A non-linear regression scheme was used in fitting Eqs. (6) and (7) or other suitable forms with respect to each sludge type and experimental data. The analysis was done in the temperature range between 180 and 600 °C depending upon the characteristics of DTG patterns for each type.

The obtained kinetic parameters are summarized in Table 5. It should be noted that the difference between the models is a number of reactions, which is in accordance with the DTG profile. A common model for sludge pyrolysis is the PBSM as represented Types II, III and V behaviors. It was found that the activation energy of the first reaction (main reaction) is almost similar for different types of sludge (ca. 60.8–76.7 kJ mol^{-1}). This reaction represents the main decomposition step of the sludge occurring at 300 °C especially for Types I, II, III and even IV (not main decomposition step for Type IV). For the second reaction, the activation energy is also comparable for Types II, III and IV (136.1, 123.0 and 142.0 kJ mol^{-1}, respectively) whilst that of Type V is 85.4 kJ mol^{-1}, which is less than the other types. For the third reaction, only for Type IV, the activation energy is reported at 131.8 kJ kg^{-1}. Notably, the third reaction only accounts for 5% of the overall fractions. The orders of all reactions were found in the range of 1.1–1.8. Any difference that distinguishes sludge to each type would be resulted from the second and third reactions.

Table 5
Kinetic parameters resulting from different models[a]

Type	Model	Reaction I		Reaction II		Reaction III	
		E	n	E	n	E	n
I	PSOM	60.8	1.8				
II	PBSM	64.5	1.3	136.1	1.5		
III	PBSM	70.4	1.3	123.0	1.6		
IV	PMOM	76.7	1.1	142.0	1.5	131.8	1.3
V	PBSM	73.2	1.6	85.4	1.8		

[a] E = activation energy (kJ mol^{-1}), n = order of reaction.

There have been a number of sewage sludge pyrolysis kinetic models reported in the literature (Conesa et al., 1997; Chu et al., 2000; Chen and Jeyaseelan, 2001; Chao et al., 2002). However, the values of kinetic parameters were varied depending on the assumptions made. Due to the different models used, the values may not be comparable. Any discussion should be done individually. Conesa et al. (1997) and Chu et al. (2000) studied the sewage sludge pyrolysis by means of TGA and reported global kinetics by three and two reaction schemes, respectively. The activation energies reported are typical (in the range of 17–332 and 43–137 kJ mol^{-1}, respectively) but the reaction order is somewhat as high as 10, which rarely occurs in general chemical reactions. Chen and Jeyaseelan (2001) on the other hand took the four consecutive first order reactions constrain and reported the activation in the same range (53–205 kJ mol^{-1}). The first order reaction model with a transition state theory was also proposed by Chao et al., 2002, with reported high activation energy of 295 kJ mol^{-1}. In the present study, the proposed models were found to well fit with the TGA behaviors. The activation energy of particular reactions was in agreement with those reported in the literature. The modeling also allows reaction order to be independently varied. Typical orders of reaction were found between 1.1 and 1.8, reasonable for most chemical reactions.

3.3. Product evolution

The detected products from TPP/MS analysis are listed in Table 6, which also represent corresponding compounds formed during pyrolysis of sewage sludge. Fig. 2 shows the typical evolution profiles of various gas products during the decomposition of sewage sludge. Although the gases are not quantified, the amount of each gas is observed to be different as indicated by the height of MS signals.

The evolution of gas can be divided into three zones according to MS peaks at 350, 500 and 750 °C leading to three classified groups of gas products. Hydrogen evolution starts at 500 °C and reaches the highest point at ca 750 °C. The second group comprises methane, ethylene, propylene,

Table 6
Suggested identification of mass spectra from MS (Conesa et al., 1998)

m/z	Ion	Name
2	H_2^+	Hydrogen
15	CH_3^+	Methane
26	HCN^+, $C_2H_2^+$	HCN, ethylene
39	$C_3H_3^+$	Propylene
43	$C_3H_7^+$	Propane
44	CO_2^+	Carbon dioxide
45	CH_3CHOH^+	Ethanol
50	CH_3Cl^+	Chloromethane
55	$C_4H_7^+$	Butane

chloromethane and butane ($m/z = 15$, 26, 39, 50 and 55) as shown in Fig. 2(b)–(i), respectively. The products in this group evolved from a single step at 500 °C. The third group comprises propane, carbon dioxide and ethanol ($m/z = 43$, 44 and 45) as shown in Fig. 2(e)–(g), respectively. These products evolved from all three steps at 350, 500 and 750 °C.

It is apparent that most gases evolve at a similar temperature regardless of sludge type. Nonetheless, there are differences in quantity and a small temperature shift may be possible depending on the nature of sludge. For the special

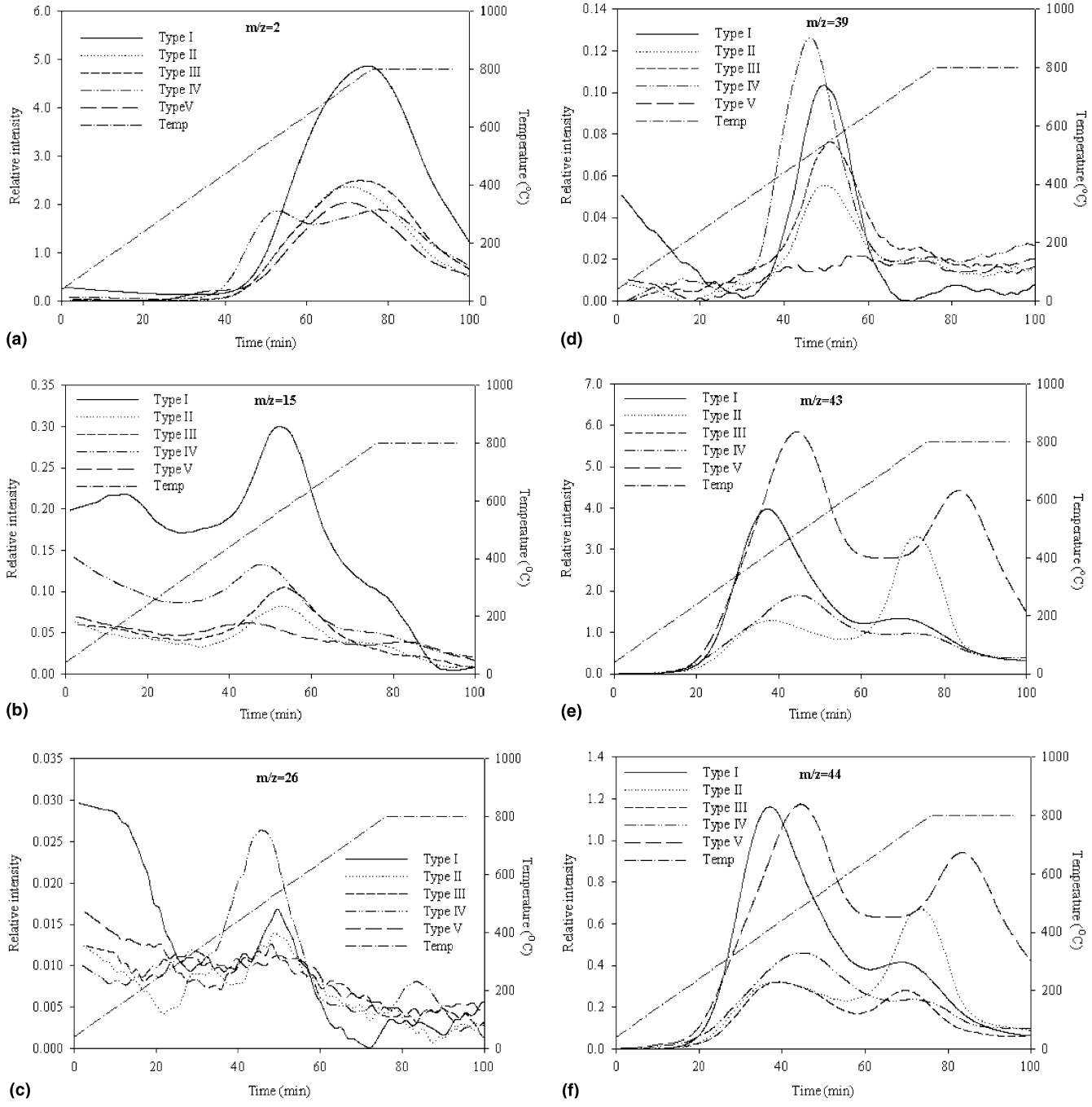

Fig. 2. Mass spectra from TPP/MS experiments.

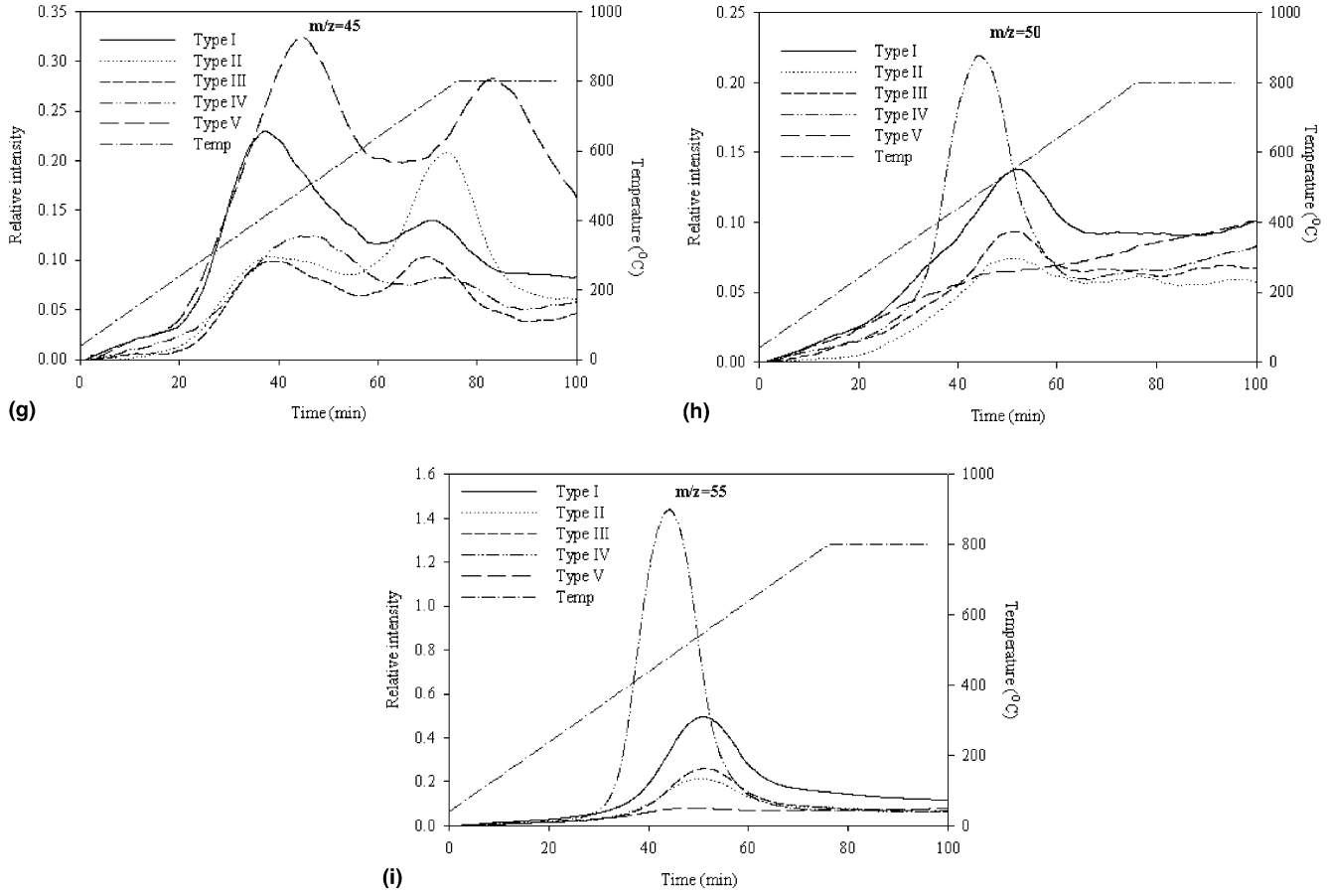

Fig. 2 (*continued*)

case, Type V has main mass loss at 250 °C but has very little effect on the gas evolution profile. The absence of gas profile might be due to larger mass number of the precut at this range. At 750 °C, although the decomposition of sludge at this temperature is very small (except Type III), the gas evolution also occurs at such high temperature for all sludges. It is possible that these gases come from either secondary gas phase reaction or liquid decomposition.

Only detected gases were discussed in this paper although other gases were also produced. The report may be different from some literatures. Conesa et al. (1998) reported a three-stage process for sewage sludge pyrolysis centered at 250, 350 and 450 °C due to three organic fractions namely non- and biodegradable organic matters and dead bacteria (Conesa et al., 1997). Instead of focusing on the sludge contents, Chen and Jeyaseelan (2001) proposed a different mechanism by a two-decomposition reaction scheme. The first reaction is primary decomposition resulting in generation of some gaseous products and intermediates decomposed at second stage. The product evolved was also slightly different from each other and from this work due to the sludge heterogeneity or even equipment used and its sensitivity.

In this work, the kinetic model proposed for sewage sludge pyrolysis (PSOM, PBSM and PMOM) correlated to different fractions decomposed at different temperatures. For example, the common type is the PBSM model, which corresponds to the two reaction scheme. Overall, the evolutions of gas are not so much different regardless the sludge types. The differences are only peak height and possibility of temperature shift. The gas evolution is just the confirmation of the stages of reaction. Although the sewage sludge pyrolysis kinetics is different among the original source, the gaseous products are qualitatively the same.

4. Conclusion

Five types of thermal decomposition behaviors of sewage sludge were observed by thermogravimetric analysis. Typically, the main decomposition of sewage sludge was in the range of 250–550 °C. The first group (Types I, II and III) was identified by main decomposition at approximately 300 °C and possible second reaction at higher temperature. Differences in the behavior may be due to different components in the sewage sludge both quantitatively and qualitatively. The second group (Types IV and V), which rarely found, has unusual properties. DTG peaks were found at 293, 388 and 481 °C for Type IV and 255 and 397 °C for Type V. The kinetics of sewage sludge pyrolysis can be described by PSOM, PBSM or PMOM. The activation energy of the first reaction, corresponding to the main pyrolysis typically at 300 °C, was rather constant (between

60.8 and 76.7 kJ mol^{-1}) whilst those of the second and third (as only in Type IV) reactions were varied in the range of 85.4–142.0 kJ mol^{-1}. Differences in the pyrolysis kinetics was laid on the second or third reactions. Typical order of the pyrolysis reaction was in the range of 1.1–1.8. Most gases evolve at a quite similar temperature regardless of the sludge type. Their evolution behaviors confirm the stages of thermal decomposition and kinetics. The pyrolysis gases comprised both saturated and unsaturated light hydrocarbons, carbon dioxide, ethanol and chloromethane.

Acknowledgements

This work was supported by the Ratchadapisakesomphot Fund of Chulalongkorn University and the Thailand Research Fund (under Waste-to-Energy Project and Royal Golden Jubilee Ph.D. Program: Grant 0051/45).

References

Caballero, J.A., Font, R., Marcilla, A., Conesa, J.A., 1997. Characterization of sewage sludges by primary and secondary pyrolysis. J. Anal. Appl. Pyrol. 40–41, 433–450.

Calvo, L.F., Otero, M., Jenkins, B.M., García, A.I., Morán, A., 2004. Heating process characteristics and kinetics of sewage sludge in different atmospheres. Thermochim. Acta 409, 127–135.

Chao, C.G., Chiang, H.L., Chen, C.Y., 2002. Pyrolytic kinetics of sludge from a petrochemical factory wastewater treatment plant—a transition state theory approach. Chemosphere 49, 431–437.

Chen, X., Jeyaseelan, S., 2001. Study of sewage sludge pyrolysis mechanism and mathematical modeling. J. Environ. Eng. 126, 585–593.

Chen, J.H., Chen, K.S., Tong, L.Y., 2001. On the pyrolysis of scrap automotive tires. J. Hazard. Mater. B 84, 43–55.

Chu, C.P., Lee, D.J., Chang, C.Y., 2000. Thermogravimetric analysis of activated sludge flocculated with polyelectrolyte. J. Environ. Eng. 126, 1082–1087.

Coats, A.W., Redfern, J.P., 1964. Kinetic parameters from thermogravimetric data. Nature 201, 68–69.

Conesa, J.A., Marcilla, A., Prats, D., Rodroguez-Pastor, M., 1997. Kinetic study of the pyrolysis of sewage sludge. Waste Manage. Res. 15, 293–305.

Conesa, J.A., Marcilla, A., Moral, R., Moreno-Caselles, J., Perez-Espinosa, A., 1998. Evolution of gases in the primary pyrolysis of different sewage sludges. Thermochim. Acta 313, 63–73.

Conesa, J.A., Marcilla, A., Caballero, J.A., Font, R., 2001. Comments on the validity and utility of the different methods for kinetic analysis of thermogravimetric data. J. Anal. Appl. Pyrol. 58–59, 617–633.

Dogru, M., Midilli, A., Howarth, C.R., 2000. Gasification of sewage sludge using a throated downdraft gasifier and uncertainty analysis. Fuel Process. Technol. 75, 55–82.

Dubdub, I.J.M., Tiong, N.P., 2001. Recycling of plastic wastes: comprehensive kinetic pyrolysis study of PVC and PET polymers using TGA. In: Proceedings of 6th World Congress of Chemical Engineer, 23–27 September, Melbourne, Australia.

Folgueras, M.B., Díaz, R.M., Xiberta, J., Prieto, I., 2003. Thermogravimetry analysis of coal and sewage sludge. Fuel 82, 1051–1055.

Gascía-Pèrez, M., Chaala, A., Yang, J., Roy, C., 2001. Co-pyrolysis of sugarcane bagasse with petroleum residue. Part I: Thermogravimetric analysis. Fuel 80, 1245–1258.

Gong, J.-S., Fu, W.-B., Zhong, B.-J., 2003. A study on the pyrolysis of asphalt. Fuel 82, 49–52.

Grønli, M.G., Várhegyi, G., Blasi, C.D., 2002. Thermogravimetric analysis and devolatilization kinetics of wood. Ind. Eng. Chem. Res. 41, 4201–4208.

Heikkinen, J.M., Hordijk, J.C., Jong, W.D., Spliethoff, H., 2004. Thermogravimetry as a tool to classify waste components to be used for energy generation. J. Anal. Appl. Pyrol. 71, 883–900.

Inguanzo, M., Domínguez, A., Menéndez, J.A., Blanco, C.G., Pis, J.J., 2002. On the pyrolysis of sewage sludge: the influence of pyrolysis conditions on solid, liquid and gas fractions. J. Anal. Appl. Pyrol. 63, 209–222.

Liu, N.A., Fan, W., Dobashi, R., Huang, L., 2002. Kinetic modeling of thermal decomposition of natural cellulosic materials in air atmosphere. J. Anal. Appl. Pyrol. 63, 303–325.

Menéndez, J.A., Domínguez, A., Inguanzo, M., Pis, J.J., 2001. Microwave pyrolysis of sewage sludge: analysis of gas fraction. J. Anal. Appl. Pyrol. 71, 657–667.

Otero, M., Díez, C., Calvo, L.F., Garcia, A.I., Morán, A., 2002. Analysis of the co-combustion of sewage sludge and coal by TG–MS. Biomass Bioenergy 22, 319–329.

Peng, W., Wu, Q., Tu, P., Zhao, N., 2001. Pyrolytic characteristics of microalgae as renewable energy source determined by thermogravimetric analysis. Bioresource Technol. 80, 1–7.

Pietro, M., Paola, C., 2004. Thermal analysis for the evaluation of the organic matters evolution during municipal solid waste aerobic composting process. Thermochim. Acta 413, 209–214.

Punnaruttanakun, P., Meeyoo, V., Kalambaheti, C., Rangsanvigit, P., Rirksomboon, T., Kitiyanan, B., 2003. Pyrolysis of API separator sludge. J. Anal. Appl. Pyrol. 68–69, 547–560.

Shen, L., Vuthaluru, H.B., Yan, H.-M., Zhang, D.K., 2001. Pyrolysis of putrescible garbage and sewage sludge mixtures in the OFS process. In: Proceedings of 6th World Congress of Chemical Engineer, 23–27 September, Melbourne, Australia.

Sørum, L., Grønli, M.G., Hustad, J.E., 2001. Pyrolysis characteristics and kinetics of municipal solid wastes. Fuel 80, 1217–1227.

Speight, J.G., 1994. Coal Technology Theory and Application. Marcel-Dekker, New York.

Thipkhunthod, P., Meeyoo, V., Rangsunvigit, P., Kitiyanan, B., Siemanond, K., Rirksomboon, T., 2005. Predicting the heating value of sewage sludges in Thailand from proximate and ultimate analyses. Fuel 84, 849–857.

Tian, F.J., Li, B.Q., Chen, Y., Li, C.Z., 2002. Formation of NO_x precursors during the pyrolysis of coal and biomass. Part V. Pyrolysis of a sewage sludge. Fuel 81, 2203–2208.

Werther, J., Ogada, T., 1999. Sewage sludge combustion. Prog. Energy Combust. 25, 55–116.

ANNEX D: The fate of trace elements in fluidised bed combustion of sewage sludge and wood.

A. Elled, L. Amand, B. Leckner, B. Andersson.

Available online at www.sciencedirect.com
ScienceDirect
Fuel 86 (2007) 843–852
FUEL
www.fuelfirst.com

The fate of trace elements in fluidised bed combustion of sewage sludge and wood

Anna-Lena Elled [a,b,*], Lars-Erik Åmand [a], Bo Leckner [a], Bengt-Åke Andersson [b]

[a] Department of Energy and Environment, Chalmers University of Technology, SE-412 96 Göteborg, Sweden
[b] University College of Borås, SE-50190 Borås, Sweden

Received 20 December 2005; received in revised form 10 August 2006; accepted 10 August 2006
Available online 11 September 2006

Abstract

Combustion tests have been carried out in a fluidised bed boiler to investigate the fate of trace elements during co-combustion of wood and municipal sewage sludge. The approach was to collect fuel and ash samples and to perform thermodynamic equilibrium calculations for gasification (reducing) and combustion (oxidising) conditions. Trace elements are found in the ash. Even most of the highly volatile Hg is captured in the bag filter ash. The bag filter ash offers higher surface area than the secondary cyclone ash and enhances the capture of Hg. There is no obvious correlation between capture and parameters investigated (sludge precipitation agent and lime addition). As, Cd, Hg, Pb, Se, Sb and Tl are predicted by equilibrium calculations to be volatile in the combustion chamber under oxidising conditions and Hg even at the filter temperature (150 °C). Reducing conditions promote, in some case more than others, the volatility of As, Cd, Pb, Sb, Se, Tl and Zn. The opposite effect was observed for Cu and Ni. Data points to the necessity of including bag filter in the gas cleaning system in order to achieve good removal of toxic trace elements.

Keywords: Co-combustion; Sewage sludge; Trace element

1. Introduction

Sludge produced by municipal waste water treatment plants has good fertiliser properties due to the high content of nutrients. Unfortunately, the content of trace elements makes the sludge unsuitable to use on farmland because of the risk of long-term contamination of the soil [1]. Landfilling of organic matter, e.g. sewage sludge, has been banned in Sweden, as well as in other European countries, and the need of alternative disposal routes increases.

Thermal processing of sewage sludge is a well proven technology, which has been practised in Europe for several years [2]. The main purpose, destruction of waste, is fulfilled at the same time as the energy is recovered and the toxic organics are destroyed. Swedish waste water treatment plants produce a small amount of sludge compared with the fuel requirements of a heat and power plant in a corresponding community. Co-combustion of sludge is, under such circumstances, favourable and associated with economical and ecological advantages but also risks [3]. The content of trace elements in sewage sludge is of crucial importance both for gaseous emissions and for the deposition of ashes, and national as well as international legislation has lately become increasingly severe [4].

The mechanisms influencing trace elements in combustion processes are complex. The fate of trace elements is influenced by the concentration and the elemental mode of occurrence in the fuel, the combustion facility, the flue gas cleaning system, the operating conditions (temperature, pressure, reducing or oxidising environment, ash formation etc.) and the presence of possible sorbents in the combustion zone [5]. In addition, the flue gas composition (HCl and SO_2) [6] and the presence of minor elements (Al, Ca,

* Corresponding author. Address: University College of Borås, SE-50190 Borås, Sweden. Tel.: +46 33 4354446.
E-mail address: annalena.elled@hb.se (A.-L. Elled).

0016-2361/$ - see front matter © 2006 Elsevier Ltd. All rights reserved.
doi:10.1016/j.fuel.2006.08.014

Fe, K, Mg, Na, P and Si) [7] are known to influence the behaviour significantly. Most of the trace elements are captured by the particle control systems, but some of the most volatile elements may escape as gaseous emissions. Hg is, for instance, a problematic element owing to its toxicity and high vapour pressure [8].

The use of sorbent to reduce trace element emissions from combustion is a recognized technique. The performance is mainly related to surface area, pore size and particle size distribution of the sorbent, but the chemical composition can be important as well. Lachas et al. [9] examined the trace element capture capabilities of kaolin and activated carbon. Kaolin was the better sorbent for Cd and Pb, and activated carbon was more effective for Hg and Se. The captured species on kaolin tended to be retained as an even layer of low concentration over most of the surface, while the captured species on activated carbon appeared mostly to be concentrated in discrete locations.

Gullet and Ragnunathan [10] tested sorbent injection during coal combustion. Hydrated lime increased the recovery of Se. Hydrated lime and limestone increased the recovery of Sb, As and Cd and kaolinite increased the recovery of Cd and Pb. The calcium-based sorbents reduced the submicrometer concentrations of the more volatile metals As, Hg, Sb and Se. Gale and Wendt [11] investigated the capture of Cd by hydrated lime and kaolinite and found that it was effectively captured by both at high temperatures through chemical reaction.

Yao et al. [12] investigated the performance of aluminosilicate- and calcium-based sorbents during sewage sludge combustion. Kaolin was found to capture trace metals effectively. Calcium-based sorbents showed some capture ability of Pb and Cd, although the effectiveness was low compared to kaolin. Kaolin shifted the distribution of Pb and Cd in the ash from fine to coarse particles and the products were insoluble in water because of reaction between kaolin and the elements [13].

Diaz-Somoano and Martínez-Tarazona [14] evaluated the retention of Zn in kaolin, limestone, alumina and fly ash during coal gasification. Alumina turned out to be the most effective sorbent. Fly ash, with high calcium content, retained Zn as well although in lower proportions. Chicken-waste wood ceramics is another example of possible sorbent. It is a porous, carbonaceous material formed by impregnating a thermosetting resin into biomass materials based on chicken-wastes (litter) and carbonizing at a high temperature. It was found to function like active carbon and it was presumed that the content of impurities in the material (Ca, K and S) increased the sorption capacity for Hg [15].

It has been concluded earlier that, despite the increased input of trace elements with sewage sludge to the combustion process, the emissions of metal compounds are well below the legal limits in the EU [16]. The present project traces the fate of elements during co-combustion of sewage sludge with wood and the main object is to determine the reason for the good capture performance. Special attention is directed to retention capacity of present fly ash and influence of reducing and oxidising conditions, type of sludge and lime addition on the distribution of trace elements.

2. Experiments

2.1. Boiler, sampling and analyses

The 12 MWth circulating fluidized bed (CFB) boiler located at Chalmers University of Technology was used for the experiments. The boiler produces heat and power and is equipped with advanced measurement techniques, specially adapted for research purposes. The facility is described elsewhere [16]. The boiler is equipped for research, but similar to conventional commercial units, with the exception that the flue gas cleaning downstream the convection path (at 150 °C) is divided into two steps: a secondary cyclone and a bag filter.

Fuel was sampled from the input streams of wood pellets and municipal sewage sludge. Samples of the solids in the combustion chamber were taken in the bottom of the chamber and in the return leg following the primary cyclone at a temperature of 850 °C. Fly ashes were sampled from the secondary cyclone and from the bag filter, both at 150 °C. The content of moisture, combustibles and ash were analysed by a MAC 400 Proximate Analyzer 785–700 system. The main components were analysed by XRF (X-ray fluorescence) and the trace elements by ICP-MS (inductive coupled plasma-mass spectrometer). Hg, as an exception, was detected by CVA (cold vapor atomic absorption). The particle size distributions of the secondary cyclone and the bag filter ashes were analysed using an ultrasonic bath and a laser diffractometer.

2.2. Fuels

The fuel mixes were chosen to achieve large differences between the tests concerning the trace elements and the content of Al, Fe, and Ca in the system. The base fuel burned was well defined and homogenous wood pellets (WP). The additional fuels were digested and mechanically dewatered municipal sewage sludges (MSS) produced in two wastewater treatment plants. Ryaverket is the second largest wastewater treatment plant in Sweden and takes care of wastewater from 775 000 inhabitants of the city of Göteborg and its surroundings. Ryaverket employs iron sulphate ($Fe_2(SO_4)_3$) for phosphorous removal. Nolhagaverket, situated in Alingsås, treats wastewater from 42 000 inhabitants and uses aluminium sulphate ($Al_2(SO_4)_3$) as precipitation agent. The properties of the fuels investigated are given in Table 1. The degree of contamination with trace element in the sludge is shown in Table 2. Ryaverket, situated in the large city, produces a

Table 1
Fuel analysis

Fuel	MSS	MSS	WP
Plant	Ryaverket	Nolhagaverket	
Precipitation chemical	$Fe_2(SO_4)_3$	$Al_2(SO_4)_3$	
Proximate analysis			
Water (% by mass, raw[a])	72.0	77.8	8.0
Ash (% by mass, dry)	46.0	42.6	0.4
Combustibles (% by mass, dry)	54.0	57.4	99.6
Volatiles (% by mass, daf[b])	94.4	85.3	81.7
Ultimate analysis (% by mass, daf[b])			
C	52.6	50.2	50.3
Cl	0.1	0.1	0.01
H	7.2	7.3	6.1
N	5.4	5.0	0.09
O	33.3	36.2	43.5
S	1.4	1.2	0.01
Lower heating value (MJ/kg)			
Hu, daf	20.50	19.50	18.80
Hu, raw	2.78	2.24	17.20
Ash analysis (g/kg dry ash)			
Al	73.3	193	12.2
Ca	40.0	38.0	164
Fe	160	42.1	20.9
K	13.3	10.7	82
Mg	9.9	5.3	26.4
Na	7.28	6.9	6.7
P	58.6	61.3	12.7
Si	127	115	79.7
Ti	4.4	9.6	0.7

[a] raw = as received.
[b] daf = dry and ash free.

Table 2
Fuel analysis

Fuel	MSS	MSS	WP
Plant	Ryaverket	Nolhagaverket	
Precipitation chemical	$Fe_2(SO_4)_3$	$Al_2(SO_4)_3$	
Trace elements (mg/kg dry fuel)			
As	5.9	5.2	0.12
Cd	0.86	0.53	0.11
Co	6.9	2.8	0.04
Cr	31	43	0.64
Cu	394	266	2.6
Hg	1.2	0.77	0.02
Mn	296	299	119
Ni	21	13	0.20
Pb	38	17	0.35
Sb	13	15	0.06
Se	13	15	5.0
Tl	9.4	10	0.06
V	23	23	0.06
Zn	652	385	15

sewage sludge that is more contaminated with trace elements than that originating from the small town.

Table 3
Test matrix

	Fuel	Precipitation chemical	Lime addition
Rya	MSS + WP	$Fe_2(SO_4)_3$	None
Aling	MSS + WP	$Al_2(SO_4)_3$	None
Rya + lime	MSS + WP	$Fe_2(SO_4)_3$	To the bed
Aling + lime	MSS + WP	$Al_2(SO_4)_3$	To the bed

Table 4
Operating conditions

Test series	Average	S-dev
Experimental time (h)	8.0	2.7
Load, MWth	6.1	0.2
Bed temperature, °C (bottom)	848	4.0
Bed temperature, °C (top)	863	12.4
Exit temperature of after burning chamber, °C	858	6.7
Temperature after economiser, °C	150	0.2
Temperature after bag filter, °C	149	2.0
Total riser pressure drop (kPa)	6.4	0.1
Excess air ratio	1.2	0.01
Primary air flow/total air flow (%)	56.2	4.2
Superficial flue gas velocity at top of riser U_{top} (m/s)	5.3	0.1

2.3. Experimental procedure

The experimental matrix is seen in Table 3. It comprises four test series: Rya, Aling, Rya + lime and Aling + lime. Each series consists of a reference test, in which only pure WP is burned, and two additional tests with sludge added to represent around 7 and 14% of the total dry mass flow to the combustion chamber. The parameters that were actively changed were the amount of sludge, the type of sludge and the lime addition ($CaCO_3$). The operating conditions are seen in Table 4. They are typical for a commercial, full scale CFB unit producing heat and/or power.

3. Theoretical analysis

The purpose of the calculation of chemical equilibria is to support the experimental investigation and facilitate interpretation of the measured data. The computer program FactSage is used and the thermodynamic data are collected from the database F*A*C*T [17].

The equilibrium composition is calculated at normal atmospheric pressure in 40 temperature steps between 25 and 1000 °C. Particular attention is given to 850 °C, as it is the bed temperature. The equilibrium composition in the convection pass is investigated at 400 and 150 °C. The input data (Al, C, Ca, Cl, Fe, H, K, Mg, N, O, P, S and Si and one trace element at a time) are estimated from the measured flows of fuel, air and lime to the boiler and related analyses. Gas, pure solids and pure liquids are considered. The effect of reducing and oxidising conditions on the fate of trace elements is investigated as well. Reducing

conditions are modelled by cutting the air supply and let the only oxygen available for reaction be that contained in the fuel. Oxidising conditions correspond to the experimental air ratio 1.2.

4. Results

4.1. Ash and element balances

The ash flows can be seen in Table 5. In the reference test (WP) the bed ash flow, diluted by sand in the bed, was several times higher than the fly ash flow. The reason is that extensive regeneration of the bed was carried out by removing bed material and adding pure silica sand in order to prevent agglomeration.

Mass and element balances verify the accuracy of the measurements. As seen in Table 6 the closures of total balances are rather good, except in the test with pure wood that can be explained by the low ash content in the fuel, leading to a modest ash flow and, hence, larger uncertainties in the measured values. In the case of a small ash flow from the fuel, the closure of such a balance is more sensitive to small disturbances in the system, e.g. temporary accumulation of ashes on tubes or other internal surfaces. The closures of the element balances are fairly good with some exceptions. Most of them can be explained, as previously, by low ash flows or accumulation in the system during prior tests and insufficient experimental time to achieve steady state in the ash composition. The large deviations regarding Sb and Tl most likely depend on underestimated concentrations of the elements in the fuels.

4.2. Coefficient of relative increase (CORI)

Substituting wood with sludge while keeping the load of the boiler constant has certain consequences. The sludge contains large fractions of water and ash, and the net calorific value is low compared to that for wood. The concentrations of S, Cl and trace elements are higher in sludge as well. The coefficient of relative increase (CORI) of ash Eq. (1) and trace elements Eq. (2) [16] describe the rate by which ash and trace elements are increased during co-combustion.

$$\frac{a_s H_w}{a_w H_s} - 1 \tag{1}$$

$$\frac{c_{is} a_s H_w}{c_{iw} a_w H_s} - 1 \tag{2}$$

Table 5
Ash flows (kg/h)

Series	WP	Rya			Aling		Rya + lime		Aling + lime		
wf[a]	0%	7%	7%	15%	6%	13%	8%	15%	6%	13%	12%
Bed ash	17	21	33	20	24	47	27	27	24	21	38
Secondary cyclone ash	5	51	44	79	31	46	53	94	36	61	72
Bag filter ash	2	3	7	8	5	6	7	11	6	14	9
Total ash flow	24	74	84	107	59	98	87	132	66	96	119

[a] wf = waste fraction; kg dry sludge/(kg dry sludge + kg dry wood).

Table 6
Mass- and element balances

Series	WP	Rya			Aling		Rya + lime		Aling + lime		
wf[a]	0%	7%	7%	15%	6%	13%	8%	15%	6%	13%	12%
Total ash balances (out/in × 100)											
	120	98	83	88	96	97	98	98	87	97	89
Total element balances (out/in × 100)											
As	233	106	72	114	129	100	123	113	126	123	88
Cd	196	124	103	159	146	164	103	121	92	98	124
Co	276	103	131	112	111	88	154	137	185	169	169
Cr	744	78	95	79	66	63	90	80	74	54	55
Cu	135	71	73	69	58	35	92	90	65	75	96
Hg	16	48	70	76	72	71	72	79	69	109	81
Mn	118	131	103	157	133	133	101	125	86	134	131
Ni	350	96	131	98	172	74	122	109	126	114	100
Pb	229	106	90	111	101	72	115	109	100	119	136
Sb	128	22	72	17	22	18	27	21	25	20	22
Tl	88	33	75	26	33	27	40	31	37	30	32
V	725	88	158	96	95	78	137	124	143	118	144
Zn	134	124	85	104	93	69	112	107	65	61	78

[a] wf = waste fraction; kg dry sludge/(kg dry sludge + kg dry wood).

a_s = ash content in the sludge, kg ash/kg dry wood,
a_w = ash content in the wood, kg ash/kg dry wood,
c_{is} = concentration of element i in the ash of sludge, kg i/kg dry ash,
c_{iw} = concentration of element i in the ash of wood, kg i/kg dry ash,
H_s = lower calorific value of sludge, MJ/kg,
H_w = lower calorific value of wood, MJ/kg.

Table 7 shows CORI values for the two MSS investigated when co-fired with WP. The value becomes zero if the base fuel and the co-fuel have the same properties. A CORI value of 200 corresponds to an increase of the trace element flow to the boiler of 18 times at a waste fraction of 15% or, expressed as energy fraction, around 10%. In general, the values of the sludge precipitated with $Fe_2(SO_4)_3$ are higher than those for the sludge precipitated with $Al_2(SO_4)_3$ with exception for Cr, Sb and Tl. The higher CORI values indicate once again that the large city sewage sludge is more contaminated compared to the small town sewage sludge.

Table 7
The coefficients of relative increase (CORI) of ash and trace elements

Additional fuel	Rya	Aling
Trace elements CORI[a]		
As	89	76
Cd	14.5	8.39
Co	301	119
Cr	91.4	124
Cu	288	191
Hg	109	70.8
Mn	3.70	3.67
Ni	200	121
Pb	207	87.6
Sb	420	451
Se	n.a.[b]	n.a.[b]
Tl	286	301
V	718	706
Zn	79	45
Ash CORI[a]	216	196

[a] CORI: according to [16].
[b] not analysed.

4.3. Relative enrichment

The ratio of the analysed concentration of a specific element in an ash and the theoretical average concentration in the total ash of the same element is called the relative enrichment (RE) [16]. Table 8 shows the RE from the reference test with pure WP and from the actual tests. The later values are average values at two different waste fractions (7 and 14%). RE of Cr, Sb, V and possibly Ni decreases with increasing waste fraction whereas the general trend for RE of the remaining elements is increasing. RE of Sb, Se and Tl are low in all ashes. The elements Cr, Cu and Zn show all the same trend: higher RE in the fly ash than in the bed ash and the difference between the secondary cyclone ash and the bag filter ash is small. The elements As, Cd, Co, Hg, Mn, Ni, Pb and V are enriched in the filter ash. The complete values of RE are found in Appendix, Table A.1.

Fig. 1 shows a close up on the RE of Hg, Cd, Pb and Mn. The relative enrichment of the volatile Hg is close to zero in the bed ash, higher in the secondary cyclone ash and highest in the bag filter ash. The less volatile Cd is enriched in the bag filter ash but also in the secondary cyclone ash. Pb is usually regarded to belong to the same volatile group as Cd and the enrichment is confirmed for the tests Rya + lime and Aling + lime. Cd appears more volatile than Pb in the tests Rya and Aling. Mn was chosen to represent the non-volatile group of trace elements, but the result indicates that Mn leaves the bed. It was pointed out earlier that the enrichment of Mn may depend on formation of fine ash particles that are mainly found in the filter ash [16].

Table 8
Average relative enrichment of trace elements in the ashes

wf[a]	Bed ash			Secondary cyclone ash			Filter ash		
	WP	MSS 7%	MSS 14%	WP	MSS 7%	MSS 14%	WP	MSS 7%	MSS 14%
As	0.13	0.40	0.45	1.02	0.82	0.90	1.27	3.69	3.37
Cd	0.03	0.26	0.46	0.59	1.37	1.44	1.79	2.33	3.77
Co	0.36	0.4	0.48	0.77	1.09	1.15	1.74	3.58	3.63
Cr	0.93	0.24	0.24	1.67	0.77	0.69	2.54	1.34	1.10
Cu	0.17	0.12	0.20	0.27	0.72	0.77	0.46	0.95	1.03
Hg	0.01	0.02	0.02	0.02	0.44	0.59	0.18	2.98	4.17
Mn	0.06	0.45	0.56	0.25	1.04	1.18	0.95	5.19	6.29
Ni	0.43	0.72	0.4	1.48	0.94	0.93	2.68	2.66	2.09
Pb	0.12	0.17	0.33	0.71	1.08	1.19	1.81	1.25	1.47
Sb	0.25	0.23	0.16	0.26	0.23	0.16	0.85	0.49	0.33
Se	0.01	0.06	0.1	0.01	0.03	0.05	0.01	0.07	0.11
Tl	0.10	0.29	0.23	0.11	0.3	0.24	0.49	0.63	0.5
V	1.06	0.41	0.46	3.16	0.92	0.97	4.87	3.26	2.66
Zn	0.12	0.18	0.24	0.45	1.09	0.97	0.31	0.74	0.87

[a] wf = waste fraction; kg dry sludge/(kg dry sludge + kg dry wood).

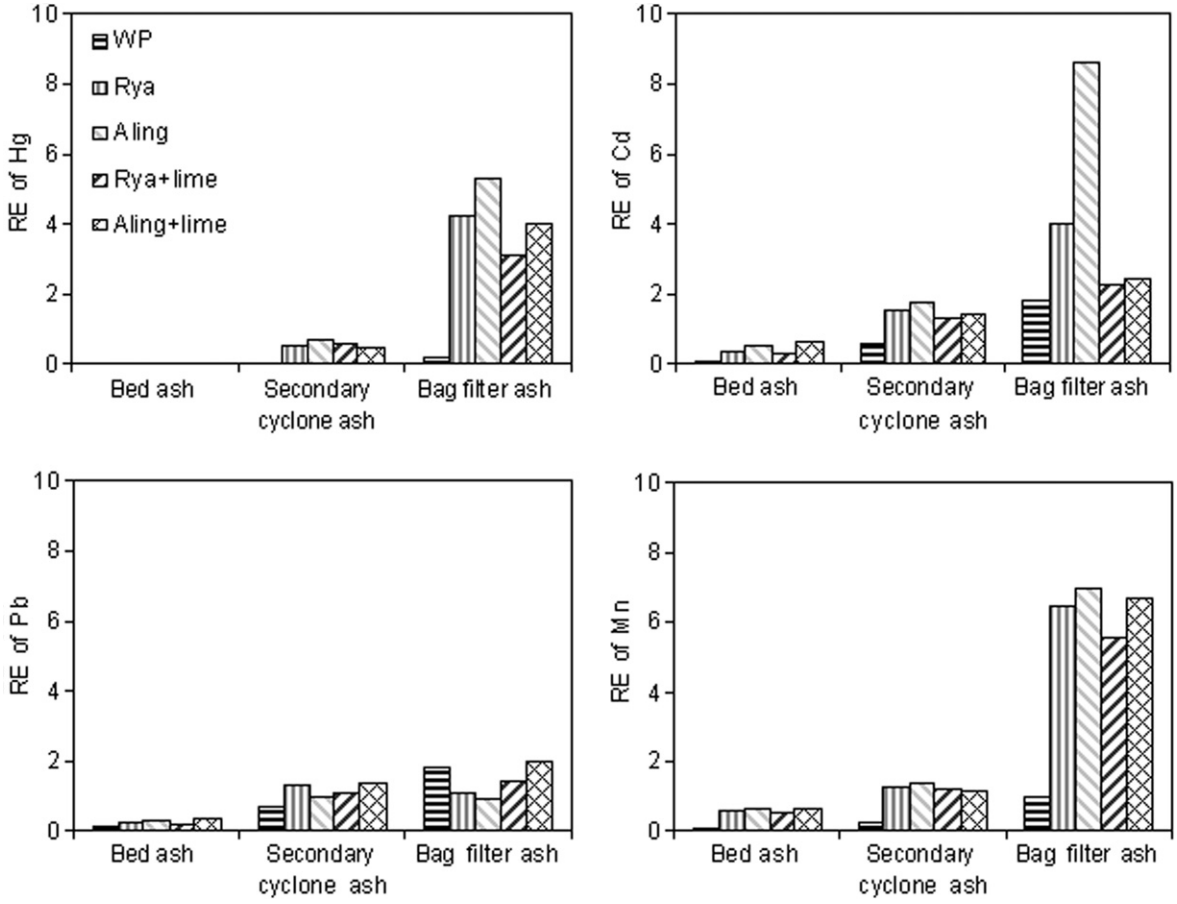

Fig. 1. The relative enrichment of Hg, Cd, Pb and Mn in the ashes.

4.4. Particle size distribution

Fig. 2A and B is an example of the particle size distribution in the secondary cyclone and the bag filter ash, respectively. The results are similar in all tests. In general, 70% of the particles in the secondary cyclone ash are 42 μm or smaller. The corresponding value in the bag filter ash is 6 μm. The secondary cyclone ash sample consists to 90%

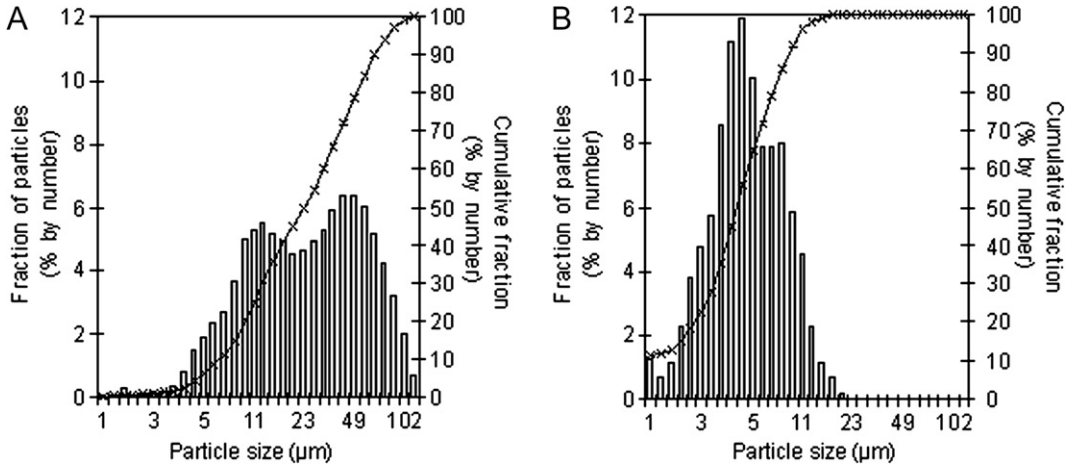

Fig. 2. Particle size distribution (% by number) in (A) secondary cyclone ash and (B) bag filter ash from Rya (μm). Lines – cumulative, bars – fractional distributions.

Table 9
The relative particle surface area (A) and concentration of Hg (C) in the bag filter ash compared with the secondary cyclone ash

	Rya	Aling	Rya + lime	Aling + lime
$A_{\text{bag filter ash}}/A_{\text{secondary cyclone ash}}$	1.28	1.18	1.44	1.43
$C_{\text{Hg, bag filter ash}}/C_{\text{Hg, secondary cyclone ash}}$	8.00	7.88	5.53	8.08

of particles between 9 and 88 μm. The same range for the samples taken from the bag filter ash is between 2 and 11 μm. Data on commercially available activated carbon and hydrated lime show that the size distributions are in the same range as the present filter ash.

Ratios of particle surface area in the bag filter ash to that of the secondary cyclone ash are seen in Table 9. The ratios increase slightly with lime addition and show that the particle surface area available for adsorption is larger in the bag filter ash than in the secondary cyclone ash. The same table shows that the ratio of the Hg concentration in the bag filter ash to that in the secondary cyclone ash is several times higher than the surface ratio, which indicates that it is not only the increased particle surface area that causes the good capture of Hg.

4.5. Thermodynamic equilibrium analyses

The trace elements Co, Cr, Cu, Mn, Ni, V and Zn are predicted to be non-volatile under oxidising conditions (150, 450 and 850 °C). The elements As, Cd, Hg, Pb, Se, Sb and Tl are all predicted to be found in the flue gas at 850 °C. The condensation temperature of As is slightly lower in the cases with sludge from Ryaverket. A few percentage of Cd is volatile in the convection pass at 400 °C but condensed at 150 °C. Hg is predicted to be completely volatilised at both temperatures. The predictions of Pb in the convection pass vary between the calculated cases due to differences in the stability range of $PbCl_2$. A few percentage of Pb is found in the flue gas at 150 °C in the cases Rya, Rya + lime and Aling + lime. Se is predicted to be completely volatilised at 400 °C but condensed at 150 °C.

The volatility of Co, Cr, Hg, Mn, Ni and V is not sensitive to reducing environment even if changes in the equilibrium composition of metal compounds in some cases are discerned. Co, Cr, Mn and V are found in the condensed phase during the whole temperature interval investigated, in contrast to Hg that is found in the gas phase. The volatility of As, Cd, Cu, Pb, Sb, Se, Tl and Zn in case Rya is seen in Fig. 3. The figure shows the mole percentage

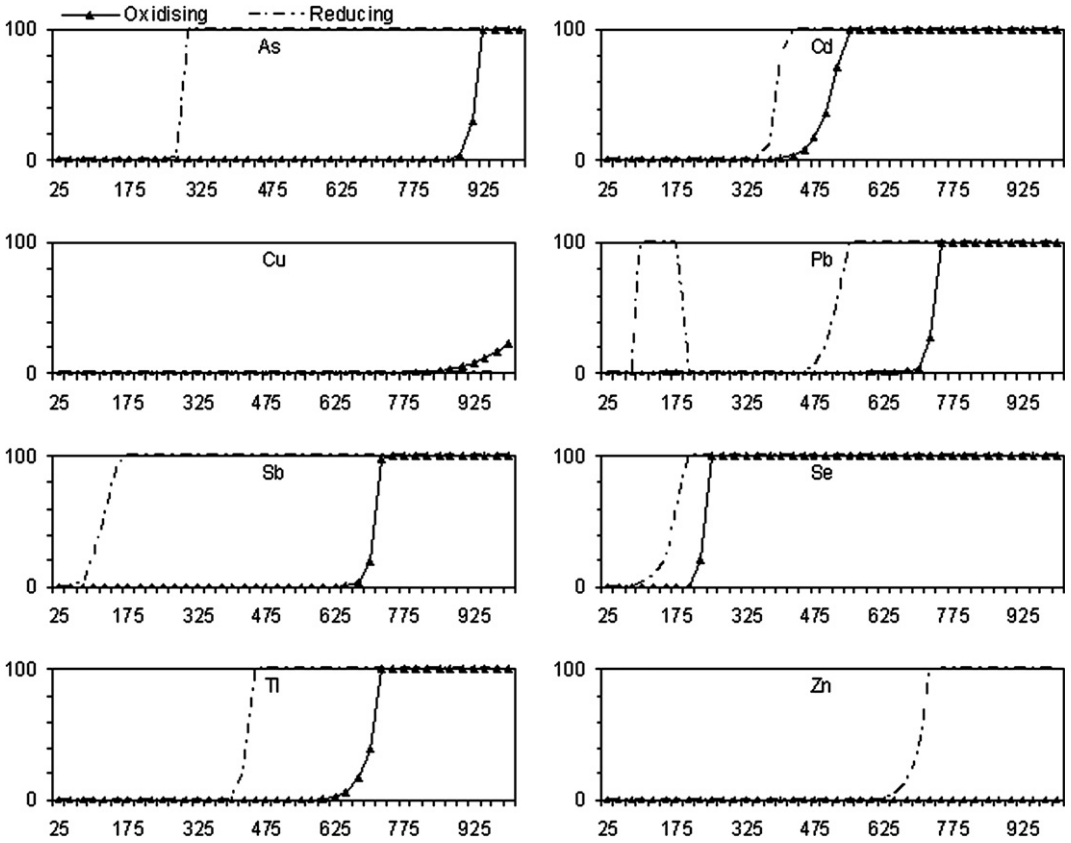

Fig. 3. Trace elements (% by mole) in the flue gas under oxidising and reducing conditions as a function of temperature (°C).

of a species found in the flue gas as a function of temperature during oxidising and reducing conditions. Reducing conditions promotes, in some case more than others, the volatility of As, Cd, Pb, Sb, Se, Tl and Zn. Reducing conditions seems to reduce the volatility of Cu at combustion temperatures. The same tendency, though less pronounced, is seen in the case of Ni (not shown in Fig. 3).

5. Discussion

The trace elements are found in various elemental and oxidised forms at different phases during combustion. They are typically enriched in fine particles due to vaporisation, nucleation and condensation mechanisms, and some may form submicron aerosols, which are difficult to control.

The experimental part of the investigation shows that the capture of trace elements performs well during co-combustion of sewage sludge and wood despite the increased flow of trace elements to the boiler. The theoretical calculation shows, on the other hand, that some of the trace elements are, from a thermodynamic point of view, inclined to be released and to be present in the flue gas even at low temperatures. Hg runs an obvious risk to be emitted, but also Pb, Sb and Se may escape under reducing conditions. The reason for the good capture during the tests is not simple to explain and is most likely due to a variety of interacting causes.

Injection of sorbent into the flue gas is a relatively simple approach to control trace element emissions. Activated carbon [8,9,15], aluminosilicate [9–13] and calcium-based sorbents [10–12], fly ash, alumina [14] and chicken-waste wood ceramics [15], all show some kind of capture abilities due to physical attraction or/and chemical reaction. Co-combustion of WP and MSS may give rise to the effects that have been shown in the work quoted, since the ash is rich on several of the active elements mentioned. The sludge contains, for instance, zeolites [18] which are shown to capture alkali metals during co-combustion of biofuels and sewage sludge [19]. It is likely that zeolites also are able to capture other metals since it is composed by the same elements as kaolin. The content of alkali metals in the wood may contribute to the capture by formation of small particles which are collected in the bag filter. Such particles, related to high surface area and perhaps to stickiness, are attractive final destinations for volatile trace elements. The level of Hg capture is known to correlate with the carbon-in-ash and the most effective fly ashes are those with unburned carbon content greater than 7% [8]. However, the carbon content in ashes from co-combustion of WP and MSS is in general lower than this value. Analyses of the bag filter ash from tests with lime addition show, to some extent, elevated content of unburned carbon (<10%) available to take part in the capture of Hg.

The system for removal of particles from the flue gas is also of importance. The secondary cyclone separates particles in the hot flue gas mechanically. The smaller particles pass the secondary cyclone and follow the flue gas to the bag filter. Particles and liquids that are not able to penetrate the filter are retained on the filter surface and form a filter cake. At regular intervals the filter is shaken and the filter cake falls apart and the fly ash is collected. The residence time of the particles is relatively long, since the filter cake can build up for several hours. This has a positive effect on the separation of heavy metals from the flue gas. The measured enrichment ratios in this investigation clearly show the need for bag filters included in the flue gas cleaning system to achieve high trace element capture levels.

6. Conclusions

- The supply of ash and trace elements to the combustion process increases dramatically when wood is replaced with municipal sewage sludge under otherwise constant conditions. The sewage sludge from the large city is more contaminated with trace elements than that from the small town.
- The trace elements are found in the ashes and especially in the filter ash having the smallest particle size fraction. Type of sludge or lime addition did not show any general trend of change in the capture of trace elements.
- The prediction of the fate of trace elements agrees fairly well with the experimental data with some exceptions, e.g. Hg. Co, Cr, Cu, Mn, Ni, V and Zn are predicted to be present in the condensed process-stream of the unit under oxidising conditions, thus retained in the ash. As, Cd, Hg, Pb, Se, Sb and Tl are predicted to be found in the flue gas at 850 °C.
- Hg is predicted to be completely volatilised in the boiler convection pass. A fraction of Cd is volatile at 400 °C but completely condensed at 150 °C. A few mole percentage of Pb are predicted to be volatile at 150 °C.
- Reducing conditions promotes the volatility of As, Cd, Pb, Sb, Se, Tl and Zn while the volatility of Cu and Ni is reduced.
- In contrast to the predictions, Co, Mn and Ni are enriched in the filter ash and the result indicates that they are released from the bed. The trace elements predicted to be volatile at combustion conditions are all, more or less, enriched in the filter ash, hence condensation on submicron particles is probably occurring.
- The higher available particle surface area in the filter ash enhances the capture of trace elements, e.g. Hg. The ash composition is likely to contribute to capture as well since it is rich on several elements known to retain trace elements.

Appendix

See Table A.1.

Table A.1
The relative enrichment of trace elements in the ashes

Series	WP	Rya			Aling		Rya + lime		Aling + lime		
wf[a]	**0%**	7%	**7%**	7%	**6%**	13%	**8%**	7%	**6%**	13%	**12%**
Relative enrichments of trace elements in the bed material											
As	**0.13**	0.44	**0.24**	0.44	**0.43**	0.44	**0.45**	0.45	**0.46**	0.45	**0.45**
Cd	**0.03**	0.2	**0.23**	0.36	**0.32**	0.55	**0.19**	0.32	**0.34**	0.42	**0.65**
Co	**0.36**	0.16	**0.41**	0.34	**0.43**	0.4	**0.40**	0.45	**0.58**	0.62	**0.6**
Cr	**0.93**	0.22	**0.26**	0.29	**0.22**	0.29	**0.25**	0.24	**0.23**	0.17	**0.2**
Cu	**0.17**	0.11	**0.09**	0.19	**0.17**	0.16	**0.1**	0.19	**0.14**	0.21	**0.26**
Hg	**0.01**	0.02	**0.02**	0.02	**0.02**	0.03	**0.02**	0.02	**0.03**	0.03	**0.03**
Mn	**0.06**	0.62	**0.41**	0.61	**0.54**	0.64	**0.37**	0.51	**0.31**	0.43	**0.62**
Ni	**0.43**	0.2	**0.44**	0.34	**2.12**	0.34	**0.36**	0.44	**0.51**	0.48	**0.4**
Pb	**0.12**	0.09	**0.13**	0.29	**0.28**	0.34	**0.11**	0.22	**0.25**	0.39	**0.39**
Sb	**0.25**	0.16	**0.48**	0.15	**0.16**	0.16	**0.17**	0.16	**0.17**	0.16	**0.16**
Se	**0.01**	0.06	**0.07**	0.11	**0.06**	0.09	**0.07**	0.11	**0.06**	0.09	**0.09**
Tl	**0.10**	0.24	**0.48**	0.23	**0.24**	0.23	**0.25**	0.23	**0.25**	0.24	**0.24**
V	**1.06**	0.27	**0.54**	0.41	**0.34**	0.4	**0.5**	0.49	**0.41**	0.40	**0.62**
Zn	**0.12**	0.15	**0.13**	0.29	**0.33**	0.31	**0.1**	0.21	**0.18**	0.16	**0.23**
Relative enrichments of trace elements in the secondary cyclone ash											
As	**1.02**	0.88	**0.49**	0.89	**0.88**	0.89	**0.93**	0.93	**0.93**	0.91	**0.90**
Cd	**0.59**	1.40	**1.36**	1.57	**1.48**	1.79	**1.27**	1.29	**1.34**	1.21	**1.37**
Co	**0.77**	0.95	**1.04**	1.23	**1.11**	1.12	**1.17**	1.12	**1.19**	1.08	**1.22**
Cr	**1.67**	0.76	**0.90**	0.84	**0.70**	0.79	**0.78**	0.74	**0.70**	0.54	**0.53**
Cu	**0.27**	0.70	**0.76**	0.77	**0.64**	0.48	**0.83**	0.87	**0.68**	0.80	**0.92**
Hg	**0.02**	0.41	**0.46**	0.53	**0.48**	0.68	**0.43**	0.56	**0.42**	0.66	**0.51**
Mn	**0.25**	1.24	**0.93**	1.22	**1.09**	1.32	**1.08**	1.18	**0.85**	1.07	**1.14**
Ni	**1.48**	0.88	**1.02**	1.06	**0.87**	0.95	**1**	0.94	**0.94**	0.86	**0.83**
Pb	**0.71**	1.1	**0.96**	1.26	**1.18**	0.96	**1.13**	1.07	**1.04**	1.23	**1.42**
Sb	**0.26**	0.16	**0.49**	0.16	**0.16**	0.16	**0.17**	0.16	**0.17**	0.16	**0.16**
V	**0.01**	0.03	**0.04**	0.05	**0.03**	0.05	**0.03**	0.06	**0.03**	0.05	**0.05**
Tl	**0.11**	0.24	**0.49**	0.23	**0.24**	0.24	**0.25**	0.24	**0.26**	0.24	**0.24**
V	**3.16**	0.72	**1.08**	1	**0.89**	0.95	**0.91**	0.91	**1.01**	0.91	**1.08**
Zn	**0.45**	1.33	**1**	1.18	**1.08**	0.94	**1.2**	1.16	**0.82**	0.73	**0.84**
Relative enrichments of trace elements in the filter ash											
As	**1.27**	3.45	**1.97**	4.68	**5.83**	5.2	**2.82**	2.78	**4.38**	3.60	**0.6**
Cd	**1.79**	1.53	**1.33**	3.99	**5.44**	8.63	**1.33**	2.23	**2.03**	1.62	**2.40**
Co	**1.74**	2.85	**2.46**	1.42	**2.15**	1.78	**3.20**	3.33	**7.23**	5.54	**6.07**
Cr	**2.54**	1.26	**1.54**	1.07	**1.05**	1.25	**1.39**	1.38	**1.44**	0.94	**0.87**
Cu	**0.46**	0.90	**0.88**	0.82	**0.86**	0.39	**1.22**	1.17	**0.90**	1.04	**1.73**
Hg	**0.18**	2.32	**2.69**	4.27	**4.09**	5.34	**2.86**	3.12	**2.95**	4.02	**4.08**
Mn	**0.95**	5.39	**5.39**	6.47	**5.80**	6.96	**3.91**	5.58	**5.48**	5.74	**6.71**
Ni	**2.68**	2.66	**2.88**	1.19	**1.68**	1.51	**2.16**	2.07	**3.91**	3.07	**2.61**
Pb	**1.81**	1.12	**0.92**	1.09	**1.41**	0.91	**1.1**	1.42	**1.70**	1.98	**1.95**
Sb	**0.85**	0.33	**1.04**	0.32	**0.34**	0.32	**0.37**	0.35	**0.38**	0.34	**0.34**
Se	**0.01**	0.07	**0.08**	0.11	**0.06**	0.1	**0.07**	0.12	**0.06**	0.10	**0.1**
Tl	**0.49**	0.5	**1.04**	0.48	**0.5**	0.48	**0.55**	0.52	**0.57**	0.51	**0.51**
V	**4.87**	3.07	**3.81**	1.4	**2.11**	1.41	**3.04**	3.55	**4.27**	3.11	**3.83**
Zn	**0.31**	0.63	**0.57**	0.99	**1.00**	0.95	**0.81**	0.64	**0.66**	0.74	**1.04**

[a] wf = waste fraction; kg dry sludge/(kg dry sludge + kg dry wood).

References

[1] Eriksson J. Halter av 61 spårelement i avloppsslam, stallgödsel, handelsgödsel, nederbörd samt jord och gröda (Concentrations of 61 trace elements in sewage sludge, manure from pigs and cattle, rainfall, soil and plants). Stockholm: Naturvårdsverket (Swedish Environmental Protection Agency); 2001. Report 5148.

[2] Werther J, Ogada T. Sewage sludge combustion. Prog Energy Combust Sci 1999;25:55–116.

[3] Åmand L-E, Leckner B, Lücke K, Werther J. Advanced air staging techniques to improve fuel flexibility, reliability and emissions in fluidized bed co-combustion. Stockholm: Värmeforsk Service AB; 2001. Report 756 of project F6-678. ISSN 0282-3772.

[4] Commission of the European Communities, European Parliament and Council. Directive 2000/76/EC On Incineration of Waste. Official Journal of the European Communities 2000; L283/33.
[5] Sloss LL, Smith IM. Trace element emissions. London: IEA Coal Reasearch; 2000, ISBN 92-9029-344-6.
[6] Miller BB, Dugwell DR, Kandiyoti R. The influence of injected HCl and SO_2 on the behaviour of trace elements during wood-bark combustion. Energy Fuels 2003;17:1382–91.
[7] Miller BB, Kandiyoti R, Dugwell DR. Trace element emissions from co-combustion of secondary fuels with coal: a comparison of bench-scale experimental data with predictions of a thermodynamic equilibrium model. Energy Fuels 2002;16:956–63.
[8] Sloss LL. Mercury – emissions and control. London: IEA Coal Reasearch; 2000, ISBN 92-9029-371-3.
[9] Lachas H, Herod AA, Reed GP, Dugwell DR, Kandiyoti R. Trace element removal from hot flue gases: screening sorbents for performance and product leachability. Energy Fuels 2003;17:521–31.
[10] Gullet B, Ragnunathan K. Reduction of coal-based metal emissions by furnace sorbent injection. Energy Fuels 1994;8:1068–76.
[11] Gale TK, Wendt JOL. In-furnace capture of cadmium and other semi-volatile metals by sorbents. Proc Combust Inst 2005;30: 2999–3007.
[12] Yao H, Mkilaha ISN, Naruse I. Screening of sorbents and capture of lead and cadmium compounds during sewage sludge combustion. Fuel 2004;83:1001–7.
[13] Yao H, Naruse I. Control of trace metal emissions by sorbents during sewage sludge combustion. Proc Combust Inst 2004;30:3009–16.
[14] Diaz-Somoano M, Martínez-Tarazona MR. Retention of Zn Compounds in solid sorbents during hot gas cleaning processes. Energy Fuels 2005;19:442–6.
[15] Ozao R, Okabe T, Nishimoto Y, Cao Y, Whitely N, Pan W-P. Gas and mercury adsorption properties of woodceramics made from chicken waste. Energy Fuels 2005;19:1729–34.
[16] Åmand L-E, Leckner B. Metal emissions from co-combustion of sewage sludge and coal/wood in fluidized bed. Fuel 2004;83:1803–21.
[17] Bale CW, Chartrand P, Degterov SA, Eriksson G, Hack K, Mahfoud BR, Melançon J, Pelton AD, Petersen S. Factsage thermochemical software and databases. Calphad 2002;26:189–228.
[18] Kurzendörfer CP, Kuhm P, Steber J. Zeolites in the environment. In: Schwuger MJ, editor. Detergents in the environment. New York: Marcel Decker Inc.; 1996, ISBN 0-8247-9396-X. p. 128–88.
[19] Åmand L-E, Leckner B, Eskilsson D, Tullin C. Deposition on heat transfer tubes during co-combustion of biofuels and sewage sludge. Fuel 2006;85:1313–22.

ANNEX E: Study on the ash fusion temperatures of coal and sewage sludge mixtures.

L. Weidong, L.Ming, L.Weifeng, L. Haifeng

Fuel 89 (2010) 1566–1572

Contents lists available at ScienceDirect

Fuel

journal homepage: www.elsevier.com/locate/fuel

Study on the ash fusion temperatures of coal and sewage sludge mixtures

Li Weidong, Li Ming, Li Weifeng, Liu Haifeng *

Key Laboratory of Coal Gasification of Ministry of Education, East China University of Science and Technology, P.O. Box 272, Shanghai 200237, People's Republic of China

ARTICLE INFO

Article history:
Received 13 April 2009
Received in revised form 19 August 2009
Accepted 27 August 2009
Available online 9 September 2009

Keywords:
Coal–sludge slurry
Co-gasification
Ash fusion temperature
Mineral matter
XRD

ABSTRACT

The coal, sewage sludge, water and chemical additives are milled to produce coal–sludge slurry as a substitute for coal–water slurry in entrained-flow gasification, co-gasification of coal and sewages sludge can be achieved. The ash fusion temperature is an important factor on the entrained-flow gasifier operation. In this study, the ash fusion temperatures (DT, ST, HT and FT) of three kinds of coals (A, B and C), two kinds of sewage sludges (W1 and W2) and series of coal–sewage blends were determined, and the mineral composition during the ash melting process was analyzed by X-ray diffraction (XRD). The results showed that the ash fusion temperatures of most coal–sewage blends are lower than those of the coals and sewage sludges. The ashes have different mineral composition at different temperature during the heating process. It was found that the mineral composition of AW1 blend ash is located in the low-temperature eutectic region of the ternary phase diagram of SiO_2–Al_2O_3–CaO. The minerals found in BW1 blend ash are almost the same as those in B coal ash. Kyanite is detected in CW1 blend ash, which results in the ash fusion temperatures of CW1 blend ash higher than those of C coal. We found that sodium mineral matters are formed because of NaOH added to W2, which can reduce the ash fusion temperature of coal–sewage blends.

1. Introduction

The sewage sludge production from wastewater treatment plants is increasing rapidly all over the world. It is estimated that approximately 26 kg of sludge is generated per person per year, on a dry weight basis [1]. In Europe, the total amount of sludge generated in urban waste water treatment plants has increased from 5.5 million (1992) to 10 million tons dry matter in 2007. In Spain, sewage sludge production from 1997 to 2005 increased 40%, rising up to 1.065 million tons in 2006 [2]. In China, sewage sludge production was about 3.5 million tones (dry weight) in 2005 [3], and increased about 10% every year.

The sewage sludge contains much toxic inorganic and organic pollutants [4]. If treated improperly, it would be a serious threat to ecological environment. The disposal of sewage sludge presents a rising challenge for the environment. Some sewage sludge disposal methods have been used, i.e., recycling in agriculture [5], landfill [6], combustion [7], pyrolysis [8,9], and gasification of sewage sludge [10]. However, these methods either cause the secondary pollution, or need a large amount of cost in the process.

A typical coal–water slurry (CWS) consists of 60–70% coal, 30–40% water and approximately 1% chemical additives [11–13]. High solids content and low viscosity are desirable CWS properties. The industrially expected value for CWS viscosity, albeit not absolute, is a Brookfield viscosity of 1000 mPa s at 100 s^{-1}. A new disposal method is to mix sewage sludge with coal to prepare coal–sludge slurry, which could instead of coal–water slurry (CWS) in the entrained-flow gasifier to realize the co-gasification of sewage sludge and coal [14]. In this method, water and caloric value in sewage sludge can be utilized sufficiently. This process does not require pre-dried sewage sludge because a certain quantity of water is needed during CWS gasification. Heavy metals in sewage sludge are trapped in ash by solidification/fixation during the fusion of coal ash [15], avoiding secondary pollution. Since the main solids in coal–sludge slurries are coal, effective gasification also meets the industrial criterion.

The authors have done much work on the slurryability of coal–sludge slurry [14]. The ash fusion temperature is another important factor on the entrained-flow gasifier operation. The entrained-flow gasifier gasification technology requires that coal ash fluid temperature should be lower than 1400 °C because of the refractory materials of gasifier. If it is off-limits, it would bring many operational problems such as reducing the life of refractory materials [16]. Because the liquid phase epitaxy slag, the reduction of ash fusion temperature can favor the entrained-flow gasifier working, and reduce the oxygen consumption. Coal–sludge slurry as a special CWS, its ash fusion temperature has different characteristics from that of coal [17–20]. Therefore, it is necessary to study the effects of sewage sludge on coal fusion temperature. The Na^+ is as fluxing medium [21,22], which also has great influence on the coal ash fusion temperatures. In this paper, several

* Corresponding author. Tel.: +86 21 64251418.
E-mail address: hfliu@ecust.edu.cn (L. Haifeng).

0016-2361/$ - see front matter © 2009 Elsevier Ltd. All rights reserved.
doi:10.1016/j.fuel.2009.08.039

Table 1
Proximate analysis and ultimate analysis of A, B, C coals and sewage sludge.

Samples	Proximate analysis w (%)				Ultimate analysis w (%)				Q_d (MJ kg^{-1})
	M_{ar}	A_d	V_d	FC_d	C_d	H_d	N_d	S_d	
A coal	7.17	6.58	39.7	53.72	69.23	4.72	0.86	0.49	28.36
B coal	9.33	10.36	29.60	60.04	71.18	6.17	0.81	0.53	22.78
C coal	9.63	15.89	29.31	54.80	67.35	4.79	0.80	0.71	23.11
Sewage sludge	80.58	41.98	50.97	7.05	30.13	5.70	2.53	1.40	14.56

M_{ar} refers to moisture on received basis; A_d, V_d and FC_d refer to ash, volatile and fixed carbon on dried basis; ultimate analysis is also on dried basis; Q refers to higher calorific value.

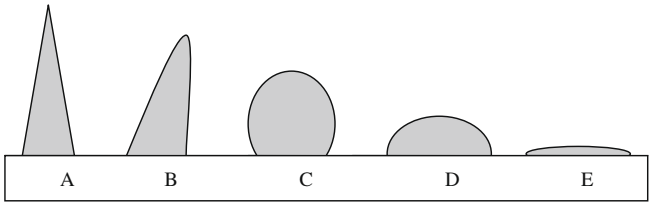

Fig. 1. Changes of cone shape during ash flow transformation (Chinese GB 219-74). (A) Original cone before heating. (B) Initial deformation temperature where first rounding of cone tip is taking place (DT). (C) Softening or sphere temperature where the cone height = cone width (ST). (D) Hemispherical temperature where cone height = 1/2 cone width (HT). (E) Fluid or flow temperature where cone height < 1.5 mm (FT).

series of experiments were carried out about the effects of sewage sludge and NaOH on the coal ash fusion temperatures. And the ash mineral composition of mixtures was detected by XRD at different temperatures.

2. Experimental

2.1. Experimental samples

Shenfu coal (A), Daliuta Coal (B), and Shigetai coal (C) from China were chosen for study. Sewage sludge was obtained from an urban wastewater treatment plant situated in Shanghai, China. The proximate and ultimate analysis of coals and sewage sludge are listed in Table 1.

As shown in Table 1, sewage sludge has special characteristics other than coals, such as higher moisture, ash, volatile, nitrogen and sulfur [23], and lower in fixed carbon and caloric value.

2.2. Ash preparation and ash fusion temperatures determination

Coal were grinded in a ball milling into particles and passed through a 150-mesh miller sieve. Sewage sludge was W1, and sewage sludge modified by sodium hydroxide (10% on the dry basis of sewage sludge) was W2. In a vessel containing a certain quantity of deionized water, The milled coal was mixed with W1 or W2. Then, the mixture was stirred by mechanical agitator kept at 400 rpm for approximately 20 min to ensure homogenization. As a result, series of coal–sludge blends (AW1, BW1, CW1, AW2, BW2, and CW2) were made. The addition amount of sewage sludge is expressed by the rate of wet sewage sludge to coal. Dried these blends and made ashes according to Chinese GB/T212-2001 standard. The dried sample is place on cupel and heated in the muffle up to 815 °C in 25 k min^{-1}. After keeping it at 815 °C for 0.5 h, the muffle temperature reduced to the room temperature, and the sample ash was made.

The ash chemical composition was determined by XRF-1800 produced by Shimadzu Corporation in Japan, and the ash fusion temperatures of coal–sewage blends were determined by 5E-AFII-auto-analyzer under reducing atmosphere according to Chinese GB219-74 standard. The reducing atmosphere was gained by incomplete combustion of black lead and charcoal in corundum tube inside the 5E-AFIIauto-analyzer during heating ash cones. There are four temperatures DT, ST, HT and FT for each cone, which are depicted in Fig. 1. For each fusibility temperature, the value reported is the average of the results obtained in two different assays. Moreover, three ash cones of the same sample were simultaneously used in the above two assays. The results are presented in Table 2.

From Table 2, it is clear that the main oxides in coal ashes are SiO_2, CaO, Al_2O_3, Fe_2O_3, SO_3. Al_2O_3 and P_2O_5 in sewage sludge ashes are much more than those in coals. And in W2 ashes, the content of Na_2O is the highest among samples because of the NaOH addition. The W1 ash fusion temperatures are close to those of bituminous coals, but the ash fusion temperatures of W2 are much higher than those of W1. Maybe, the excess Na_2O contained in W2 increases the ash fusion temperatures of sewage sludge because of 1548 °C melting point of Na_2O. Dong [22] also found that the sample fusion temperature decreases till certain dosage and after that the fusion temperature increases with further addition of Na to sample.In order to explain the ash fusion behaviors, X-ray diffraction (XRD) was used to detect mineral composition in ashes at different temperatures. Each ash was heated in a reducing atmosphere from 800 °C [24] to FT with the interval of 100 °C, and then dampened in water [25]. Mineral composition and type were identified by XRD diffractograms [26]. Diffractograms were made using a Rigaku D/max 2550VB/PC X-ray power diffractometer produced by Japan neo-Confucianism Company. Diffraction intensities were recorded in the 2θ range of 0°–80°.

Table 2
Ash chemical composition and ash fusion temperatures of A, B C coals and W1, W2 sewage sludges.

Samples	Ash chemical composition (wt.%)								Ash fusion temperature (°C)			
	SiO_2	Al_2O_3	Fe_2O_3	MgO	CaO	Na_2O	P_2O_5	SO_3	DT	ST	HT	FT
A coal ash	21.46	9.88	9.63	1.58	29.74	2.30	0.04	22.68	1190	1229	1235	1240
B coal ash	31.44	15.74	7.94	2.37	20.58	1.39	0.03	17.98	1181	1251	1237	1253
C coal ash	45.04	17.65	8.70	1.66	10.75	2.13	0.08	10.60	1157	1182	1206	1224
W1 ash	27.99	25.53	5.66	2.07	11.40	0.91	16.71	6.71	1183	1206	1210	1222
W2 ash	18.02	20.70	3.74	1.51	7.31	26.30	12.48	7.23	1291	1348	1369	1374

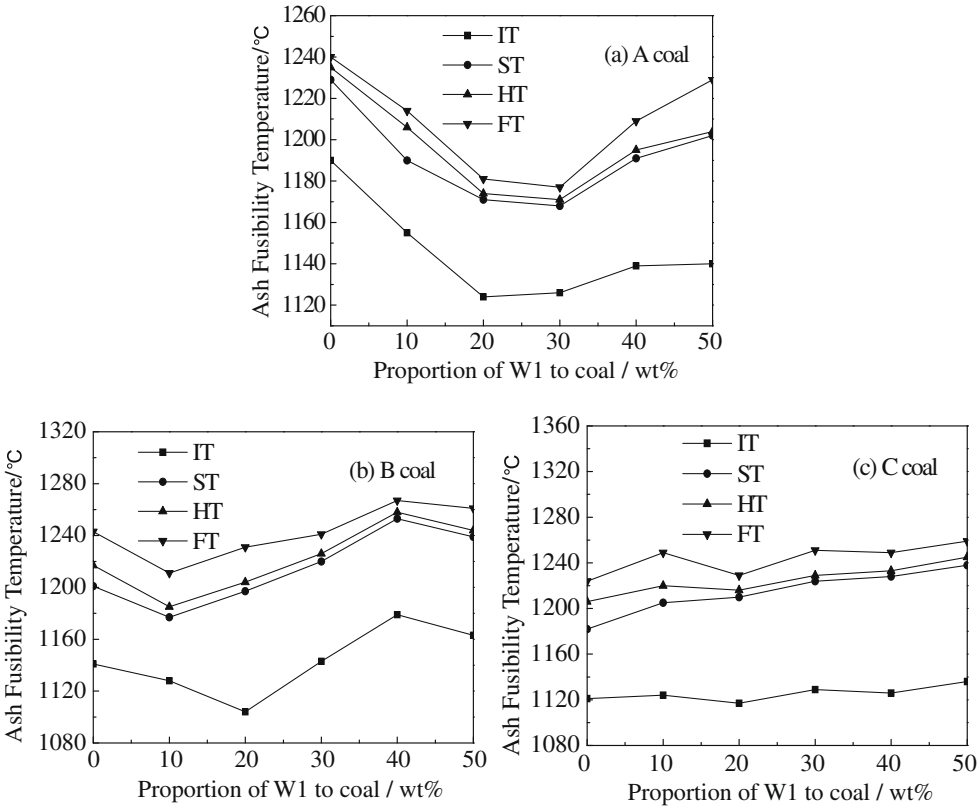

Fig. 2. The influence of W1 on the IT, ST, HT and FT of A, B and C coals.

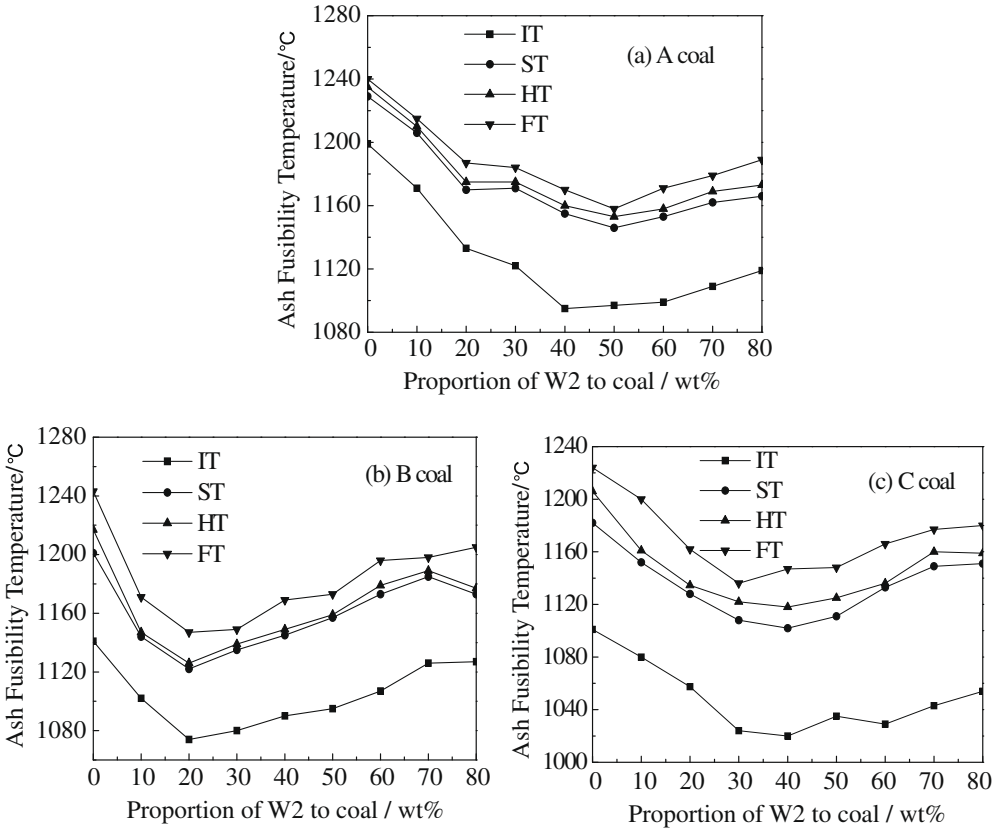

Fig. 3. The influence of W2 on the IT, ST, HT and FT of A, B and C coals.

3. Results and discussion

3.1. The influence of sewage sludge on ash fusion temperatures of coals

The influence of W1 or W2 on ash fusion temperatures of three coals is presented in Figs. 2 and 3, respectively. The ash fusion temperatures are plotted against the proportion of sewage sludge to coal (expressed in weight percentage).

It can be known from Fig. 2a, AW1 blend ash fusion temperatures decrease initially and then increase while the proportion of W1 to A coal from 0 to 50 wt.%. The blend ash fusion temperatures reduce to minimum at the 30 wt.% proportion of W1 to A coal, and FT is1177 °C. Fig. 2b presents a similar trend to Fig. 2a, but the decrease degree is a little smaller. The effect of W1 on C coal ash fusion temperature presents an obvious difference to A and B coals. The CW1 ash fusion temperatures increase appreciably with increase of W1 percentage to C coal.

The ash fusion temperatures of three kinds of blends of W2 and coals (AW2, BW2 and CW2) show the same tendency as AW1 and BW1. When the ash fusion temperatures get to the minimum, the proportion of W2 to A, B and C coals are 50, 20 and 30 wt.%. Comparing Fig. 3 with Fig. 2, it can be concluded that W2 can further reduce coals ash fusion temperatures than W1. With further addition W2 to the coals, the ash fusion temperatures increase. After more and more sewage sludge addition to the coal, the sewage sludge dominates the properties of coal–sludge blends. So, the ash fusion temperatures increase later and get close to the sewage sludge.

3.2. Minerals composition detected by XRD

Different samples have different absorbed or reflected X-ray, which is not only related to mineral type, but also to the mineral content. For a certain kind of mineral, the diffraction intensity

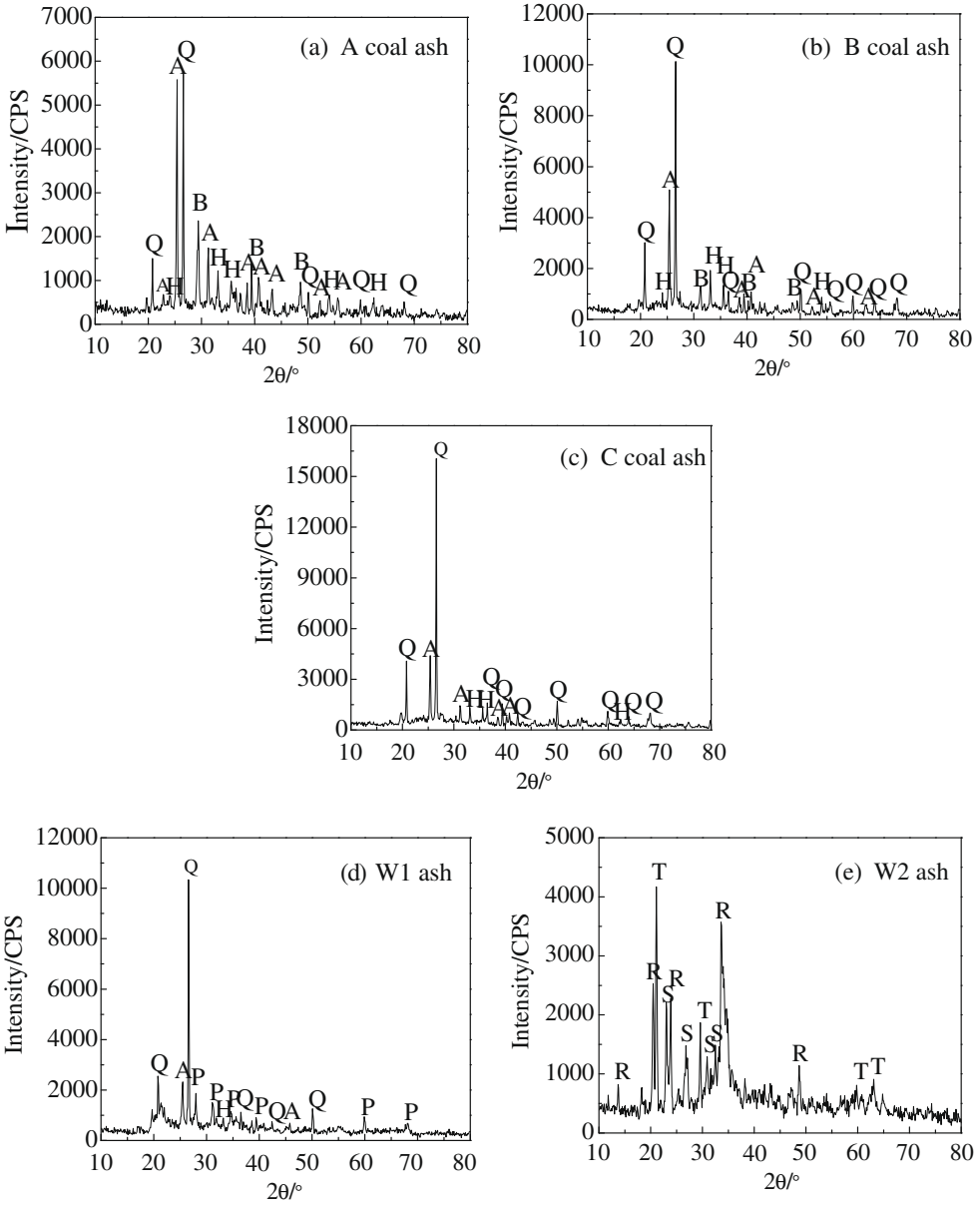

Fig. 4. XRD diffractograms of coal ashes (A, B and C) and sludge ashes (W1 and W2) produced at 800 °C. Q-Quartz, A-Anhydrite, B-Calcite, H-Hematite, P-Chloroapatite, R-Sodium calcium silicate, S-Nahpolite, T-Nepheline.

can be approximately in response to its content [24]. Firstly, the mineral composition in coal–sewage blend ashes made at 800 °C was analyzed by XRD.

Fig. 4a–e presents the XRD patterns of 800 °C ashes of three coals and two kinds of sewage sludge. The results showed that the main mineral matters in A and B coal ashes are quartz, anhydrite, calcite and hematite, while in C coal ash are quartz, anhydrite and hematite. It can be seen from Fig. 4d that W1 XRD diffractogram is similar to those of coals. Chloroapatite is also detected apart from quartz, anhydrite and hematite. The presence of chloroapatite is due to

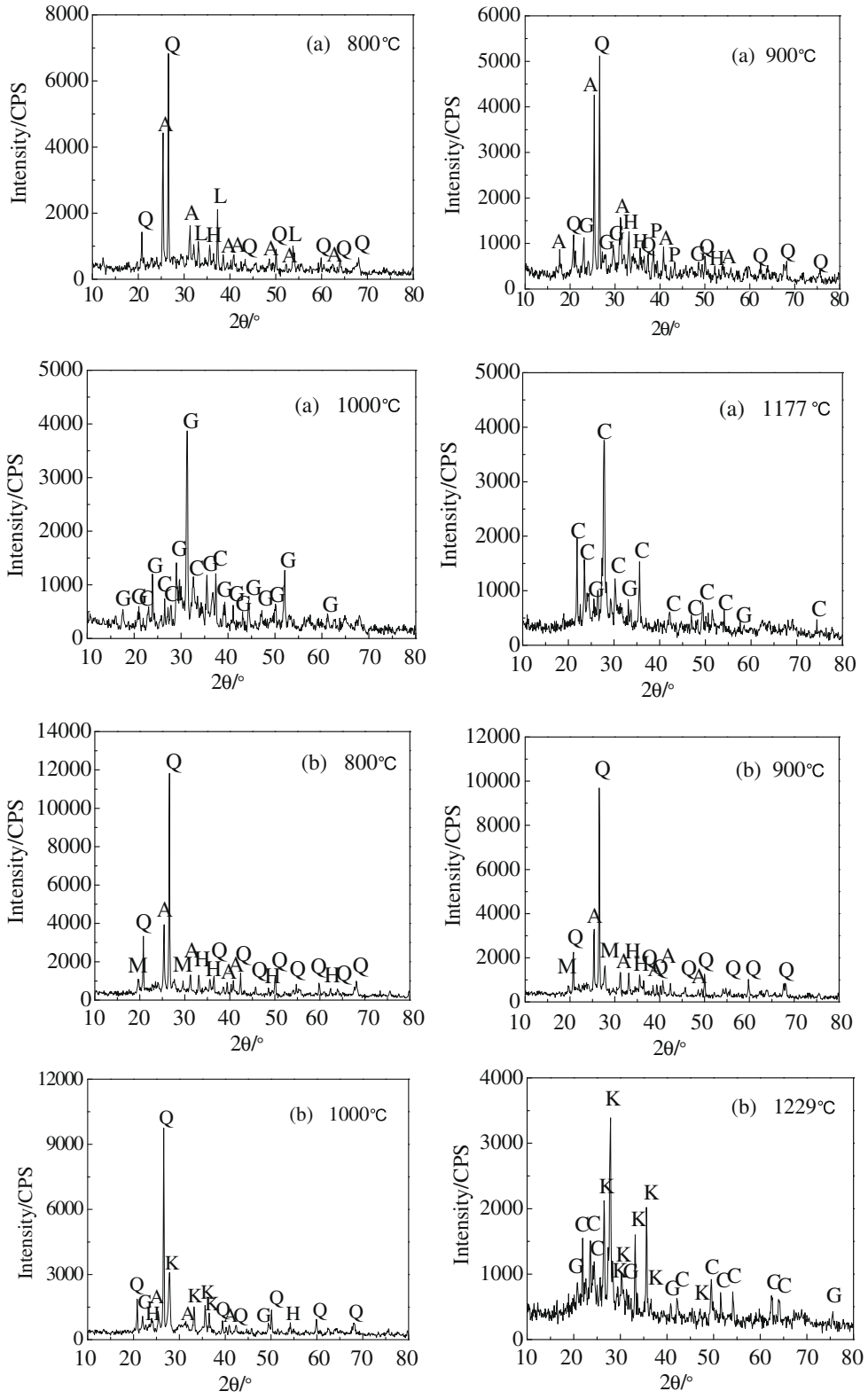

Fig. 5. XRD diffractograms of coal–W1 blend ashes at 800, 900, 1000 °C and FT. (a) A coal–30 wt.% W1 blend ash; (b) C coal–20 wt.% W1 blend ash Q-Quartz, A-Anhydrite, H-Hematite, L-Lime, K-Kyanite, M-Montmorillonite, C-Anorthite, G-Gehlenite, P-Chloroapatite N-Albite.

the high content of phosphate in sewage sludge. In W2 ashes, main mineral matters are nahpolite, nepheline and sodium calcium silicate, which are formed from Na_2O reaction with quartz, Al_2O_3, CaO and other minerals.

Ternary phase diagrams such as $CaO–SiO_2–Al_2O_3$ have shown their usefulness in prediction ash fusion temperatures [26]. Due to this fact, $SiO_2–Al_2O_3–CaO$ were employed to explain the coal–sewage blend ash fusion temperatures.

Fig. 5 shows the ash XRD diffractograms of A coal–30 wt.% W1 blend and C coal–20 wt.% W1 blend at 800, 900, 1000 °C and FT. In A coal–30 wt.% W1 blend ash, apart from quartz, anhydrite and hematite, chloroapatite and lime are also detected at 800 °C.

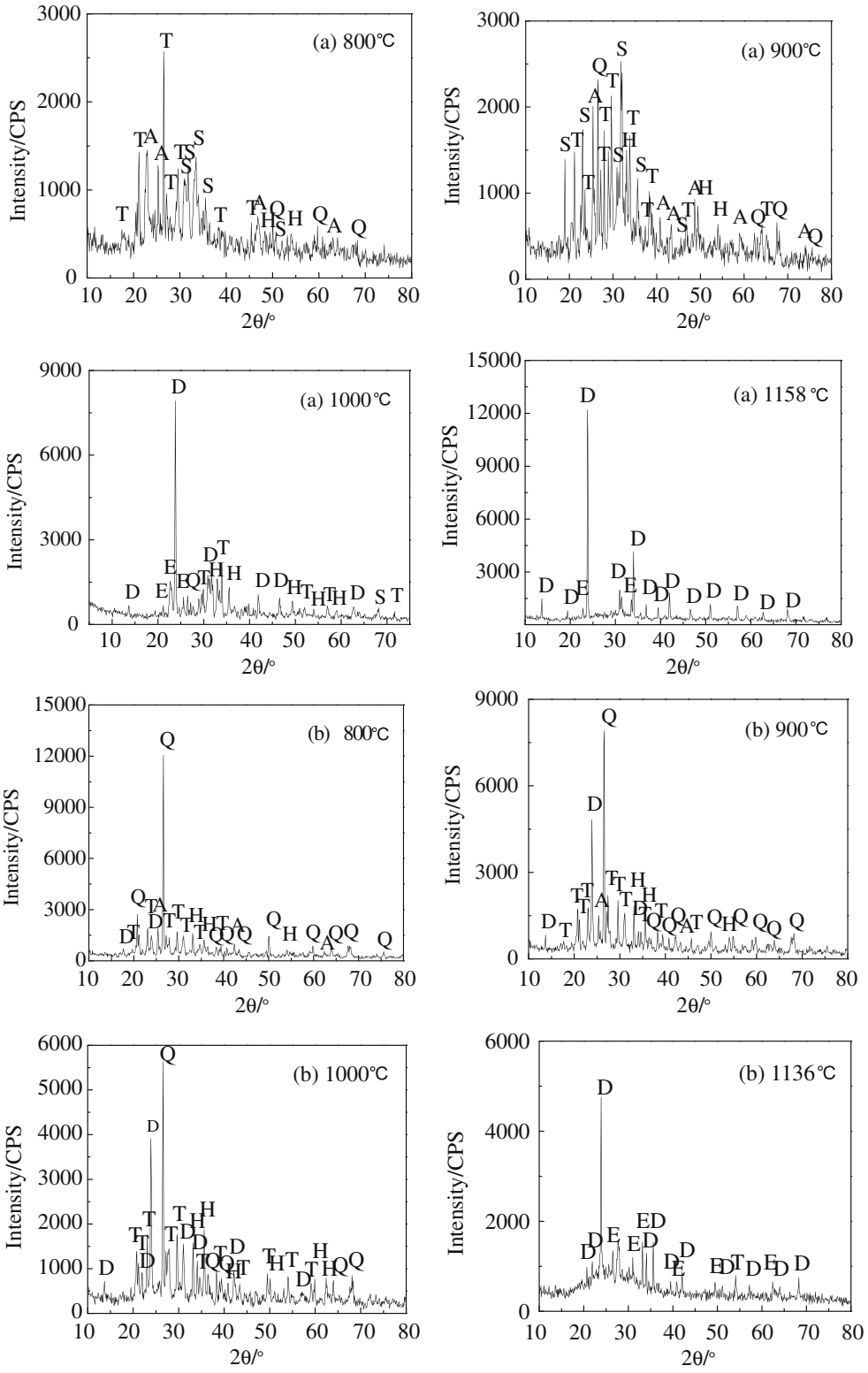

Fig. 6. XRD diffractograms of coal–W2 blend ashes at 800, 900, 1000 °C and FT. (a) A coal–50 wt.% W2 blend ash; (b) C coal–30 wt.% W2 blend ash Q-Quartz, A-Anhydrite, H-Hematite, S-Nahpolite, T-Nepheline, D-Nosean, E-Sodium–calcium phosphate.

The diffraction peak of quartz decreases with the increase of temperature, because it reacts with Al_2O_3 and CaO to form gehlenite.At 1000 °C, anhydrite and quartz disappear, while the gehlenite is observed. The XRD peak of chloroapatite disappears at 1177 °C (FT), and then the main mineral matters in blend ashes forms to anorthite. Gehlenite is also detected, but the XRD peak was weak. Co-existing of anorthite and gehlenite will produce a low-melting eutectic mixture. This is the main reason for the lower ash melting temperatures of blend ashes.

In C coal–20 wt.% W1 blend ash, montmorillnbite is detected at 800 °C, and then it disappears at 1000 °C because of formation of kyanite. Kyanite begins to decompose and transform into mullite at about 1300 °C [27]. Quartz, anhydrite, and hematite disappear, and kyanite, anorthite and gehlenite co-exist in blend ashes at FT. The presence of kyanite could explain why the addition of W1 does not reduce C coal ash fusion temperatures.

B coal–10 wt.% W1 blend ash show the same minerals as found in B coal ash samples (quartz, anhydrite, calcite and hematite). This is the reason why a low proportion of sludge does not affect mineral composition, although it lowers ash fusion temperatures.

Fig. 6 shows the XRD diffractograms of A coal–50 wt.% W2 blend ash and C coal–30 wt.% W2 blend ash at 800, 900, 1000 °C, FT. The diffractograms of A coal–50 wt.% W2 blend ash shows an intermediate behavior between A coal ash and W2 ash. At 800 °C, quartz, anhydrite, hematite, nahpolite and nepheline are detected. In the AW2 blend ash of 900 °C, the main minerals are nahpolite and nepheline, quartz and anhydrite. Anhydrite disappears at 1000 °C, and nahpolite and nepheline begin to transform to nosean and sodium–calcium phosphate. With temperature increase, the quantity of nosean increases. At 1158 °C, only nosean and a little sodium–calcium phosphate are detected. B coal–20 wt.% W2 blend ash and C coal–30 wt.% W2 blend ash show similar minerals behaviors to A coal–50 wt.% W2 blend ashes. We found that sodium mineral matters are formed because of NaOH added to W2, the ash fusion temperatures of which are lower. Therefore, W2 reduces coals ash fusion temperatures more effectively than W1. As mentioned above, sodium is an efficient fusion agent. Alkali metal as a corrector of network is easy to crystallize with SiO_2. With the increase of addition of sodium, bridged oxygen bond between silicon and oxygen would convert to non-bridged oxygen bond, which cause original tetrahedral structure loose, and even some leading to decomposition. Then tetrahedral structure will change into unstable Si–O cyclic structure, which easy to produce new minerals combined with other elements.

4. Conclusions

The ash fusion temperatures of coal, sewage sludge and series of coal–sewage blends were investigated. The results showed that the fusion temperatures of most coal–sewage blends ashes are lower than those of the coals and sewage sludges.

The ash fusion temperature change of coal–sludge blends is mainly caused by mineral composition. Temperatures and the ratio of sewage sludge and coal have significant effects on the mineral behavior. It was found that the mineral composition of AW1 (A:W1 is 100:30) coal–30 wt.% W1 blend ash is located in the low-temperature eutectic region of the ternary phase diagram SiO_2–Al_2O_3–CaO. The minerals found in BW1 blend ash are almost the same as those in B coal ashes. Kyanite is detected in CW1 blend ash, which results in the ash fusion temperatures of C coal. The main reason of W2 reducing ash fusion temperatures of coals was due to the addition of sodium in sodium hydroxide.

Acknowledgements

This work is supported by National Natural Science Foundation of China (Grant No. 50776033), New Century Excellent Talents in University (NCET-08-0775), PetroChina Innovation Foundation (2009D-5006-04-05), Program for Changjiang Scholars and Innovative Research Team in University (PCSIRT–IRT 0620) and National Key State Basic Research Development Program of China (973 Program, 2004CB217700).

References

[1] Borrely SI, Cruz AC, Del Mastro NL, Sampa MHO, Somessari ES. Radiation processing of sewage sludge: a review. Prog Nucl Energy 1998;33:3–21.
[2] Carbonell G, Pro J, Gomez N, Babin MM, Fernandez C, Alonso E, et al. Sewage sludge applied to agricultural solid: ecotoxicological effects on representative solid organisms. Ecotoxicol Environ Saf 2009;72:1309–19.
[3] Wang JL, Wang JZ. Application of radiation technology to sewage sludge processing: a review. J Hazard Mater 2007;143:2–7.
[4] Rulken W. Sewage sludge as a biomass resource for the production of energy: overview and assessment of the various options. Energy Fuels 2008;22:9–15.
[5] Walid BA, Noureddine G, Abdelbasset L, Gijs DL, Marc V, Naceur J, et al. Effect of 5-year application of municipal solid waste compost on the distribution and mobility of heavy metal sin a Tunisian calcarrous soil. Agric Ecosyst Environ 2009;130:156–63.
[6] Alina S, Maria S, Ola H. Energy use and recovery strategies within wastewater treatment and sludge handling at pulp and paper mills. Bioresour Technol 2009;100:3497–505.
[7] Vesilind PA, Ransey TB. Effect of drying temperature on the fuel value of wastewater sludge. Wastewater Manage Res 1996;14:189–96.
[8] Conesa JA, Marcilla A, Prats D, Pastor MR. Kinetic study of the pyrolysis of sewage sludge. Waste Manage Res 1997;15:293–305.
[9] Konar SM, Boocock DGB, Mao V, Liu J. Fuels and chemicals from sewage sludge 3: hydrocarbon liquids from the catalytic pyrolysis of sewage sludge lipids over activated alumina. Fuel 1994;73:642–8.
[10] Ferrasse JH, Seyssiecq I, Roche N. Thermal gasification: a sensible solution for sewage sludge valorization. Chem Eng Technol 2003;26:941–5.
[11] Zhou MS, Yang DJ, Qiu XQ. Influence of dispersant on bound water content in coal–water slurry and its quantitative determination. Energy Convers Manage 2008;49:3063–8.
[12] Zhou MS, Yang DJ, Qiu XQ. Effect of the sodium lignosulphonate from different material on rheological behavior of coal water slurry. J Chem Eng Chin Univ 2007;21:386–91.
[13] Wei YC, Li BQ, Li W. Effect of coal characteristics on the properties of coal water slurry. Coal Prep 2005;25:239–49.
[14] Li WD, Li WF, Liu HF, Yu ZH. Influence of sewage sludge on the slurryability of coal–water slurry. Fuel 2009 [available on line].
[15] Marrero TW, McAuley BP, Sutterlin WR, Steven-Morris J, Manahan SE. Fate of heavy metals and radioactive metals in gasification of sewage sludge. Waste Manage 2004;24:193–8.
[16] Li HX, Chen FL. Coal blending to reduce the ash fusion temperature of high fusibility Huainan coal. J China Coal Soc 2002;27:529–33.
[17] Bryant GW, Browning GJ, Emanuel H, Gupta SK, Gupta RP, Lucas JA, Wall TF, et al. The fusibility of blended coal ash. Energy Fuels 2000;14:316–25.
[18] Belen FM, Maria DR, Jorge X, Purificacion GM, Juan PJ. Influence of sewage sludge addition on coal ash fusion temperatures. Energy Fuels 2005;19:2562–70.
[19] Paterson N, Zhuo Y, Dugwell D, Kandiyoti R. Formation of hydrogen cyanide and ammonia during the gasification of sewage sludge and bituminous coal. Energy Fuels 2005;19:1016–22.
[20] Ninomiya Y, Zhang L, Sakano T, Kanaoka CH, Masui M. Transformation of mineral and emission of particulate matter during co-combustion of coal with sewage sludge. Fuel 2004;83:751–64.
[21] Cheng Y, Li HX, Wu CL. Effect of fluxes on ash fusion characteristics of Huainan coal. Coal Technol 2005;12:90–2.
[22] Dong F, Guo GY, Wang N, Wang BF. Influence of Na_2O on continuous casting mould fluxes melting properties. J Baotou Univ Iron Steel Technol 2003;3:198–200.
[23] Reed GP, Paterson NP, Zhuo Y, Dugwell DR, Kandiyoti R. Trace element distribution in sewage sludge gasification: source and temperature effects. Energy Fuels 2005;19:298–304.
[24] Srinivasachar S, Helble JJ, Boni AA, Shah N, Huffman GP, Huggins FE. Mineral behavior during coal combustion 2. Illite transformations. Prog Energy Combust Sci 1993;16:293–302.
[25] Qiu JR, Li F, Zheng Y, Zheng CG, Zhou HC. The influences of mineral behaviors on blended coal ash fusion characteristics. Fuel 1999;78:963–9.
[26] Dyk JCV, Baxter LL, Heerden JHPV, Coetzer RLJ. Chemical fractionation tests on South African coal sources to obtain species-specific information on ash fusion temperatures. Fuel 2005;84:1768–77.
[27] Lin BY, Zhang JW, Si SQ, Pan BM, Li JZ, Zhao YA. Kyanite, andalusite, sillimanite (second print). Beijing, China: The Publishing House of Metallurgical Industry; 2003. p. 88–94.